ISSN: 2153-1196 Volume 10, Number 2, February 2019

Scientific Research Publishing

Journal of Modern Physics

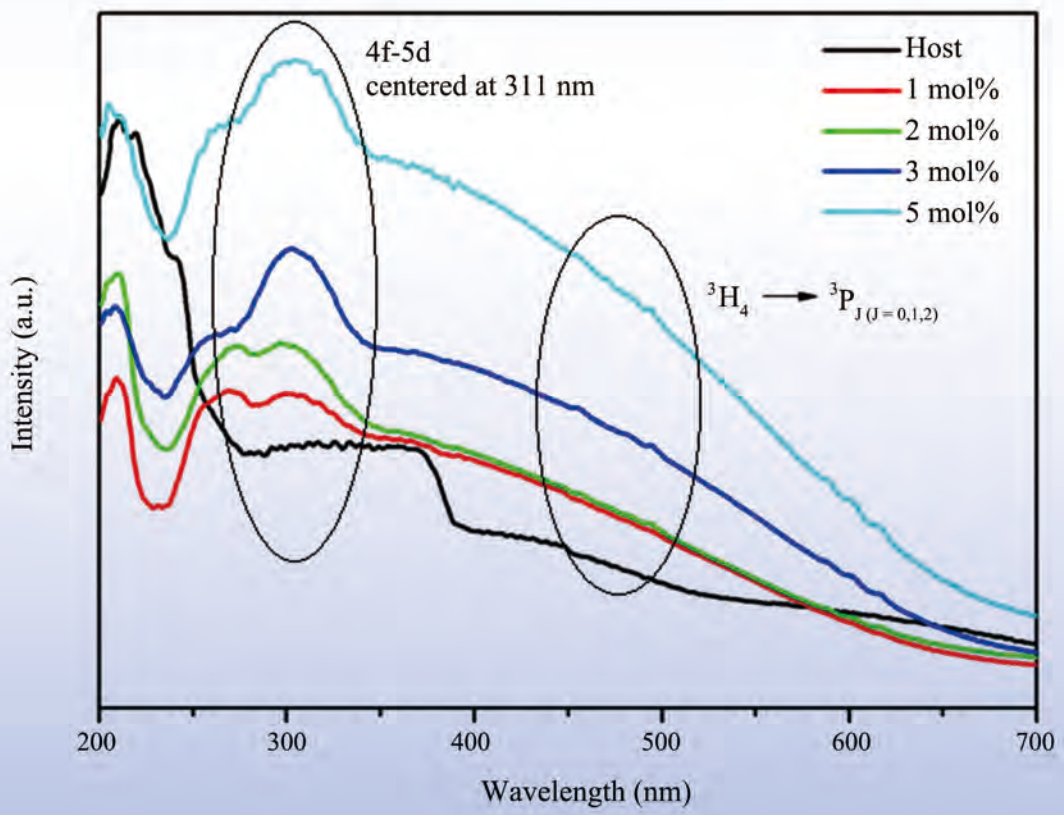

ISSN: 2153-1196
9 772153 119007 02

www.scirp.org/journal/jmp

Journal Editorial Board

ISSN: 2153-1196 (Print) ISSN: 2153-120X (Online)
http://www.scirp.org/journal/jmp

Editor-in-Chief

Editorial Board

Scientific Research Publishing

Journal of Modern Physics, 2019, 10, 91-194
http://www.scirp.org/journal/jmp
ISSN Online: 2153-120X
ISSN Print: 2153-1196

Table of Contents

Volume 10 Number 2 February 2019

The figure on the front cover is from the article published in Journal of Modern Physics, 2019, Vol. 10, No. 2, pp. 91-101 by Hung-Rung Shih *et al.*

Journal of Modern Physics (JMP)
Journal Information

SUBSCRIPTIONS

The *Journal of Modern Physics* (Online at Scientific Research Publishing, www.SciRP.org) is published monthly by Scientific Research Publishing, Inc., USA.

Subscription rates:
Print: $89 per issue.
To subscribe, please contact Journals Subscriptions Department, E-mail: sub@scirp.org

SERVICES

Advertisements
Advertisement Sales Department, E-mail: service@scirp.org

Reprints (minimum quantity 100 copies)
Reprints Co-ordinator, Scientific Research Publishing, Inc., USA.
E-mail: sub@scirp.org

COPYRIGHT

PRODUCTION INFORMATION

For manuscripts that have been accepted for publication, please contact:
E-mail: jmp@scirp.org

Journal of Modern Physics, 2019, 10, 91-101
http://www.scirp.org/journal/jmp
ISSN Online: 2153-120X
ISSN Print: 2153-1196

Structure and Photoluminescence Properties of Pr^{3+} Ion-Doped BaY_2ZnO_5 Phosphor Prepared Using a Sol-Gel Method

Hung-Rung Shih[1], Mu-Tsun Tsai[2], Lay-Gaik Teoh[3], Yee-Shin Chang[4*]

[1]Department of Mechanical and Computer-Aided Engineering, National Formosa University, Taiwan
[2]Department of Materials Science and Engineering, National Formosa University, Taiwan
[3]Department of Mechanical Engineering, National Pingtung University of Science and Technology, Taiwan
[4]Department of Electronic Engineering, National Formosa University, Taiwan
Email: *yeeshin@nfu.edu.tw

How to cite this paper: Shih, H.-R., Tsai, M.-T., Teoh, L.-G. and Chang, Y.-S. (2019) Structure and Photoluminescence Properties of Pr^{3+} Ion-Doped BaY_2ZnO_5 Phosphor Prepared Using a Sol-Gel Method. *Journal of Modern Physics*, **10**, 91-101.
https://doi.org/10.4236/jmp.2019.102008

Received: January 7, 2019
Accepted: February 9, 2019
Published: February 12, 2019

Abstract

The Pr^{3+} ion-doped BaY_2ZnO_5 phosphor with the orthorhombic structure was synthesized successfully using a sol-gel method in this study. The SEM images show that the BaY_2ZnO_5:Pr^{3+} phosphor particles are aggregational but have an isotropic distribution for 2 mol% Pr^{3+} ions doped. Under an excitation wavelength of 311 nm, the emission bands that appear in the emission spectra are due to the $^3P_0 \rightarrow {}^3H_{4,5,6}$, $^1D_2 \rightarrow {}^3H_4$ and $^3P_0 \rightarrow {}^3F_2$ electron transition of Pr^{3+} ion, and it is the same as that for solid state reaction preparation. Comparing to the solid state reaction preparation, the intensities of the $^3P_0 \rightarrow {}^3H_4$ transition were increased by about 6.5 times for sol-gel method. The enhancement in emission intensity is because the activators have more homogeneous contribution in host for the sol-gel method preparation. In addition, the color tone did not change very obviously, which located around the green light region for Pr^{3+} ion concentrations increasing. The color stability is better for sol-gel method than that for the solid state reaction preparation.

Keywords

Phosphor, Rare Earth Oxides, Optical Properties

1. Introduction

Oxide phosphors have recently gained much attention for applications such as screens infield-emission displays (FEDs) [1], plasma display panels (PDPs) [2] [3] and for white color light-emitting diodes (LEDs) [4] because the intrinsic problems such as their higher chemical stability and resistance to moisture rela-

tive to that of traditional phosphors are rare earth or transition metal activated sulphides such as ZnS, SrS, and CaS. A lot of efforts have been done to discover the novel host materials as well as activators with high photoluminescence properties including emission intensity, high quantum yield and so on for phosphor applications [5] [6].

The emission of lanthanide ion, Pr^{3+} ion, in the visible region occurs because of the transition of the $^3P_0$ level, which contains two dominant transitions from the fluorescent $^3P_0$ level to the lower $^3H_6$ and $^3H_4$ states [7]. The emission spectra of Pr^{3+} are significantly different in different hosts and can take the form of red, green, or even blue emissions [8] [9].

BaY_2ZnO_5 has the orthorhombic structure with space of Pbnm [10], and it consists of YO_7, BaO_{11}, and ZnO_5 polyhedra. BaY_2ZnO_5 is an excellent host for various activator ions-doped phosphors. Some previous studies investigated the effect of the size, morphology of particles, and activator concentrations on the photoluminescence properties of BaY_2ZnO_5:RE^{3+} phosphors [11] [12] [13] [14]. According to our previous study [14], the emission spectra show that the $^3P_0 \rightarrow {}^3H_{4,5,6}$ transitions are dominant for the Pr^{3+}-doped BaY_2ZnO_5 phosphor. The color tone changes from green to greenish and finally yellow, as the Pr^{3+} ion concentration increases.

Many efforts have been done to enhance the emission intensities of phosphors and the improvement of particle morphologies via fluxes addition, chemical methods utilized to mix activators well or by doping with ions of different radii. Various chemical methods have been investigated for synthesizing fine-sized grains, because these have been reported to enhance the emission efficiency and intensity of phosphors [15] [16]. These methods include sol-gel [17] [18] [19], hydrothermal [20] [21] [22], and precipitate techniques [23]. Among these methods, the sol-gel process is an attractive route that starts from molecular precursors and forms an oxide network via inorganic polymerization reactions, and offers both product and processing advantages, such as high purity, ultrahomogeneity, and reduction of the calcining temperature, which could decrease the grain size and enhance the emission efficiency and intensity of phosphors.

In this investigation, the Pr^{3+} ions-doped BaY_2ZnO_5 phosphor was prepared using a sol-gel method to reduce the preparation parameters, improve the surface morphology, and hope to increase to the luminescence efficiency of phosphor. The influences of Pr^{3+} ion concentrations on the resulting structure and the photoluminescence (PL) properties of BaY_2ZnO_5:Pr^{3+} phosphor were also studied. The results indicated that the calcination conditions are lower than that of the solid state reaction, and the intensities of emission peak increased by about 6.5 times for the sol-gel method.

2. Experimental Procedure

In this study, BaY_2ZnO_5 compounds doped with various concentrations of Pr^{3+} ions were synthesized using a sol-gel method. The raw materials of barium ni-

tride [$Ba(NO_3)_2$], yttrium acetate [$Y(OOCCH_3)_3{\cdot}4H_2O$], zinc acetate [$Zn(OOCCH_3)_2$] and praseodymium acetate [$Pr(OOCCH_3)_3{\cdot}xH_2O$] with a purity of 99.99% were supplied by Alfa Aesar. At the first, barium nitride (0.01 mole), zinc acetate (0.01 mole), yttrium acetate (0.02 - 2x mole) and praseodymium acetate (2x mole, x = 0 - 0.005) were separately dissolved in 100 ml of deionized water, respectively. Secondly, barium nitride, zinc acetate, yttrium acetate and praseodymium acetate solutions were mixed in a round bottom flask. When the precursor was completely dissolved in the solution, predetermined amounts of citric acid and ethylene glycol (equal molar ratio) were added to the solution mentioned above as a chelating agent and stabilizing agent, respectively. The amounts of citric acid and ethylene glycol were determined by the ratio of citric acid to metal cations. At last, the powders obtained were calcined in air at 1200˚C for 6 h.

Characterization

Powders were analyzed for crystal structure by X-ray diffractometry (XRD; Rigaku Dmax-33 x-ray diffractometer, Tokyo, Japan) using Cu-Karadiation with a source power of 30 kV and a current of 20 mA to identify the possible phases formed after heat treatment. The surface morphologies of phosphors were examined using high resolution scanning electron microscopy (HR-SEM, S4200, Hitachi). Optical absorption spectra were measured at room temperature using a Hitachi U-3010 UV-vis spectrophotometer. Both the excitation and emission spectra of the phosphors were measured using a Hitachi F-7000 fluorescence spectrophotometer with a 150 W xenon arc lamp as the excitation source at room temperature.

3. Results and Discussion

3.1. Structures

Figure 1 shows the X-ray diffraction patterns of the $Ba(Y_{1-x}Pr_x)_2ZnO_5$(x = 0 - 0.05) powders calcined in air at 1200˚C for 6 h. The XRD results show that all of the diffraction peaks of the $BaY_2ZnO_5:Pr^{3+}$ phosphors can be attributed to the orthorhombic structure (JCPDS 89-5856) for Pr^{3+} ion concentration from 0 to 5 mol%, and there is no second phase appears in the spectra, which demonstrates that the Pr^{3+} ion substitutes the Y^{3+} ion. The calcination conditions are lower than that of 1250˚C/12h for conventional ceramics processing reported by the solid state reaction [14]. When the Pr^{3+} content is further increased, the intensities of the diffraction peaks seem to be decrease, and the diffraction peak of the (131) shift to a lower diffraction angle. The shift of the peak position is $\Delta\theta$ = 0.68˚ for the Pr^{3+} ion concentration is 0 and 5 mol%. It is due to the Pr^{3+} ion (0.99 Å, 6-coordinated) has a larger radius than that of Y^{3+} ion (0.90 Å, 6-coordinated), the lattice distorts and intra-stress occurs, nonuniform strain in the vicinity of the Pr^{3+} ions is induced when a trivalent praseodymium ion is introduced to replace trivalent yttrium ion in the $BaY_2ZnO_5:Pr^{3+}$ system.

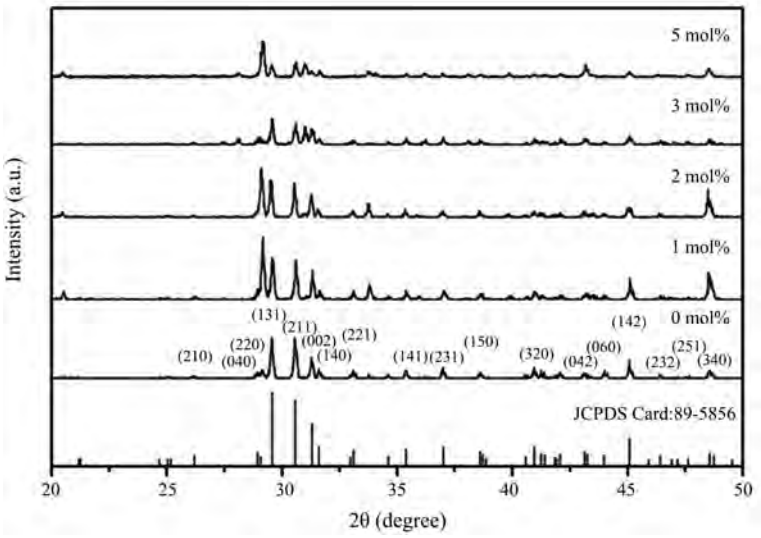

Figure 1. The X-ray diffraction patterns for different concentration of Pr^{3+} ion-doped BaY_2ZnO_5 phosphors prepared using sol-gel method.

Table 1 is the grain size calculated using the Scherrer's equation for different concentrations of Pr^{3+} ion-doped BaY_2ZnO_5 phosphor. The grain sizes for BaY_2ZnO_5:Pr^{3+} phosphors are all in the nanoscale range, and increase initially then decrease for Pr^{3+} ion concentration increase further. The largest grain size occurs when Pr^{3+} ion concentration is 2 mol%. The results are in good accordance with the analysis of XRD patterns for the intensity of (131) diffraction peak is increase then decrease as the Pr^{3+} ion concentration increases.

3.2. Microstructures

The size of phosphor particles should be as homogeneous as possible without any aggregates or agglomerates. Moreover, the surface of the phosphor particles should also be as smooth as possible and have a high degree of crystallization to improve efficiency. **Figure 2** shows the FE-SEM surface morphology of BaY_2ZnO_5 doped with 0, 1, 2, and 5 mol% Pr^{3+} ions. By the results, most of these phosphor particles have polyhedral shapes and irregular. These particles are agglomerates of smaller particles during the calcination process due to that they are on the nano-scale with large surface energies when the particles produced using this sol-gel method. When the Pr^{3+} ion concentration doping is 2 mol% (**Figure 2(c)**), the particles seem to be more uniform distribution and regular sizes. These phosphor powders with better surface morphologies will display a preferable photoluminescence property, and it will be good accordance with the optical properties measurement.

Figure 3 shows the absorption spectra of the BaY_2ZnO_5 doped with different Pr^{3+} ion concentrations phosphor calcined at 1200˚C in air for 6 h. For the host material, it shows two absorption broads in the UV region. The strong absorption band in the region from 200 to 270 nm is attributed to the band-to-band transitions, whereas the weaker broad band from 270 to 400 nm can be attri-

buted to the tightly bound Frankel excitons, which are usually observed close to the bandgap in large-bandgap crystals [24] [25]. The absorption edge of the BaY_2ZnO_5 host is located at ~378 nm. When Pr^{3+} ion doped, a stronger broad band in the range of 250 - 350 nm and a series of small peaks between 400 and 500 nm appear in the spectrum, and that are associated with the f-f transition of the Pr^{3+} ion. The stronger broad band centered at 311 nm can be attributed to the 4f - 5d characteristics transition absorption of Pr^{3+} ion. According to the studies [26] [27] [28], the typical Pr^{3+}-activated oxide phosphors always demonstrate strong 4f - 5d transition band absorption at approximately 200 - 330 nm, and it is in accordance with the results for our study. In addition, there also appears a series of absorption peaks from 440 to 500 nm and 580 to 620 nm, this can be attributed to the 4f orbital characteristics transition for the $^3H_4 \rightarrow {}^3P_J$ (J = 0, 1, 2) transition of the Pr^{3+} ion.

Table 1. The grain Size of $Ba(Y_{1-x}Pr_x)_2ZnO_5$(x = 0 - 0.05) phosphor calculated using the Scherrer's equation.

Pr^{3+} ion concentration	D_g (nm)
0	45.21
1	56.11
2	77.48
3	67.80
5	58.11

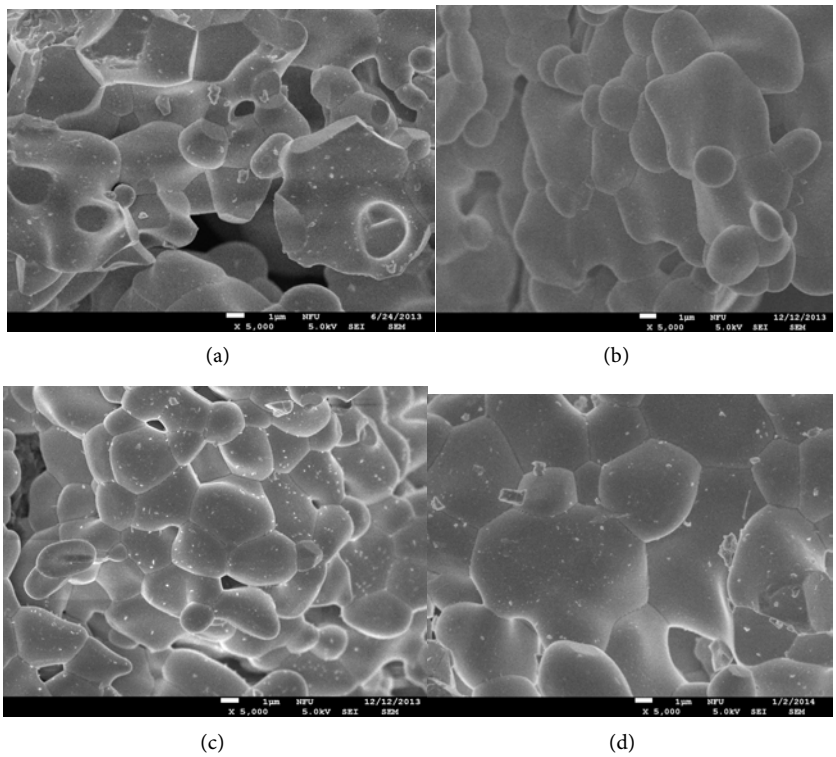

(a) (b)

(c) (d)

Figure 2. The FE-SEM micrographs of BaY_2ZnO_5 doped with different Pr^{3+} ion concentrations: (a) 0, (b) 1, (c) 2 and (d) 5 mol%.

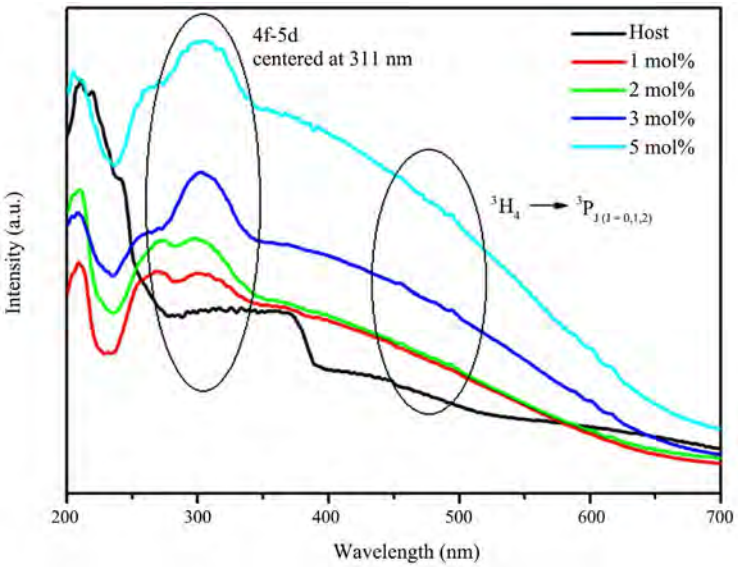

Figure 3. The absorption spectra of BaY_2ZnO_5 doped with different Pr^{3+} ion phosphor prepared using sol-gel method.

Figure 4(a) shows the excitation spectra for BaY_2ZnO_5 doped with various Pr^{3+} ion concentrations calcined in air at 1200˚C for 6 h using the sol-gel method, the singles were obtained by monitoring the emission wavelength of 513 nm for the $^3P_0 \rightarrow {}^3H_4$ transition. A strong broad band from 250 - 350 nm and some sharp peaks in the longer wavelength region can be observed in the excitation spectra. It is similar to the results observed in the absorption spectra, the 4f - 5d transition of Pr^{3+} ion centered at 311 nm was located in the broad band region. These sharp peaks centered at 458 nm, 485 nm and 495 nm in the longer wavelength region from 450 to 500 nm can be assigned to the f-f transitions of Pr^{3+} ion for the $^3H_4 \rightarrow {}^3P_2$, $^3H_4 \rightarrow {}^3P_1$ and $^3H_4 \rightarrow {}^3P_0$, transition, respectively [29] [30]. The excitation intensity has a maximum value for Pr^{3+} ion 2 mol% doped, and then decreasing as the Pr^{3+} ion concentration increases which is due to concentration quenching effect.

Figure 4(b) is the comparison for excitation spectra of BaY_2ZnO_5:2mol%Pr^{3+} phosphor synthesized using the solid state reaction and sol-gel method. As can be seen, different synthesization did not change the shape of excitation curve but did change the intensities of the excitation peak. The excitation intensity of 4f - 5d transition for BaY_2ZnO_5:2mol%Pr^{3+} phosphor synthesized by the sol-gel method is 1.5 times higher than that for the solid state reaction. In Addition, The peak of the 4f - 5d transition shifts from 315 (solid state reaction) to 311 nm (sol-gel method). This shift was associated with the size of the BaY_2ZnO_5:2mol%Pr^{3+} phosphors. It is caused by BaY_2ZnO_5:2mol%Pr^{3+} phosphor prepared using a sol-gel method (calcination at 1200˚C) with a smaller particle sizes then that for solid state reaction (calcination at 1250˚C). According to the studies [31], for a smaller particle size, lattice parameters were usually smaller than those of the bigger one because of the huge surface stress, which leads a stronger ligands field and hence the blue shift was often observed.

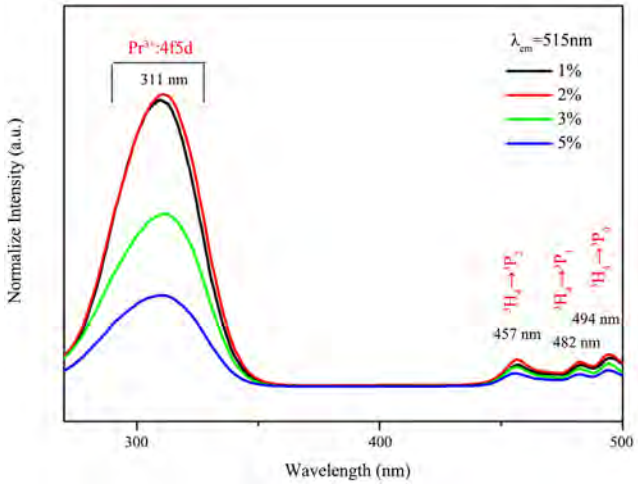

(a)

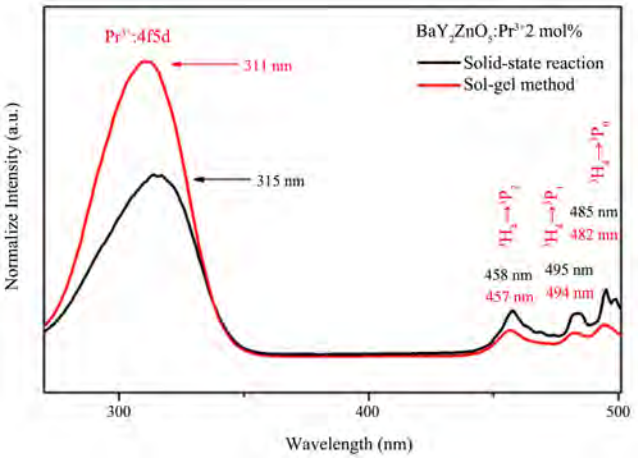

(b)

Figure 4. The excitation spectra of BaY_2ZnO_5 doped with different Pr^{3+} ion phosphor prepared using soli-gel method, and (b) the comparison of excitation spectra for BaY_2ZnO_5:2mol%Pr^{3+} phosphor prepared using sol-gel method and solid state reaction.

Figure 5(a) is the emission spectra under an excitation of 311 nm for BaY_2ZnO_5 doped with various Pr^{3+} ion concentrations prepared using the sol-gel method, and **Figure 4(b)** is the comparison of the emission spectra for BaY_2ZnO_5 doped with 2 mol% Pr^{3+} ions prepared by the solid state reaction and sol-gel method. As can be seen in **Figure 5(a)**, there are several light emitting peaks in the visible light ranges for 490 - 520 nm, and 530 - 560 nm, respectively. The emission peaks at 496, 499 and 515 nm are assigned to the $^3P_0 \rightarrow {}^3H_4$ transitions, those at 530, 539 and 555 nm are the $^3P_0 \rightarrow {}^3H_5$ transitions. It reached a maximum when the Pr^{3+} concentration was 2 mol%, and decreased with the increasing Pr^{3+} concentration, which indicated that the concentration quenching is active when $x > 0.02$. Comparison to the solid state reaction (**Figure 5(b)**), the intensities of the $^3P_0 \rightarrow {}^3H_4$ transition for BaY_2ZnO_5:2mol%Pr phosphor increased by about 6.5 times for sol-gel method. The enhancement in emission intensity is because the activators have more homogeneous contribution in host for the

sol-gel method preparation.

For $BaY_2ZnO_5:Pr^{3+}$ phosphor prepared using the sol-gel method, different concentrations of Pr^{3+} ion-doping has no effect on the wave shape, but did change the emission peaks intensities. The Commission Internationale de I'Eclairage (CIE) color coordinates of the different color tones for $Ba(Y_{1-x}Pr_x)ZnO_5$ phosphors prepared using the sol-gel method that are excited at 311 nm are shown in Figure 6. As the Pr^{3+} ion concentration increasing, the color tone did not change very obviously, and which located around the green light region. It possesses a better color stability for sol-gel method synthesization, because the color tone changes from green to greenish and finally to yellow light region as the Pr^{3+} ion concentrations increasing for solid state reaction preparation.

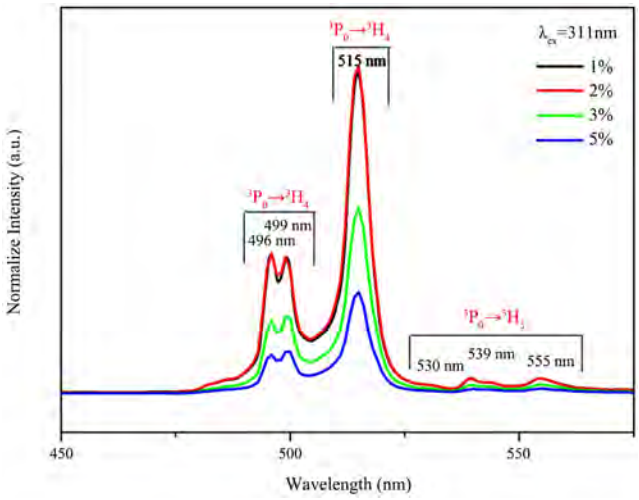

(a)

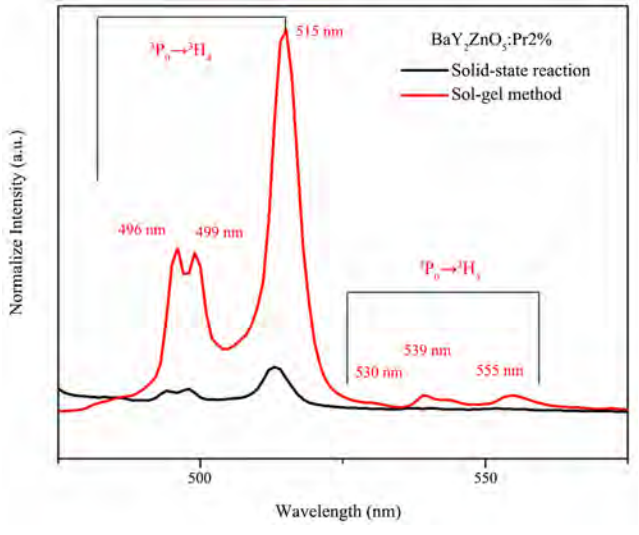

(b)

Figure 5. The emission spectra of BaY_2ZnO_5 doped with different Pr^{3+} ion phosphor prepared using soli-gel method, and (b) the comparison of excitation spectra for BaY_2ZnO_5:2mol%Pr^{3+} phosphor prepared using sol-gel method and solid state reaction.

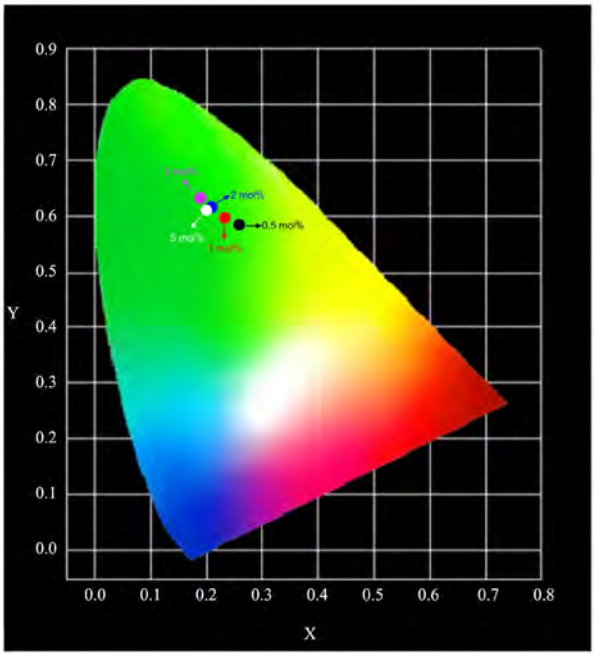

Figure 6. CIE chromaticity diagram for BaY_2ZnO_5 doped with various Pr^{3+} ion concentration.

4. Conclusion

In this study, the orthorhombic structure for Pr^{3+} ion-doped BaY_2ZnO_5 was synthesized successfully using a sol-gel method, and the calcination conditions are lower than that for the conventional ceramics processing. The SEM images show that the BaY_2ZnO_5:Pr^{3+} phosphor particles are aggregational but have an isotropic distribution for 2 mol% Pr^{3+} ions doped. Under an excitation wavelength of 311 nm, the emission bands that appear in the emission spectra are due to the $^3P_0 \rightarrow {}^3H_{4,5,6}$, $^1D_2 \rightarrow {}^3H_4$ and $^3P_0 \rightarrow {}^3F_2$ electron transition of Pr^{3+} ion, and it is the same as that for solid state reaction preparation. The optimum condition for Pr^{3+} ion concentration doped is 2 mol%, and the intensities of the $^3P_0 \rightarrow {}^3H_4$ transition are increased by about 6.5 times for sol-gel method. The enhancement in emission intensity is because the activators have more homogeneous contribution in host for the sol-gel method preparation. In addition, the color tone did not change very obviously, which located around the green light region for Pr^{3+}ion concentrations increasing. The color stability is better for sol-gel method than that for solid state reaction preparation.

Acknowledgements

The authors would like to thank the Ministry of Science and Technology of the Republic of China for financially supporting this project under grant MOST 107-2622-E-150-005-CC3.

Conflicts of Interest

The authors declare no conflicts of interest regarding the publication of this paper.

References

[1] Hsu, W.T., Wu, W.H. and Lu, C.H. (2003) *Materials Science and Engineering*: *B*, **104**, 40-44. https://doi.org/10.1016/S0921-5107(03)00268-X

[2] Mauch, R.H. (1996) *Applied Surface Science*, **92**, 589-597. https://doi.org/10.1016/0169-4332(95)00301-0

[3] Yi, L., Hou, Y., Zhao, H., He, D., Xu, Z., Wang, Y. and Xu, X. (2000) *Displays*, **21**, 147-149. https://doi.org/10.1016/S0141-9382(00)00046-9

[4] Zhao, X., Wang, X., Chen, B., Meng, Q., Di, W., Ren, G. and Yang, Y. (2007) *Journal of Alloys and Compounds*, **433**, 352-355. https://doi.org/10.1016/j.jallcom.2006.06.096

[5] Wakefield, G., Keron, H.A., Dobson, P.J. and Hutchison, J.L. (1999) *Journal of Colloid and Interface Science*, **215**, 179-182. https://doi.org/10.1006/jcis.1999.6225

[6] Jung, H.K., Park, D.S. and Park, Y.C. (1999) *Materials Research Bulletin*, **34**, 43-51. https://doi.org/10.1016/S0025-5408(98)00216-5

[7] Pedrini, C., Bouttet, D., Dujardin, C., Moine, B., Dafinei, I., Lecoq, P., Koselja, M. and Blazek, K. (1994) *Optical Materials*, **3**, 81-88. https://doi.org/10.1016/0925-3467(94)90010-8

[8] Piper, W., DeLuca, J. and Ham, F. (1974) *Journal of Luminescence*, **8**, 344-348. https://doi.org/10.1016/0022-2313(74)90007-6

[9] Sommerdijk, J., Bril, A. and De Jager, A. (1974) *Journal of Luminescence*, **8**, 341-343. https://doi.org/10.1016/0022-2313(74)90006-4

[10] Kaduk, J.A., Wing, N.W., Greenwood, W., Dillingham, J. and Toby, B.H. (1999) *Journal of Research of the National Institute of Standards and Technology*, **104**, 147-171. https://doi.org/10.6028/jres.104.011

[11] Liang, C.H., Chang, Y.C. and Chang, Y.S. (2008) *Applied Physics Letters*, **93**, Article ID: 211902. https://doi.org/10.1063/1.2998299

[12] Liang, C.H., Teoh, L.G., Liu, K.T. and Chang, Y.S. (2012) *Journal of Alloys and Compounds*, **517**, 9-13. https://doi.org/10.1016/j.jallcom.2011.11.088

[13] Shih, H.R. and Chang, Y.S. (2017) *Journal of Electronic Materials*, **46**, 6603-6608. https://doi.org/10.1007/s11664-017-5717-0

[14] Shih, H.R., Tsai, Y.Y., Liu, K.T., Liao, Y.Z. and Chang, Y.S. (2013) *Optical Materials*, **35**, 2654-2657. https://doi.org/10.1016/j.optmat.2013.08.007

[15] Shih, H.R., Tsai, M.T., Chen, H.L., Xiang, Y.X. and Chang, Y.S. (2014) *Materials Research Bulletin*, **55**, 33-37.

[16] Williams, D.K., Bihari, B., Tissue, B.M. and McHale, J.M. (1998) *The Journal of Physical Chemistry B*, **102**, 916-920.

[17] Zhang, J., Zhang, Z., Tang, Z., Lin, Y. and Zheng, Z. (2002) *Journal of Materials Processing Technology*, **121**, 265-268.

[18] Li, Y., Duan, X., Liao, H. and Qian, Y. (1998) *Chemistry of Materials*, **10**, 17-18.

[19] Hirano, M. (2000) *Journal of Materials Chemistry*, **10**, 469-472.

[20] Hirano, M., Imai, M. and Inagaki, M. (2000) *Journal of the American Ceramic Society*, **83**, 977-979. https://doi.org/10.1111/j.1151-2916.2000.tb01310.x

[21] Tas, A.C., Majewski, P.J. and Aldinger, F. (2002) *Journal of Materials Research*, **17**, 1425-1433.

[22] Nedelec, J.M., Mansuy, C. and Mahiou, R. (2003) *Journal of Molecular Structure*, **651-653**, 165-170.

[23] Li, J. and Kuwabara, M. (2003) *Science and Technology of Advanced Materials*, **4**, 143-148.

[24] Hashizume, K., Matsubayashi, M., Vachal, M. and Tani, T. (2002) *Journal of Luminescence*, **98**, 49. https://doi.org/10.1016/S0022-2313(02)00251-X

[25] Liang, C.H., Qi, X.D. and Chang, Y.S. (2010) *Journal of the Electrochemical Society*, **157**, 1169.

[26] Hoefdraad, H.E. and Blasse, G. (1975) *Physica Status Solidi* (*A*), **29**, K95-K97.

[27] Donega, C.D.M., Meijerink, A. and Blasse, G. (1995) *Journal of Physics and Chemistry of Solids*, **56**, 673-685.

[28] Dorenbos, P. (2000) *Journal of Luminescence*, **91**, 91. https://doi.org/10.1016/S0022-2313(00)00197-6

[29] Lin, Y.F., Chang, Y.H., Chang, Y.S., Tsai, B.S. and Li, Y.C. (2006) *Journal of the Electrochemical Society*, **153**, G543.

[30] Raju, G.S.R., Park, J.Y., Jung, H.C., Balarkrishnaiah, R., Moon, B.K. and Jeong, J.H. (2011) *Current Applied Physics*, **11**, S292-S295.

[31] Huang, S.C., Wu, J.K., Hsu, W.J., Chang, H.H., Hung, H.Y., Lin, C.L., Su, H.Y., Bagkar, N., Ke, W.C., Kuo, H.T. and Liu, R.S. (2009) *International Journal of Applied Ceramic Technology*, **6**, 465.

Journal of Modern Physics, 2019, 10, 102-127
http://www.scirp.org/journal/jmp
ISSN Online: 2153-120X
ISSN Print: 2153-1196

A Topological Transformation of Quantum Dynamics

Vu B. Ho

Advanced Study, 9 Adela Court, Mulgrave, Australia
Email: vubho@bigpond.net.au

How to cite this paper: Ho, V.B. (2019) A Topological Transformation of Quantum Dynamics. *Journal of Modern Physics*, **10**, 102-127.
https://doi.org/10.4236/jmp.2019.102009

Received: January 14, 2019
Accepted: February 11, 2019
Published: February 14, 2019

Abstract

In this work, we discuss the topological transformation of quantum dynamics by showing the wave dynamics of a quantum particle on different types of topological structures in various dimensions from the fundamental polygons of the corresponding universal covering spaces. This is not the view from different perspectives of an observer who simply uses different coordinate systems to describe the same physical phenomenon but rather possible geometric and topological structures that quantum particles are endowed with when they are identified with differentiable manifolds that are embedded or immersed in Euclidean spaces of higher dimension. We present our discussions in the form of Bohr model in one, two and three dimensions using linear wave equations. In one dimension, the fundamental polygon is an interval and the universal covering space is the straight line and in this case the standing wave on a finite string is transformed into the standing wave on a circle which can be applied into the Bohr model of the hydrogen atom. In two dimensions, the fundamental polygon is a square and the universal covering space is the plane and in this case, the standing wave on the square is transformed into the standing wave on different surfaces that can be formed by gluing opposite sides of the square, which include a 2-sphere, a 2-torus, a Klein bottle and a projective plane. In three dimensions, the fundamental polygon is a cube and the universal covering space is the three-dimensional Euclidean space. It is shown that a 3-torus and the manifold $K \times S^1$ defined as the product of a Klein bottle and a circle can be constructed by gluing opposite faces of a cube. Therefore, in three-dimensions, the standing wave on a cube is transformed into the standing wave on a 3-torus or on the manifold $K \times S^1$. We also suggest that the mathematical degeneracy may play an important role in quantum dynamics and be associated with the concept of wavefunction collapse in quantum mechanics.

Keywords

Quantum Topology, Topological Transformation, Quantum Dynamics, Differentiable Geometry and Topology, Differentiable Manifolds, Schrödinger Wave Mechanics, Bohr Model in One, Two and Three Dimensions, de Broglie Wave-Particle Duality

1. Introductory Summary

In our previous works on spacetime structures of quantum particles, we showed that quantum particles can be endowed with various geometric and topological structures of differentiable manifolds and classified according to the mathematical structures that are determined by the wavefunctions that are used to express the geometrical objects associated with the quantum particles, such as the Gaussian curvature and the Ricci scalar curvature. We also showed that many physical properties associated with quantum particles can be determined only by the topological structures rather than the geometric structures, such as angular momentum, electric charge and magnetic monopole [1] [2]. These physical entities can be classified according to topological invariants of the corresponding homotopy groups. Therefore, quantum dynamics is also related closely to the topological structures of a quantum particle [3]. By viewing quantum particles as differentiable manifolds, we also discussed their motion by extending the isometric transformations in classical physics to the isometric embedding between smooth manifolds [4]. In mathematics and physics, the motion of physical objects in an ambient space can be described by geometric transformations under which the properties of the configuration of the objects remain unchanged, such as isometric transformations that preserve the distance from a configuration space onto itself. In classical dynamics, the motion of solid objects can be described by the Poincaré group, which is the non-abelian Lie group of Minkowski spacetime isometries [5] [6]. If we consider quantum particles as differentiable manifolds, then we will need to extend the description of the dynamics of quantum particles in classical physics as point-particles to the dynamics of particles as differentiable manifolds in an ambient space. Furthermore, being viewed as differentiable manifolds, quantum particles are assumed to possess internal geometrical and topological structures that in turns possess internal symmetries that give rise to intrinsic dynamics. If quantum particles are assumed to remain as stable structures, then their intrinsic dynamics should be described by smooth isometric transformations, which are smooth isometric embeddings into the spatiotemporal manifold. The smooth isometric embeddings of differentiable manifolds can also be viewed as geometric solitons which are formed by a continuous process of materialising spacetime structures rather than the motion of a solid physical object through space with respect to time as described in classical physics. However, even though it seems reasonable to apply smooth isometric

embeddings into quantum dynamics in which quantum particles are assumed to possess stable geometric structures, such approach will leave out the role played by the topological structures of the differentiable manifolds associated with quantum particles during a dynamical evolution. We may suggest that there should be some kind of internal mechanism that controls the dynamical evolution of the topological structures of a quantum particle responsible for its physical displacement as a differentiable manifold. Such control theories should be rigorously formulated in terms of conformal embeddings, conformal mappings and immersions in differential geometry and topology. In fact, recent developments have shown that unsmooth isometric embeddings can be performed topologically in the sense that these isometric embeddings can change the shape of a physical object without changing its scale. For example, as will be discussed in details in Section 2, the common 2-torus is normally defined as a doughnut-shaped surface embedded in three-dimensional Euclidean space R^3. The 2-torus can be constructed from the fundamental square by identifying opposite sides of the square, and the embedding requires the fundamental square to be stretched in the third spatial dimension therefore distorts distances. Even so, it is shown that isometric embeddings of the square torus into the ambient three-dimensional Euclidean space can also be performed by modifying the standard torus using C^1 regularity of isometric embeddings to construct C^1 fractal structures from an infinite sequence of waves of corrugations [7]. In spite of that, as illustrations, in this work we will only discuss the topological transformations of quantum dynamics by showing the wave dynamics of a quantum particle on different types of topological structures in various dimensions from the fundamental polygons of the corresponding universal covering spaces. We present and illustrate our discussions in the form of Bohr model in one, two and three dimensions. It should be emphasised that these should not be regarded as the view from the different perspectives of an observer who simply uses different coordinate systems to describe the same physical phenomenon but possible geometric and topological structures that quantum particles are endowed with.

At the macroscopic scale where physical objects are observable, the shape of a physical object depends on the conditions of the environment to which the object belongs. In general, physical objects can change their shapes and other physical features to imitate their environments during the process of evolutionary adaptations. The evolutionary adaptations can be represented in terms of mathematics as processes of geometric and topological evolutions. If we adopt the concept of self-similarity from the fractal theory then at the microscopic scale within the domain of quantum particles we may assume that quantum particles may also have the ability to alter their endowed geometric and topological characteristics to adapt to the environments which are assumed to be composed of physical fields. These physical fields manifest themselves as forces to determine the mathematical structures of quantum particles. We will assume that the topological structures of their associated differentiable manifolds also play an

important role in determining the physical structure of a quantum particle and its quantum dynamics. If quantum particles are formed from mass points by contact forces then they may have the ability to change their topological structures to adapt the topological structures of the physical system in which they are part of. For example, if an electron moves in a straight line with a constant speed then it will keep its shape as a particle whose particular geometric and topological structures are stable. However, if it is forced to move in a circle, like moving around the nucleus of a hydrogen atom, then it can turn into the shape of a closed string which vibrates as a standing wave. At each moment of time, the spatial shape of the vibrating string forms a one-dimensional differentiable manifold. Therefore, the geometric and topological processes of evolutionary adaption of quantum particles will determine whether the dynamics is a classical or quantum dynamics. This can be described mathematically as follows. In classical dynamics, the motion of a particle with constant speed in a straight line and the motion of an identical particle with constant speed in a circle are two different dynamical processes that are formulated differently using Newton's second law of motion $m\mathrm{d}^2\boldsymbol{r}/\mathrm{d}t^2 = \boldsymbol{F}$. For the particle that moves in a straight line with constant speed v the acceleration is equal to zero therefore the external net force acting on it is equal to zero. In this case the position x along the straight line is described as $x = vt + x_0$. On the other hand, for the particle which moves in a circle with constant speed v the acceleration a is nonzero and is related to the constant speed v of the motion as $a = v^2/r$. However, these two seemingly distinctive classical dynamics are in fact the same for the case of the electron moving around the nucleus of the Bohr model of a hydrogen atom. To the electron, moving in a circle is also an inertial motion as in the case of moving in a straight line as long as the speed is constant. This problem of dual character of classical and quantum dynamics is probably due to the fact that quantum particles may possess internal geometric and topological structures which may be identified with those of differentiable manifolds. It could be possible that physical laws obeyed by quantum particles are related more closely to the topological structures of a physical system. For example, as will discussed in details later on, even though geometrically the wave dynamics of a quantum particle in a circle is distinctively different from that in a straight line, but topologically they are equivalent because a circle is formed from the fundamental interval of the straight line, which is the universal covering space of the circle. However, in order to give a clearer picture of different geometrical and topological methods that are used to formulate physical laws in physics we now give examples that show how different identifications of physical entities to geometrical objects can lead to different formulations of physical descriptions of the dynamics of classical and quantum mechanics. In physics, classical dynamics describes the motion of physical objects at the macroscopic scale in which the state of motion of an object is determined by the equation of motion which can be derived from the principle of least action. For example, consider a particle moving in a plane under the influ-

ence of a force. The normal acceleration a_n of the particle can be found as $a_n = -v^2/\rho$, where v is the speed of the particle and ρ is the radius of curvature. This result can also be obtained by using the variational principle $\delta S = 0$, where S is defined by $S = \int p\mathrm{d}s = \int p\sqrt{1+\left(\mathrm{d}y/\mathrm{d}x\right)^2}\mathrm{d}x$, with p is the momentum of the particle [8]. This result not only reveals an intrinsic relationship between geometrical methods and the variational principle in classical mechanics but also reaffirms the belief that the principle of least action can also be used to formulate the physical laws in a deterministic manner. However, we showed that this is not the case when the principle of least action is extended into the domain of quantum mechanics. We showed that the identification of the momentum p of a quantum particle with the de Broglie wavelength λ, which in turns is identified with the curvature κ of the path of a particle, *i.e.* $\kappa = 2\pi/\lambda$, leads to an interesting feature; namely the action principle $\delta S = 0$ is satisfied not only by the stationary path corresponding to the classical motion, but also by any path. In this case the Bohr quantum condition possesses a topological character in the sense that the principal quantum number n is identified with the winding number, which is used to represent the fundamental group of paths [9].

The dual character of classical and quantum dynamics of quantum particles that possess internal geometric and topological structures of differentiable manifolds can also be extended to spaces of higher dimension. In Section 4 we will discuss the topological transformation of the two-dimensional wave dynamics in which quantum particles are assumed to be endowed with the geometric and topological structures of differentiable manifolds of closed vibrating surfaces, such as a 2-sphere, a 2-torus, a Klein bottle, or a hemispherical projective plane. These surfaces can be formed from the fundamental squares of the universal covering plane by the process of gluing opposite sides of the square. As shown in our works on the principle of least action [2] [3] [9], we can generalise Feynman's postulate of random path to formulate a quantum theory in which the transition amplitude between states of a quantum mechanical system is a sum over random surfaces, provided the functional P in the action integral $S = \int P\mathrm{d}A$ is taken to be proportional to the Gaussian curvature K of a surface. Consider classes of surfaces which are described by the higher dimensional homotopy groups. As in the case of the fundamental homotopy group of paths, if we choose from among the homotopy class a representative spherical surface, in which case we can write $\oint P\mathrm{d}A = \left(q_e/4\pi\right)\oint K\mathrm{d}A = \left(q_e/4\pi\right)\oint \mathrm{d}\Omega = nq_e$. Also as in Bohr model of the hydrogen atom, we may consider a quantum process in which a physical entity transits from one surface to another with some radiation-like quantum created in the process. Since this kind of physical process can be considered as a transition from one homotopy class to another, the radiation-like quantum may be the result of a change of the topological structure of the physical system, and so it can be regarded as a topological effect. It is also noted that the action integral $\left(q_e/4\pi\right)\oint K\mathrm{d}A$ is identical to Gauss's law in electrodynamics therefore the constant q_e can be identified with the charge of a

particle, which represents the topological structure of a physical system and the charge of a physical system must exist in multiples of q_e. Hence, the charge of a physical system may depend on the topological structure of the system and is classified by the homotopy group of closed surfaces. We want to mention here that in differential geometry the Gaussian curvature K is related to the Ricci scalar curvature R by the relation $R = 2K$, and it has been shown that the Ricci scalar curvature can be identified with the potential of a physical system, therefore our assumption of the existence of a relationship between the Gaussian curvature and the surface density of a physical quantity can be justified [1]. Furthermore, by extending Feynman's method of sum over random surfaces to the temporal dynamics in which the magnetic monopole can also be considered as a topological structure of the temporal continuum then we can establish a relationship between the electric charge q_e and the magnetic monopole q_m associated with a quantum particle, similar to Dirac relation $\hbar c/q_e q_m = 2$ [10]. Let P_T be a 3-dimensional physical entity which will be identified with the surface density of a magnetic substance, such as the magnetic charge of an elementary particle. We therefore assume that an elementary particle is assigned not only with an electric charge q_e but also a magnetic charge q_m. We further assume that the quantity P_T is proportional to the temporal Gaussian curvature K_T. Now, if we consider a surface action integral of the form $S = \int P_T \mathrm{d}A_T = \int (q_m/2\pi) K_T \mathrm{d}A_T = n_T q_m$ then the constant q_m can be identified with the magnetic charge of a particle. In particular, the magnetic charge q_m represents the topological structure of a physical system must exist in multiples of q_m. Hence, the magnetic charge of a physical system, such as an elementary particle, may depend on the topological structure of the system and is classified by the homotopy group of closed surfaces. We now show that it is possible to obtain Dirac relationship between the electric charge q_e and the magnetic charge q_m by considering a spatiotemporal curvature K which is defined as a product of the temporal Gaussian curvature K_T and the spatial Gaussian curvature K_S as $K = K_T \times K_S$. The spatiotemporal submanifold that gives rise to this form of curvature is homeomorphic to $S^2 \times S^2$. If K_T and K_S are independent from each other then we can write $\oint K\mathrm{d}A = \oint K_T \times K_S \mathrm{d}A_T \mathrm{d}A_S = \oint K_T \mathrm{d}A_T \times \oint K_S \mathrm{d}A_S$. If we assume further that $\oint K\mathrm{d}A = k$, where k is an undetermined constant, then we obtain a general relationship between the electric charge q_e and the magnetic charge q_m as $k/q_e q_m = n_S n_T$. In particular, if $n_S = 1$, $n_T = 2$ and $k = \hbar c$, or $n_S = 2$, $n_T = 1$ and $k = \hbar c$, then we recover the relationship obtained by Dirac, $\hbar c/q_e q_m = 2$. We can then extend our discussions into three dimensions even though we also showed that the entire geometric and topological structures of quantum particles are not observable to an observer in the three-dimensional Euclidean space R^3 if they are formulated as three-dimensional differentiable manifolds embedded or immersed in the four-dimensional Euclidean space R^4 [11]. Nonetheless, it is shown that different three-dimensional manifolds, such

as a 3-torus and the $K\times S^1$, which is the product of a Klein bottle and a circle, can be formed by gluing the opposite faces of the fundamental polygon, which is a three-dimensional cube [12], therefore, in Section 5, we will discuss the topological transformation of a three-dimensional wave dynamics in which quantum particles are assumed to be endowed with the geometric and topological structures of differentiable manifolds of a 3-torus or the $K\times S^1$.

Probably, the most prominent feature that emerges from formulating quantum physics in terms of differential geometry and topology is the possibility to express geometric and topological structures of quantum particles by using quantum wavefunctions. We showed that in one dimension, the geometric structure of a 1D differentiable manifold that is represented by the curvature κ can be expressed in terms of a wavefunction ψ as $\kappa=\left(1+\left(\mathrm{d}\psi/\mathrm{d}x\right)^2\right)^{-3/2}\left(\mathrm{d}^2\psi/\mathrm{d}x^2\right)$, and in two dimensions the Ricci scalar curvature R of a 2D differentiable manifold can be expressed in terms of a wavefunction ψ as $R=2\left(\psi_{11}\psi_{22}-\psi_{12}^2\right)^2\Big/\left(1+\psi_1^2+\psi_2^2\right)^2$, where $\psi_\mu=\partial\psi/\partial x^\mu$ and $\psi_{\mu\nu}=\partial^2\psi/\partial x^\mu\partial x^\nu$. However, in three dimensions, despite no direct relationship between the Ricci scalar curvature and the wavefunction that describes a manifold has been established, we have shown that such relationship can be constructed through physical identifications rather than from purely geometrical formulations. For example, we showed that the Ricci scalar curvature that describes the geometrical structure of a quantum particle satisfies the three-dimensional diffusion equation $\partial_t R=k\nabla^2 R$. Solutions to the diffusion equation can be found as $R\left(x,y,z,t\right)=\left(M\Big/\left(\sqrt{4\pi kt}\right)^3\right)\mathrm{e}^{-\left(x^2+y^2+z^2\right)/4kt}$, which determines the probabilistic distribution of an amount of geometrical substance M which manifests as observable matter. As shown in appendix 1, if a pseudo-Euclidean metric is defined in the form $\mathrm{d}s^2=Dc^2\mathrm{d}t^2-A\left(x,y,z,t\right)\left(\mathrm{d}x^2+\mathrm{d}y^2+\mathrm{d}z^2\right)$, where D is constant, then the quantity $A\left(x,y,z,t\right)$ can be determined [1]. However, for quantum particles that are endowed with the geometric and topological structures of differentiable manifolds, it would be more suitable to consider Bianchi manifolds with a metric which has separate scale factors given by the line element $\mathrm{d}s^2=Dc^2\mathrm{d}t^2-a_1\left(t\right)^2\mathrm{d}x^2-a_2\left(t\right)^2\mathrm{d}y^2-a_3\left(t\right)^2\mathrm{d}z^2$. Spaces with this form of metric are homogeneous but not generally isotropic therefore quantum particles with this metric will change its volume and shape. The deformation is determined by the shear constructed from the scale factors $a_i\left(t\right)$ [13]. On the other hand, we have also shown that the Ricci scalar curvature that describes the geometrical structures of a quantum particle can also be constructed from Schrödinger wavefunctions in wave mechanics. As shown in appendix 2, the relationship between the Schrödinger wavefunction ψ and the Ricci scalar curvature R can be established as

$$R=\left(\sum_{\mu=1}^3\left(\mathrm{d}x^\mu/\mathrm{d}t\right)^2-\hbar\left(\partial_t\psi+\sum_{\mu=1}^3\partial_\mu\psi\left(\mathrm{d}x^\mu/\mathrm{d}t\right)\right)/m\psi\right)\Big/k.$$

The purpose of this work is to discuss the topological transformation of quantum dynamics by showing the wave dynamics of a quantum particle on dif-

ferent types of topological structures in various dimensions from the fundamental polygons of the corresponding universal covering spaces. Therefore, the topological structures of differentiable manifolds that are associated with quantum particles will hold a dominant role in our discussions. This in fact is a common feature of natural existence not only at the microscopic scale of quantum particles that we assume in this work but also at any scale. A more complete formulation of the dynamics of quantum particles would be a wave dynamics on geometries whose mathematical structures can be classified according to the uniformisation theorem and Thurston geometrisation conjecture. In two dimensions, there are three geometries, which are Euclidean E^2, spherical S^2 and hyperbolic H^2. In three dimensions, Thurston geometrisation conjecture states that every closed three-dimensional manifold can be decomposed into submanifolds which can be constructed from eight types of geometric structures, which are spherical geometry S^3, Euclidean geometry E^3, hyperbolic geometry H^3, the geometry of $S^2 \times R$, the geometry of $H^2 \times R$, the geometry of the universal cover of $SL(2,R)$, Nil geometry, and Solv geometry [14] [15]. And a rigorous treatment of the wave dynamics on these geometries would be geometric wave equations on differentiable manifolds, in particular, linear wave equations on Lorentzian manifolds [16]. However, for the purpose of physical illustration, we will follow a modest approach in which we will present our discussions in the form of Bohr model in one, two and three dimensions using linear wave equations. In one dimension, the fundamental polygon is an interval and the universal covering space is the straight line and in this case the standing wave on a finite string is transformed into the standing wave on a circle which can be applied into the Bohr model of the hydrogen atom. The wave dynamics on a circle can also be described in terms of projective geometry. Since a circle is a 1-sphere which is also a 1-torus therefore the Bohr model of the hydrogen atom can also be viewed as a standing wave on a 1-torus. In two dimensions, the fundamental polygon is a square and the universal covering space is the plane and in this case the standing wave on the square is transformed into the standing wave on different surfaces that can be formed by gluing opposite sides of the square, which include a 2-sphere, a 2-torus, a Klein bottle and a projective plane. We will show when the wave dynamics on a projective plane is described in terms of projective geometry then it is identical to the wave dynamics on a 2-sphere. In three dimensions, the fundamental polygon is a cube and the universal covering space is the three-dimensional Euclidean space. It is shown that a 3-torus and the manifold $K \times S^1$ defined as the product of a Klein bottle and a circle can be constructed by gluing opposite faces of a cube therefore in three-dimensions the standing wave on a cube is transformed into the standing wave on a 3-torus or on the manifold $K \times S^1$. We also discuss a transformation of a stationary wave on the fundamental cube into a stationary wave on a 3-sphere despite it still remains unknown whether a 3-sphere can be constructed directly from a cube by gluing its opposite faces. In spite of this uncertainty, however, we speculate that

mathematical degeneracy in which an element of a class of objects degenerates into an element of a different but simpler class may play an important role in quantum dynamics. For example, a 2-sphere is a degenerate 2-torus when the axis of revolution passes through the centre of the generating circle. Therefore, it seems reasonable to assume that if an n-torus degenerates into an n-sphere then wavefunctions on an n-torus may also be degenerated into wavefunctions on an n-sphere. Furthermore, since an n-sphere can degenerate itself into a single point, therefore the mathematical degeneracy may be related to the concept of wavefunction collapse in quantum mechanics where the classical observables such as position and momentum can only be obtained from the collapse of the associated wavefunctions for physical measurements. This consideration suggests that quantum particles associated with differentiable manifolds may possess the more stable mathematical structures of an n-torus rather than those of an n-sphere, therefore, also as a brief investigation into different methods of embeddings of differentiable manifolds in Euclidean spaces, in the next section we will examine the geometric and topological structures of the familiar 2-torus and how it can be isometrically embedded in the ambient three-dimensional Euclidean space R^3.

2. On the Geometric and Topological Structures and the Isometric Embeddings of a 2-Torus

In geometry, when a circle revolves about an axis which does not touch the circle in the three-dimensional Euclidean space R^3 then it generates the surface of revolution of a 2-torus, as shown in the following Figure 1.

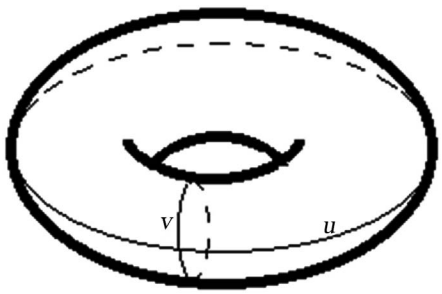

Figure 1. The surface of revolution of a 2-torus.

On the other hand, in topology, a torus can also be defined as the Cartesian product of two circles $S^1 \times S^1$. The homeomorphism between a ring torus and the Cartesian product of two circles leads to an important feature about the embedding of the 2-torus into a higher dimensional Euclidean space. Normally, a 2-torus is simply viewed as a doughnut-shaped surface embedded in three-dimensional Euclidean space R^3. However, if a 2-torus is defined as the Cartesian product $S^1 \times S^1$, called Clifford torus, then since each circle is embedded in a two-dimensional Euclidean space R^2 therefore the product space is a four-dimensional Euclidean space R^4. As a consequence, the embedding of

the Clifford torus in four-dimensional Euclidean space R^4 is symmetric and isometric but the embedding of the 2-torus in three-dimensional Euclidean space R^3 is asymmetric and non-isometric [17]. The difference can be specified by using the Gaussian curvature as follows [18]. In the three-dimensional Euclidean space R^3, the parametric equations for a doughnut-shaped torus given in terms of the parameters (u,v) as $x=(c+a\cos v)\cos u$, $y=(c+a\cos v)\sin u$, $z=a\sin v$, where a is the radius of the tube and c is the radius from the centre of the torus to the centre of the tube, and $u,v\in[0,2\pi)$. The line element can then be found as $\mathrm{d}s^2=(c+a\cos v)^2\,\mathrm{d}u^2+a^2\mathrm{d}v^2$. From this line element the Gaussian curvature can be found as $K=\cos v/a(c+a\cos v)$. The ring torus corresponds to $c>a$ for which $K>0$ for the outer region of the torus and $K<0$ for the inner region. On the other hand, the Clifford torus is a flat square torus which is isometric to the fundamental square whose opposite sides are identified as shown below **Figure 2**.

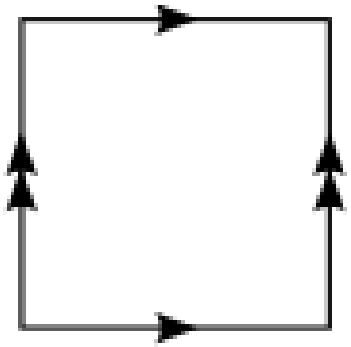

Figure 2. The fundamental square of the Clifford torus.

The isometric embedding of the Clifford torus in the four-dimensional Euclidean space R^4 shows that it is flat and obeys the Euclidean geometry. Then it had emerged the interesting question whether it is possible to isometrically embed the flat 2-torus in three-dimensional Euclidean space R^3. Remarkably, the Nash embedding theorem in topology states that such isometric embedding is possible [19] [20] [21]. It has also been shown that isometric embeddings of the square flat torus into the ambient three-dimensional Euclidean space R^3 can be performed by modifying the standard torus using C^1 regularity of isometric embeddings to construct C^1 fractal structures from an infinite sequence of waves of corrugations. By implementing the Convex Integration Theory, it is possible to visualise isometric embeddings of a flat torus into the ambient three-dimensional Euclidean space R^3. In general, in order to evaluate the curvature at every point of a surface it is required that the surface must be of class C^2. For the case of the flat 2-torus, since the curvature is vanished at every point of the surface therefore it cannot be isometrically embedded with C^2 regularity. However, this does not prevent its isometric embeddings into the three-dimensional Euclidean space R^3 if the embeddings belong to the class C^1, and there are infinitely many such isometric embeddings [7]. Another im-

portant development involving fractals that we want to mention here is the study of fractal solutions of linear and nonlinear dispersive partial differential equations on the torus, in particular, fractal solutions of linear and nonlinear Schrödinger wave equations [22]. Fractal images are visual representations of fractal spaces that can also be determined by a system of differential equations that exhibit chaotic dynamics [23] [24]. However, the purpose of this work is to discuss the topological transformation of quantum dynamics of quantum particles therefore in the following we will focus only on linear wave equations on different topological structures that can be formed from the fundamental polygons of their corresponding universal covering spaces in one, two, and three dimensions.

3. Geometric and Topological Transformation of Bohr Model of the Hydrogen Atom

In order to successfully construct a model for the hydrogen atom which predicts correctly the spectrum of the energy radiated from the atom, Bohr proposed three postulates which state that the centripetal force required for the electron to orbit the nucleus in a stable circle is the Coulomb force $mv^2/r = kq^2/r^2$, the permissible orbits are those that satisfy the condition that the angular momentum of the electron equals $n\hbar$, that is $mvr = n\hbar$, and when the electron moves in one of the stable orbits it does not radiate, however, it will radiate when it makes a transition between the stable orbits [25]. On the other hand, in his work on the concept of matter wave, de Broglie proposed that an electron has both a wave and a particle nature by regarding the electron as a standing wave around the circumference of an orbit, as shown in the following **Figure 3** [26].

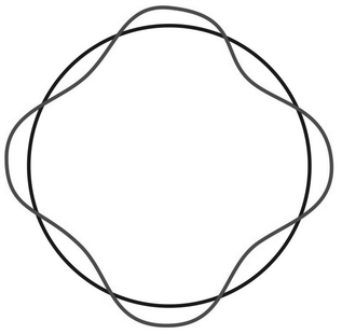

Figure 3. A standing wave around the circumference of a circle.

It is seen that de Broglie's requirement leads to the wave condition $2\pi r = n\lambda$. This is equivalent to assuming that the standing wave around a circle, which is a 1-sphere, is similar to a standing wave on the fundamental interval of a straight line R which is the universal covering space of the circle S^1, where the translations taking the interval to the next images will generate the holonomy group [27]. In mathematics, the circle of radius r is normally considered as a 1-sphere defined by the relation $S^1 = \left\{x \in R^2 : |x| = r\right\}$. In fact, the circle is also classified

as a 1-torus T^1 which is a topological space equivalent to the quotient space R/Z, therefore, when the fundamental polygon of the universal covering space R is transformed into a circle we actually also transformed it into a 1-torus T^1. Since there is no difference between the topological structures of the 1-sphere S^1 and the 1-torus T^1, the transformation of quantum dynamics from the fundamental polygon into both of them is the same, but as expected, we will show in the next two sections that in higher dimensions this is not the case. Consider a standing wave on a string defined in the domain $D=\{0<x<L\}$ that satisfies the wave equation

$$\frac{1}{c^2}\frac{\partial^2\psi}{\partial t^2}-\frac{\partial^2\psi}{\partial x^2}=0 \tag{1}$$

with the boundary conditions $\psi(0,t)=0$, $\psi(L,t)=0$ and initial conditions $\psi(x,0)=f(x)$, $\partial\psi/\partial t(x,0)=g(x)$. The general solution to the wave equation given in Equation (1) can be found as [28]

$$\psi(x,t)=\sum_{n=1}^{\infty}\left(A_n\cos\frac{n\pi ct}{L}+B_n\sin\frac{n\pi ct}{L}\right)\sin\frac{n\pi x}{L} \tag{2}$$

where

$$A_n=\frac{2}{L}\int_0^L f(x)\sin\frac{n\pi x}{L}\mathrm{d}x,\quad B_n=\frac{2}{cn\pi}\int_0^L g(x)\sin\frac{n\pi x}{L}\mathrm{d}x \tag{3}$$

Now imagine we convert the finite string into a circle with a radius R where the end points $x=0$ and $x=L$ are joined so that $2\pi R=L$. In order to describe a standing wave on the circle we first consider a two-dimensional wave equation

$$\frac{1}{c^2}\frac{\partial^2\psi}{\partial t^2}-\frac{\partial^2\psi}{\partial x^2}-\frac{\partial^2\psi}{\partial y^2}=0 \tag{4}$$

Using the relationship between the polar coordinates (r,θ) and the Cartesian coordinates (x,y) defined by the relations $x=r\cos\theta$, $y=r\sin\theta$, the two-dimensional wave equation given in Equation (4) is rewritten in the form

$$\frac{1}{c^2}\frac{\partial^2\psi}{\partial t^2}-\frac{\partial^2\psi}{\partial r^2}-\frac{1}{r}\frac{\partial\psi}{\partial r}-\frac{1}{r^2}\frac{\partial^2\psi}{\partial\theta^2}=0 \tag{5}$$

Using the method of separation, solutions to the wave equation given in Equation (5) can be expressed in the form $\psi=R(r)\Theta(\theta)T(t)$, then we obtain

$$\frac{1}{c^2}\frac{1}{T}\frac{\mathrm{d}^2T}{\mathrm{d}t^2}-\frac{1}{R}\frac{\mathrm{d}^2R}{\mathrm{d}r^2}-\frac{1}{r}\frac{1}{R}\frac{\mathrm{d}R}{\mathrm{d}r}-\frac{1}{r^2}\frac{\mathrm{d}^2\Theta}{\mathrm{d}\theta^2}=0 \tag{6}$$

If we consider the wave motion only on the circle of constant radius $r=R$ then the wave equation given in Equation (6) reduces to two separate ordinary differential equations

$$\frac{\mathrm{d}^2T}{\mathrm{d}t^2}+c^2\beta^2T=0,\quad \frac{\mathrm{d}^2\Theta}{\mathrm{d}\theta^2}+R^2\beta^2\Theta=0 \tag{7}$$

Solutions to the equations given in Equation (7) can be found as

$$T(t) = A\cos\beta ct + B\sin\beta ct, \quad \Theta(\theta) = C\cos\beta R\theta + B\sin\beta R\theta \tag{8}$$

Using the conditions $\Theta(0) = 0$ and $\Theta(2\pi) = 0$, we obtain $C = 0$ and $\beta = n/2R$. Therefore, $\Theta_n(\theta) = \sin(n\theta/2)$ and the general solutions are given as

$$\psi(\theta,t) = \sum_{n=1}^{\infty}\left(A_n\cos\frac{nct}{2R} + B_n\sin\frac{nct}{2R}\right)\sin\frac{n\theta}{2} \tag{9}$$

In fact, the resulting wavefunction $\psi(\theta,t)$ in Equation (9) can be obtained directly from Equation (2) by replacing $x = R\theta$ with the condition $2\pi R = L$. It is also interesting to note that the wavefunction $\psi(\theta,t)$ given in Equation (9) can also be considered as a wavefunction on a projective elliptic geometry in which the points of an n-dimensional projective space are identified with the lines that go through the origin of the $(n + 1)$-dimensional space and are represented by vectors in the $(n + 1)$-dimensional Euclidean space R^{n+1}. The distance between two points in a projective space can be defined using the metric that specifies the angle between two vectors $\boldsymbol{u}$ and $\boldsymbol{v}$ as $d(\boldsymbol{u},\boldsymbol{v}) = \cot^{-1}\left(|\boldsymbol{u}\cdot\boldsymbol{v}|/|\boldsymbol{u}||\boldsymbol{v}|\right)$ [29].

It is also worth mentioning here that the energy spectrum of the Bohr model can be determined if we apply de Broglie wavelength λ defined in terms of the momentum of a quantum particle as $\lambda = h/mv$. Using the wavelength given by the relation $2\pi R = n\lambda$ we obtain $h/mv = 2\pi R/n$, and this leads to the Bohr's postulate of the quantisation of angular momentum $mvR = n\hbar$. Using this relationship and the Coulomb's law $mv^2/R = kq^2/R^2$ then we obtain the expression for the radius of the nth stationary orbit as $R_n = n^2\hbar^2/mkq^2$. Then the energy spectrum E_n can be calculated as follows

$$E_n = T + V = \frac{mv^2}{2} - \frac{kq^2}{R} = -\frac{kq^2}{2R} = -\frac{mk^2q^4}{2\hbar^2n^2} \tag{10}$$

where R now is the radius of the nth stationary orbit.

4. Geometric and Topological Transformation of a Two-Dimensional Wave Dynamics

In this section we will extend the discussion in Section 3 by considering the transformation of a standing wave on a fundamental square of the universal covering plane R^2 into a standing wave on a 2-dimensional surface which is formed by identifying and gluing the opposite edges of the square. This may be seen as an extension of the Bohr model of the hydrogen atom from one-dimensional manifolds of the 1-sphere and 1-torus embedded in the ambient two-dimensional Euclidean space R^2 into two-dimensional manifolds embedded or immersed in the ambient three-dimensional Euclidean space R^3. As shown in **Figure 4** below, different types of two-dimensional manifolds can be formed by the process of identifying and gluing the opposite pair of the edges a square, including the surfaces of a 2-sphere S^2, a 2-torus T^2, a Klein bottle K^2, and a projective plane P^2 [17].

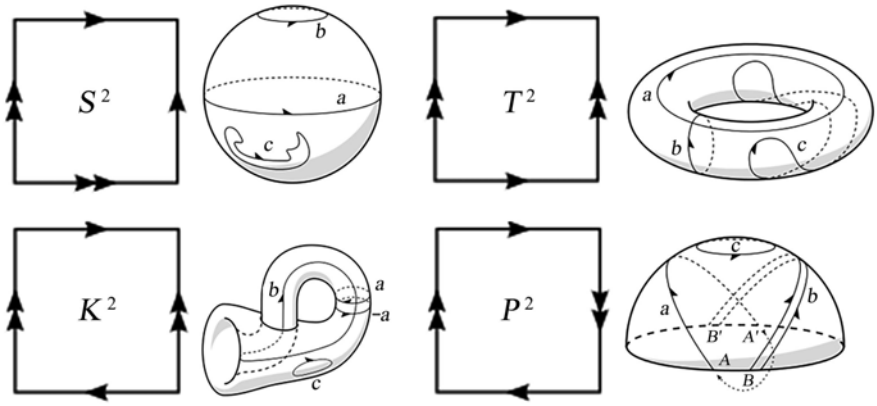

Figure 4. A 2-sphere, a 2-torus, a Klein bottle, a projective plane, and their corresponding fundamental squares.

Each of the four manifolds has a particular fundamental polygon depending on how the edges are identified. However, the universal covering space for all of them is the two-dimensional Euclidean space R^2 where the translations taking the square to the next images will also generate the holonomy group [27]. As in the case of the Bohr model of the hydrogen atom in which the electron is assumed to move in stationary circular orbits, an extended Bohr model on surfaces such as a 2-sphere is similar to Schrödinger wave mechanics in spherical coordinates therefore a moving electron on the surface of a 2-sphere also does not radiate and is described as a standing wave. Therefore we may assume that a standing wave in the universal covering space R^2 can also be transformed into a standing wave on one of the four curved surfaces that can be formed from the fundamental squares as shown above. Consider the standing wave on a square in the domain $D=\{0<x<L, 0<y<L\}$ that satisfies the two-dimensional wave equation given in Equation (4) with the boundary conditions $\psi(0,y,t)=0$, $\psi(L,y,t)=0$, $\psi(x,0,t)=0$, $\psi(x,L,t)=0$ and initial conditions $\psi(x,y,0)=f(x,y)$, $\partial\psi/\partial t(x,y,0)=g(x,y)$. Then the general solution can be found as

$$\psi(x,y,t)=\sum_{n=1}^{\infty}\sum_{m=1}^{\infty}\left(A_{mn}\cos\lambda_{mn}t+B_{mn}\sin\lambda_{mn}t\right)\sin\frac{m\pi x}{L}\sin\frac{n\pi y}{L} \tag{11}$$

where $\lambda_{mn}=(c\pi/L)\sqrt{m^2+n^2}$, and the coefficients A_{mn} and B_{mn} are given as

$$\begin{aligned} A_{mn}&=\frac{4}{L^2}\int_0^L\int_0^L f(x,y)\sin\frac{m\pi x}{L}\sin\frac{n\pi y}{L}\mathrm{d}x\mathrm{d}y,\\ B_{mn}&=\frac{4}{L^2\lambda_{mn}}\int_0^L\int_0^L g(x,y)\sin\frac{m\pi x}{L}\sin\frac{n\pi y}{L}\mathrm{d}x\mathrm{d}y \end{aligned} \tag{12}$$

The standing wave described by the function $\psi(x,y,t)$ given in Equation (11) is restricted to the fundamental polygon of the universal covering space R^2. Following the Bohr model of the hydrogen atom in which standing waves on circular orbits are topologically equivalent to standing waves on the fundamental interval of the universal covering line, now we consider the transformation of a standing wave on the fundamental squares into a standing wave on the four cor-

responding surfaces of a 2-sphere S^2, a 2-torus T^2, a Klein bottle K^2 and a projective plane P^2. In order to describe a standing wave on the transformed surfaces from the fundamental squares, we consider a three-dimensional wave equation given in Cartesian coordinates (x,y,z) of the form

$$\frac{1}{c^2}\frac{\partial^2\psi}{\partial t^2}-\frac{\partial^2\psi}{\partial x^2}-\frac{\partial^2\psi}{\partial y^2}-\frac{\partial^2\psi}{\partial z^2}=0 \tag{13}$$

First, consider a standing wave on the surface of a 2-torus. In differential geometry, the relationship between the Cartesian coordinates (x,y,z) and the toroidal coordinates (ξ,η,φ) is given as follows [30] [31]

$$x=\frac{a\sinh\eta\cos\varphi}{\cosh\eta-\cos\xi},\quad y=\frac{a\sinh\eta\sin\varphi}{\cosh\eta-\cos\xi},\quad z=\frac{a\sin\xi}{\cosh\eta-\cos\xi} \tag{14}$$

where the domains of the toroidal coordinates are given as $0\le\xi<2\pi$, $0\le\eta<\infty$, and $0\le\varphi<2\pi$. From the relations given in Equation (14), it can be shown that surfaces of constant $\xi=\xi_0$ correspond to 2-spheres given by the equation $x^2+y^2+\left(z-a\cot\xi_0\right)^2=a^2/\sin^2\xi_0$, and surfaces of constant $\eta=\eta_0$ correspond to 2-tori given by the equation $z^2+\left(\sqrt{x^2+y^2}-a\coth\eta_0\right)^2=a^2/\sinh^2\eta_0$. Then in terms of the toroidal coordinates (ξ,η,φ), the three-dimensional wave equation given in Equation (13) can be rewritten as

$$\begin{aligned}&\frac{1}{c^2}\frac{\partial^2\psi}{\partial t^2}-\frac{\left(\cosh\eta-\cos\xi\right)^3}{a^2\sinh\eta}\left(\frac{\partial}{\partial\xi}\left(\frac{\sinh\eta}{\cosh\eta-\cos\xi}\frac{\partial\psi}{\partial\xi}\right)\right.\\&\left.+\frac{\partial}{\partial\eta}\left(\frac{\sinh\eta}{\cosh\eta-\cos\xi}\frac{\partial\psi}{\partial\eta}\right)+\frac{\partial}{\partial\varphi}\left(\frac{1}{\sinh\eta\left(\cosh\eta-\cos\xi\right)}\frac{\partial\psi}{\partial\varphi}\right)\right)=0\end{aligned} \tag{15}$$

where $\sinh x$ and $\cosh x$ are hyperbolic functions. Solutions to Equation (15) can be found by separating the variables of the form $\psi(\xi,\eta,\varphi,t)=\sqrt{\cosh\xi-\cos\eta}U(\xi)H(\eta)\Phi(\varphi)T(t)$ and then dividing the result by $\left(\cosh\xi-\cos\eta\right)^{5/2}U(\xi)H(\eta)\Phi(\varphi)T(t)/\sinh^2\xi$. In this case Equation (15) reduces to the form

$$\begin{aligned}&\frac{\sinh^2\xi}{c^2\left(\cosh\xi-\cos\eta\right)^3}\frac{\mathrm{d}^2T}{\mathrm{d}t^2}-\frac{1}{4}\sinh^2\xi-\cosh\xi\sinh\xi\frac{1}{U}\frac{\mathrm{d}U}{\mathrm{d}\xi}\\&-\sinh^2\xi\frac{1}{U}\frac{\mathrm{d}^2U}{\mathrm{d}\xi^2}-\sinh^2\xi\frac{1}{H}\frac{\mathrm{d}^2H}{\mathrm{d}^2\eta}-\frac{1}{\Phi}\frac{\mathrm{d}^2\Phi}{\mathrm{d}\varphi^2}=0\end{aligned} \tag{16}$$

If we consider standing waves only on the surfaces of the toroids which are defined by setting the variable η equal to a constant, $\eta=\eta_0$, then Equation (16) becomes

$$\begin{aligned}&\frac{\sinh^2\xi}{c^2\left(\cosh\xi-\cos\eta_0\right)^3}\frac{1}{T}\frac{\mathrm{d}^2T}{\mathrm{d}t^2}-\frac{1}{4}\sinh^2\xi-\cosh\xi\sinh\xi\frac{1}{U}\frac{\mathrm{d}U}{\mathrm{d}\xi}\\&-\sinh^2\xi\frac{1}{U}\frac{\mathrm{d}^2U}{\mathrm{d}\xi^2}-\frac{1}{\Phi}\frac{\mathrm{d}^2\Phi}{\mathrm{d}\varphi^2}=0\end{aligned} \tag{17}$$

By separating the functions in Equation (17), we obtain the following system

of ordinary differential equations

$$\frac{\mathrm{d}^2T}{c^2\mathrm{d}t^2}+k^2T=0 \tag{18}$$

$$\frac{\mathrm{d}^2\Phi}{\mathrm{d}\varphi^2}+m^2\Phi=0 \tag{19}$$

$$\frac{\mathrm{d}^2U}{\mathrm{d}\xi^2}+\coth\xi\frac{\mathrm{d}U}{\mathrm{d}\xi}-\left(\frac{m^2}{\sinh^2\xi}-\frac{k^2}{\left(\cosh\xi-\cos\eta_0\right)^3}-\frac{1}{4}\right)U=0 \tag{20}$$

It is seen from Equations (18-20) that time-independent geometric structures of the extended Bohr model of the hydrogen atom on the surface of a 2-torus can be described by toroidal functions. It is also seen from Equation (18) that if the time dependence of the wave equation is given of the form $\exp\left(-i\omega t\right)$, where $\omega=ck$, then the wave equation reduces to the Helmholtz equation $\nabla^2\psi=\kappa^2\psi$. It has been shown that solutions to the Helmholtz equation in the toroidal coordinates can be obtained in terms of series representation of the associated Legendre function [32] [33]. It is also noted that a standing wave on the surface of a 2-sphere given by the equation $x^2+y^2+\left(z-a\cot\xi_0\right)^2=a^2/\sin^2\xi_0$ can also be obtained from Equation (16) by setting the variable ξ equal to a constant, $\xi=\xi_0$. However, it is more convenient if we follow the common practice using spherical coordinates $\left(r,\theta,\phi\right)$ which are related to the Cartesian coordinates $\left(x,y,z\right)$ as $x=r\sin\theta\cos\phi$, $y=r\sin\theta\sin\phi$, $z=r\cos\theta$. In spherical coordinates $\left(r,\theta,\phi\right)$ the wave equation given in Equation (13) takes the form

$$\frac{1}{c^2}\frac{\partial^2\psi}{\partial t^2}-\frac{\partial^2\psi}{\partial r^2}-\frac{2}{r}\frac{\partial\psi}{\partial r}-\frac{1}{r^2\sin\theta}\frac{\partial}{\partial\theta}\left(\sin\theta\frac{\partial\psi}{\partial\theta}\right)-\frac{1}{r^2\sin^2\theta}\frac{\partial^2\psi}{\partial\phi^2}=0 \tag{21}$$

Solutions to Equation (21) can be found by separating the variables of the form $\psi\left(r,\theta,\phi,t\right)=R\left(r\right)\Theta\left(\theta\right)\Phi\left(\phi\right)T\left(t\right)$. However, if we consider the wave dynamics only on the surface of constant radius $r=R$ then the wavefunction can be written in the form $\psi\left(\theta,\phi,t\right)=\Theta\left(\theta\right)\Phi\left(\phi\right)T\left(t\right)$ and the wave equation given in Equation (21) reduces to the following system of ordinary differential equations

$$\frac{1}{c^2}\frac{\mathrm{d}^2T}{\mathrm{d}t^2}+k^2T=0 \tag{22}$$

$$\frac{\mathrm{d}^2\Phi}{\mathrm{d}\phi^2}+m^2\Phi=0 \tag{23}$$

$$\frac{1}{\sin\theta}\frac{d}{d\theta}\left(\sin\theta\frac{\mathrm{d}\Theta}{\mathrm{d}\theta}\right)+\left(k^2R^2-\frac{m^2}{\sin^2\theta}\right)\Theta=0 \tag{24}$$

It should be mentioned here that the 2-sphere S^2 with the constant radius $r=R$ is a spherical membrane which is assumed to vibrate therefore the wavefunction $\psi\left(R,\theta,\phi,t\right)$ actually represents the height of the mass points that form the spherical membrane by contact forces. If we let $k^2R^2=l\left(l+1\right)$ and $\omega=ck$ then general solutions can be found as

$$\psi(\theta,\phi,t)=\sum_{l=0}^{\infty}\sum_{m=-l}^{l}\left(A_{ml}\cos\omega t+B_{ml}\sin\omega t\right)P_l^m(\cos\theta)\mathrm{e}^{im\phi} \tag{25}$$

The combination $P_l^m(\cos\theta)\mathrm{e}^{im\phi}$ becomes the spherical harmonics $Y_l^m(\theta,\phi)$ when it is normalised. We have shown that a standing wave on the fundamental squares in the universal covering space R^2 can be transformed into a standing wave on a 2-torus or a 2-sphere, respectively. Now, since the 2-dimensional Euclidean space R^2 is also the universal covering space of the Klein bottle K^2 and the projective plane P^2 therefore we can also discuss the possibility to transform a standing wave on their fundamental squares into a standing wave on either of these surfaces. A transformed wave dynamics can be achieved if parametric equations for these two surfaces can be established. For example, the immersion of the Klein bottle in the three-dimensional Euclidean space R^3 is given by the implicit equation $\left(x^2+y^2+z^2+2y-1\right)\left(\left(x^2+y^2+z^2-2y-1\right)^2-8z^2\right)+16xz\left(x^2+y^2+z^2-2y-1\right)=0$, and the parametric equations for the immersion of the Klein bottle are given as

$$x=\left(r+\cos\frac{u}{2}\sin v-\sin\frac{u}{2}\sin 2v\right)\cos u \tag{26}$$

$$y=\left(r+\cos\frac{u}{2}\sin v-\sin\frac{u}{2}\sin 2v\right)\sin u \tag{27}$$

$$z=\sin\frac{u}{2}\sin v+\cos\frac{u}{2}\sin 2v \tag{28}$$

where $u,v\in[0,2\pi)$ and $r>2$. The parameter r is the radius of the self-intersecting circle in the (x,y)-plane, the parameter u gives the angle in the (x,y)-plane, and the parameter v specifies the position of the cross section [34] [35]. Using the parametric equations of the Klein bottle given in Equations (26-28), the wave equation on the fundamental square can be transformed into the wave equation on the surface of the Klein bottle. In general, it is shown in differential geometry that if a metric of the form $\mathrm{d}s^2=g_{\alpha\beta}\mathrm{d}x^\alpha\mathrm{d}x^\beta$ can be established on any surface then the Laplacian $\nabla^2\psi$ of a scalar function ψ can be written in the form $\nabla^2\psi=\left(1/\sqrt{g}\right)\partial\left(\sqrt{g}g^{\alpha\beta}\,\partial\psi/\partial x^\beta\right)/\partial x^\alpha$ [36]. Despite the fact that the spherical metric with spherical coordinates (r,θ,ϕ) is obtained from the line element $\mathrm{d}s^2=\mathrm{d}r^2+r^2\mathrm{d}\theta^2+r^2\sin^2\theta\mathrm{d}\phi^2$, and the toroidal metric with toroidal coordinates (u,v,θ) is obtained from the line element $\mathrm{d}s^2=\left(a^2/(\cosh u-\cos v)^2\right)\left(\mathrm{d}u^2+\mathrm{d}v^2+\sinh^2 u\mathrm{d}\theta^2\right)$, however, metrics on the Klein bottle and the projective plane are problems that are being investigated. For example, a metric of revolution g_0 for the first eigenvalue on a Klein bottle can be constructed as [37]

$$g_0=\frac{9+\left(1+8\cos^2 v\right)^2}{1+8\cos^2 v}\left(\mathrm{d}u^2+\frac{\mathrm{d}v^2}{1+8\cos^2 v}\right) \tag{29}$$

A more complicated metric on a Klein bottle can also be constructed, for ex-

ample, in the work from the reference [38]. Even though there is no particular metric that has been established for the surface of the projective plane, we know that it can be represented as the set of all straight lines that pass through the origin and has the structure of a compact surface, as shown in the following **Figure 5** [39].

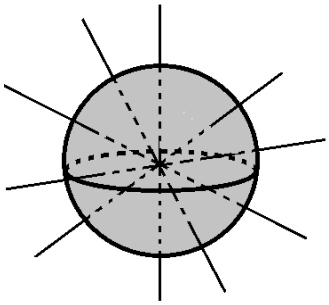

Figure 5. Straight lines representing a projective plane.

Therefore, if the distance between two points in the projective space that immerses in the three-dimensional Euclidean space R^3 can be defined using the metric that specifies the angle between two vectors $\boldsymbol{u}$ and $\boldsymbol{v}$ as $d(\boldsymbol{u},\boldsymbol{v}) = \cot^{-1}\left(|\boldsymbol{u}\cdot\boldsymbol{v}|/|\boldsymbol{u}||\boldsymbol{v}|\right)$ then even though they have different geometric natures standing waves on the projective plane can also be described by the solutions given in Equation (25) for standing waves on the surface of a 2-sphere.

5. Geometric and Topological Transformation of a Three-Dimensional Wave Dynamics

In this section we extend further the discussions on the transformations of wave dynamics from a standing wave on fundamental cubes to a standing wave on three-dimensional manifolds that can be formed from the fundamental cubes by the process of gluing opposite surfaces of the cube. This can also be seen as an extension of the Bohr model of the hydrogen atom from a one-dimensional manifold embedded in the ambient two-dimensional Euclidean space R^2 into three-dimensional manifolds embedded or immersed in four-dimensional Euclidean space R^4. As shown in **Figure 6** below, a 3-torus can be constructed by identifying the opposite faces of the first cube and the manifold $K \times S^1$, which is the product of a Klein bottle and a circle, can be constructed according to the second cube [12].

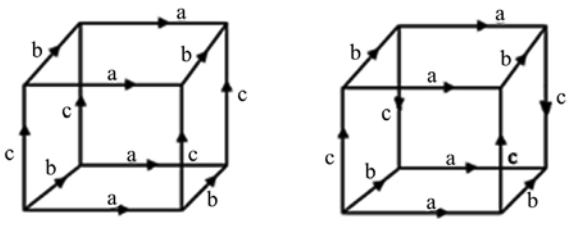

Figure 6. Fundamental cubes of a 3-torus and the manifold which is the product of a Klein bottle and a circle.

Now, consider a standing wave in a cube in a region of three-dimensional Euclidean space defined by the domain $D=\{0<x<L,0<y<L,0<x<L\}$. The standing wave is assumed to satisfy a three-dimensional wave equation written in the Cartesian coordinates (x,y,z) of the form given in Equation (13), with the boundary conditions $\psi(x,y,z,t)=0$ on the boundary of D and the initial conditions $\psi(x,y,z,0)=f(x,y,z)$, $\partial\psi/\partial t(x,y,z,0)=g(x,y,z)$. Then the general solution can be found as

$$\psi(x,y,z,t)=\sum_{n=1}^{\infty}\sum_{m=1}^{\infty}\sum_{l=1}^{\infty}\left(A_{lmn}\cos\lambda_{mn}t+B_{lmn}\sin\lambda_{mn}t\right)\sin\frac{m\pi x}{L}\sin\frac{m\pi y}{L}\sin\frac{n\pi z}{L} \quad (30)$$

where $\lambda_{mn}=(c\pi/L)\sqrt{l^2+m^2+n^2}$, and the coefficients A_{lmn} and B_{lmn} can be found in terms of the functions $f(x,y,z)$ and $g(x,y,z)$ using the orthogonal conditions. However, the main problem that we are interested in now is how to transform the standing wave in the fundamental cubes into a standing wave on a 3-torus or the manifold $K\times S^1$. In order to describe the wave dynamics on a hypersurface embedded or immersed in four-dimensional Euclidean space R^4 we need a four-dimensional wave equation written in the Cartesian coordinates (x,y,z,w) of the form

$$\frac{1}{c^2}\frac{\partial^2\psi}{\partial t^2}-\frac{\partial^2\psi}{\partial x^2}-\frac{\partial^2\psi}{\partial y^2}-\frac{\partial^2\psi}{\partial z^2}-\frac{\partial^2\psi}{\partial w^2}=0 \quad (31)$$

As in the case of two-dimensional surfaces discussed in Section 4, in order to use the wave equation given in Equation (31) to describe a wave dynamics on the surface of a 3-torus we first need to construct a line element $\mathrm{d}s^2=g_{\alpha\beta}\mathrm{d}x^\alpha\mathrm{d}x^\beta$ for the 3-torus and then apply the Laplacian $\nabla^2\psi=\left(1/\sqrt{g}\right)\partial\left(\sqrt{g}g^{\alpha\beta}\,\partial\psi/\partial x^\beta\right)/\partial x^\alpha$. The parametric equations for a 3-torus are given as [40]

$$x=(a\cos\theta+b)\cos\varphi,\quad y=(a\cos\theta+b)\sin\varphi,\quad z=a\sin\theta\sin\zeta,\quad w=a\sin\theta\cos\zeta \quad (32)$$

From the parametric equations given in Equation (32), the line element for the 3-torus embedded in the ambient four-dimensional Euclidean space R^4 can be found and given as

$$\mathrm{d}s^2=a^2\left(\mathrm{d}\theta^2+\left(\cos\theta+\frac{b}{a}\right)^2\mathrm{d}\varphi^2+\sin^2\theta\mathrm{d}\zeta^2\right) \quad (33)$$

From the line element given in Equation (33), in terms of the orthogonal coordinates (θ,φ,ζ), the wave equation on the surface of a 3-torus takes the form

$$\frac{1}{c^2}\frac{\partial^2\psi}{\partial t^2}-\frac{1}{a^2}\left(\frac{\partial^2\psi}{\partial\theta^2}+\left(-\frac{\sin\theta}{\cos\theta+\frac{b}{a}}+\frac{\cos\theta}{\sin\theta}\right)\frac{\partial\psi}{\partial\theta}+\frac{1}{\left(\cos\theta+\frac{b}{a}\right)^2}\frac{\partial^2\psi}{\partial\varphi^2}+\frac{1}{\sin^2\theta}\frac{\partial^2\psi}{\partial\zeta^2}\right)=0 \quad (34)$$

It is shown that solutions to the wave equation on 3-torus given in Equation (34) exist and, in particular, they can be written as a Fourier decomposition [41]. For the wave dynamics on surface of the manifold $K\times S^1$, which is the product of a Klein bottle and a circle, we may consider a mixed metric which is a combination of a metric on a circle and a metric on a Klein bottle. A metric on a circle is found using the line element in polar coordiantes $\mathrm{d}s^2=\mathrm{d}r^2+r^2\mathrm{d}\theta^2$ in which the radius is constant, $r=R$, therefore, we have $\mathrm{d}s^2=R^2\mathrm{d}\theta^2$. Together with the metric of revolution g_0 for the first eigenvalue on a Klein bottle given in Equation (29), we obtain

$$\mathrm{d}s^2=k_1R^2\mathrm{d}\theta^2+k_2\left(\frac{9+\left(1+8\cos^2 v\right)^2}{1+8\cos^2 v}\left(\mathrm{d}u^2+\frac{\mathrm{d}v^2}{1+8\cos^2 v}\right)\right) \tag{35}$$

where k_1 and k_2 are undetermined constants.

As a further discussion, we now discuss the transformation of a stationary wave on a cube into a stationary wave on a 3-sphere despite it still remains unknown whether a 3-sphere can be constructed directly from a cube by gluing its opposite faces. Despite this uncertainty, however, as mentioned before, we speculate that mathematical degeneracy in which an element of a class of objects degenerates into an element of a different but simpler class may play an important role in quantum dynamics therefore if an *n*-torus degenerates into an *n*-sphere then wavefunctions on an *n*-torus may also be degenerated into wavefunctions on an *n*-sphere. Consider a *d*-dimensional hypersphere S_r^d of radius *r* embedded in the ambient $(d+1)$-dimensional Euclidean space R^{d+1}. If spherical coordinates $\left(r,\theta,\theta_1,\cdots,\theta_{d-2},\phi\right)$ are defined in terms of the Cartesian coordinates $\left(x_1,x_2,\cdots,x_{d+1}\right)$ as $x_1=r\cos\theta$, $x_2=r\sin\theta\cos\theta_1$, $\cdots$, $x_{d+1}=r\sin\theta\cdots\sin\theta_{d-2}\sin\phi$ then the Laplacian $\nabla_{S^d}^2$ on the hypersphere S_r^d is given as follows [42]

$$\nabla_{S^d}^2\psi=\frac{1}{r^2}\left(\frac{\partial^2\psi}{\partial\theta^2}+(d-1)\cot\theta\frac{\partial\psi}{\partial\theta}+\frac{1}{\sin^2\theta}\nabla_{S^{d-1}}^2\psi\right) \tag{36}$$

For the case of a 3-sphere S^3 embedded in four-dimensional Euclidean space R^4, the wave equation given in Equation (36) takes the form

$$\frac{1}{c^2}\frac{\partial^2\psi}{\partial t^2}-\frac{1}{r^2}\left(\frac{\partial^2\psi}{\partial\theta^2}+2\cot\theta\frac{\partial\psi}{\partial\theta}+\frac{1}{\sin^2\theta}\nabla_{S^2}^2\psi\right)=0 \tag{37}$$

where $\nabla_{S^2}^2$ is Laplacian operator on a 2-sphere S^2. Solutions to Equation (37) can be established by separating the variables of the form $\psi\left(r,\theta,\theta_1,\theta_2,t\right)=R\left(r\right)\Theta\left(\theta,\theta_1,\theta_2\right)T\left(t\right)$. However, if we only consider the wave on the surface of constant radius $r=R$ then the wave equation given in Equation (37) reduces to the following system of ordinary differential equations

$$\frac{1}{c^2}\frac{\mathrm{d}^2T}{\mathrm{d}t^2}+k^2T=0 \tag{38}$$

$$\frac{\partial^2\Theta}{\partial\theta^2}+2\cot\theta\frac{\partial\Theta}{\partial\theta}+\frac{1}{\sin^2\theta}\nabla_{S^2}^2\Theta-k^2R^2\Theta=0 \tag{39}$$

In particular, for stable quantum particles in which ψ is time-independent therefore we can set $k=0$, and in this case the eigenfunctions of $\nabla_{S^3}^2$ are the hyperspherical harmonics $\Theta_{nl}^m(\theta,\theta_1,\theta_2)$ which are solutions of the equation

$$\nabla_{S^3}^2\Theta_{nl}^m(\theta,\theta_1,\theta_2)=-l(l+2)\Theta_{nl}^m(\theta,\theta_1,\theta_2) \tag{40}$$

It can be shown that $\Theta_{nl}^m(\theta,\theta_1,\theta_2)$ are given as [43]

$$\Theta_{nl}^m(\theta,\theta_1,\theta_2)=2^{l+1/2}\sqrt{\frac{(n+1)\Gamma(n-l+1)}{\pi\Gamma(n+l+2)}}\Gamma(l+1)\sin^l\theta C_{n-l}^{l+1}(\cos\theta)Y_l^m(\theta_1,\theta_2) \tag{41}$$

where C_{n-l}^{l+1} are the Gegenbauer polynomials and Y_l^m are the 3D spherical harmonics in which $n=0,1,2,\cdots$, $0\le l\le n$, and $-l\le m\le l$. The number of hyperspherical harmonics for a given value of n is $(n+1)^2$.

6. Conclusion

In this work, we have discussed the topological transformation of quantum dynamics by showing the wave dynamics of a quantum particle from the fundamental polygons of the corresponding universal covering spaces in one, two and three dimensions. As stated in the introductory summary, this is not the view from different perspectives of an observer who simply uses different coordinate systems to describe the same physical phenomenon but rather possible geometric and topological structures that quantum particles are endowed with when they are identified with differentiable manifolds that are embedded or immersed in Euclidean spaces of higher dimension. For the purpose of physical illustration, we followed a modest approach in which we presented our discussions in the form of Bohr model in one, two and three dimensions using linear wave equations. In one dimension, we considered the topological transformation of a standing wave on a finite string into the standing wave on a circle which can be applied into the Bohr model of the hydrogen atom. The wave dynamics on a circle can also be described in terms of projective elliptic geometry. In two dimensions, we discussed the topological transformation of a standing wave on a square into a standing wave on different surfaces that can be formed by gluing opposite sides of the square, which include a 2-sphere, a 2-torus, a Klein bottle and a projective plane. In particular, we showed that when the wave dynamics on a projective plane is described in terms of projective elliptic geometry, then it is identical to the wave dynamics on a 2-sphere. In three dimensions, we considered the topological transformation of a standing wave on a cube into a standing wave on a 3-torus or on the manifold $K\times S^1$. We also discussed a transformation of a stationary wave on a cube into a stationary wave on a 3-sphere despite it still remains unknown whether a 3-sphere can be constructed directly from a cube by gluing its opposite faces. However, it seems reasonable to assume that if an n-torus degenerates into an n-sphere, then wavefunctions on an n-torus may also be degenerated into wavefunctions on an n-sphere. Furthermore, since an n-sphere can degenerate itself into a single point, the mathematical degeneracy may be related to the concept of wavefunction collapse in quan-

tum mechanics where the classical observables such as position and momentum can only be obtained from the collapse of the associated wavefunctions for physical measurements. This consideration suggests that quantum particles associated with differentiable manifolds may possess the more stable mathematical structures of an n-torus rather than those of an n-sphere. Even though it has not been discussed in this work, we would like to add the following remark in relation to physical states of quantum particles that would make the topological transformations that have been presented in this work possible. If quantum particles are formed from mass points by contact forces, then they may have the ability to change their topological structures to adapt the topological structures of the physical system in which they are part of. In physics, such ability is related to the physical states of fluid rather than solid states as being assumed for quantum particles in particle physics. And, interestingly, it can be shown that equations of fluid dynamics that describe the fluid state of quantum particles can be derived from Dirac equation in quantum mechanics [44].

Acknowledgements

We would like to thank the reviewers for their constructive criticisms and comments and the administration of JMP for their editorial advice during the preparation of this work.

Conflicts of Interest

The author declares no conflicts of interest regarding the publication of this paper.

References

[1] Ho, V.B. (2018) *International Journal of Physics*, **6**, 105-115.

[2] Ho, V.B. (2018) *GJSFR-A*, **18**, 37-58.

[3] Ho, V.B. (2018) *International Journal of Physics*, **6**, 47-52.

[4] Ho, V.B. (2017) On the Motion of Quantum Particles and Euclidean Relativity. Preprint, ResearchGate, viXra 1710.0253v1.

[5] Tung, W.K. (1985) Group Theory in Physics. World Scientific. https://doi.org/10.1142/0097

[6] Cornwell, J.F. (1987) Group Theory in Physics. Academic.

[7] Borrelli, V., Jabrane, S., Lazarus, F. and Thibert, B. (2012). Hevea Project: The Folder.

[8] Yourgrau, W. and Mandelstam, S. (1979) Variational Principles in Dynamics and Quantum Theory. Dover Publications, New York.

[9] Ho, V.B. (1996) Geometrical and Topological Methods in Classical and Quantum Physics. PhD Thesis, Monash University, Clayton.

[10] Dirac, P.A.M. (1928) P*roceedings of the Royal Society A*: *Mathematical*, *Physical and Engineering Sciences*, **117**, 610-624. https://doi.org/10.1098/rspa.1928.0023

[11] Ho, V.B. (2018) *International Journal of Physics*, **6**, 139-146.

[12] Hatcher, A. (2001) Algebraic Topology.

[13] Pontzen, A. (2016), Bianchi Universes. Scholarpedia.

[14] Thurston, W.P. (2002) The Geometry and Topology of Three-Manifolds. Electronic version 1.1.

[15] Scott, P. (1983) *Bulletin of the London Mathematical Society*, **15**, 401-487. https://doi.org/10.1112/blms/15.5.401

[16] Bär, C. (2017) Geometric Wave Equations. Lecture Notes, University of Potsdam, Potsdam.

[17] Wikipedia, Clifford Torus.

[18] Wolfram MathWorld, Torus.

[19] Andrews, B. (2002) *Continuity*, **7810**, 157-208.

[20] Tao, T. (2016) Notes on the Nash Embedding Theorem.

[21] Huynh, K.M. (2018) The Nash Embedding Theorem. UCLA Mathematics Department.

[22] Chousionis, V., Erdogan, M.B. and Tzirakis, N. (2014) Fractal Solutions of Linear and Nonlinear Dispersive Partial Differential Equations. arXiv:1406.3283

[23] Rossler, O.E. (1976) *Physics Letters A*, **57**, 397-398. https://doi.org/10.1016/0375-9601(76)90101-8

[24] Peitgen, H.O., Jurgens, H. and Saupe, D. (2004) Chaos and Fractals. Srpinger-Verlag, New York.

[25] Bohr, N. (1913) *Philosophical Magazine*, **26**, 1-25.

[26] De Broglie, L. (1925) *Annales de Physique*, **10**, 22-128.

[27] Lachieze-Rey, M. and Luminet, J.P. (2003) Cosmic Topology.

[28] Strauss, W.A. (1992) Partial Differential Equation. John Wiley & Sons, New York.

[29] Wikipedia. Elliptic Geometry.

[30] Arfken, G. (1970) Mathematical Methods for Physicists. Academic, New York.

[31] Wolfram MathWorld, Laplace's Equation in Toroidal Coordinates.

[32] Weston, V.H. (1958) *Quarterly of Applied Mathematics*, **16**, 237-257. https://doi.org/10.1090/qam/104001

[33] Weston, V.H. (1960) *Journal of Mathematics and Physics*, **39**, 64-71. https://doi.org/10.1002/sapm196039164

[34] Wolfram MathWorld, Klein Bottle.

[35] Wikipedia. Klein Bottle.

[36] Fritz, J. (1978) Partial Differential Equations. Springer, Berlin.

[37] Jakobson, D., Nadirashvili, N. and Polterovich, I. (2005) Extremal Metric for the First Eigenvalue on a Klein Bottle. arXiv:math/0311484v2

[38] Gonzales-Diaz, P.F. and Garay, L.J. (1999) *Physical Review D*, **59**, Article ID: 064026.

[39] Tillmann, S. (2012) Real Projective Manifolds. Tsinghua University, Beijing.

[40] Plebanski, J. and Krasinski, A. (2006) An Introduction to General Relativity and Cosmology. Cambridge University Press, Cambridge.

[41] Petersen, O.L. (2014) The Wave Equation and Redshift in Bianchi Type I Spacetimes. Master's Thesis in Mathematics, Royal Institute of Technology, Sweden.

[42] Meremianin, A.V. (2009) *Journal of Mathematical Physics*, **50**, Article ID: 013526.

[43] Domokos, G. (1967) *Physical Review*, **159**, 1387-1403.

[44] Ho, V.B. (2018) *Journal of Modern Physics*, **9**, 2402-2419.

Appendices

Appendix 1

In this appendix, we show in detail the derivation of the equations that are used to determine the metric tensor of the line element given as $\mathrm{d}s^2 = Dc^2\mathrm{d}t^2 - A(x,y,z,t)\left(\mathrm{d}x^2 + \mathrm{d}y^2 + \mathrm{d}z^2\right)$. In differential geometry, the Riemann curvature tensor $R^{\alpha}{}_{\mu\beta\nu}$ is defined in terms of the affine connection $\Gamma^{\gamma}_{\alpha\beta}$ as

$$R^{\alpha}{}_{\mu\beta\nu} = \frac{\partial\Gamma^{\alpha}_{\mu\beta}}{\partial x^{\nu}} - \frac{\partial\Gamma^{\alpha}_{\mu\nu}}{\partial x^{\beta}} + \Gamma^{\lambda}_{\mu\beta}\Gamma^{\alpha}_{\lambda\nu} - \Gamma^{\lambda}_{\mu\nu}\Gamma^{\alpha}_{\lambda\beta} \tag{1}$$

The contraction of the Riemann curvature tensor given in Equation (1) with respect to the indices α and β gives the Ricci tensor

$$R_{\mu\nu} = \frac{\partial\Gamma^{\sigma}_{\mu\nu}}{\partial x^{\sigma}} - \frac{\partial\Gamma^{\sigma}_{\mu\sigma}}{\partial x^{\nu}} + \Gamma^{\lambda}_{\mu\nu}\Gamma^{\sigma}_{\lambda\sigma} - \Gamma^{\lambda}_{\mu\sigma}\Gamma^{\sigma}_{\lambda\nu} \tag{2}$$

In order to formulate the field equations for the gravitational field it is necessary to introduce a symmetrical metric tensor $g_{\alpha\beta}$ in terms of which the affine connection $\Gamma^{\gamma}_{\alpha\beta}$ is defined as

$$\Gamma^{\lambda}_{\mu\nu} = \frac{1}{2}g^{\lambda\sigma}\left(\frac{\partial g_{\sigma\nu}}{\partial x^{\mu}} + \frac{\partial g_{\sigma\mu}}{\partial x^{\nu}} - \frac{\partial g_{\mu\nu}}{\partial x^{\sigma}}\right) \tag{3}$$

With the line $\mathrm{d}s^2 = Dc^2\mathrm{d}t^2 - A(x,y,z,t)\left(\mathrm{d}x^2 + \mathrm{d}y^2 + \mathrm{d}z^2\right)$, we obtain the following non-zero components of the affine connection

$$\Gamma^1_{01} = \Gamma^1_{10} = \frac{1}{2cA}\frac{\partial A}{\partial t},\quad \Gamma^2_{02} = \Gamma^2_{20} = \frac{1}{2cA}\frac{\partial A}{\partial t}$$

$$\Gamma^3_{03} = \Gamma^3_{30} = \frac{1}{2cA}\frac{\partial A}{\partial t},\quad \Gamma^0_{11} = \frac{1}{2cD}\frac{\partial A}{\partial t}$$

$$\Gamma^1_{11} = \frac{1}{2A}\frac{\partial A}{\partial x},\quad \Gamma^2_{11} = -\frac{1}{2A}\frac{\partial A}{\partial y},\quad \Gamma^3_{11} = -\frac{1}{2A}\frac{\partial A}{\partial z}$$

$$\Gamma^1_{12} = \Gamma^1_{21} = \frac{1}{2A}\frac{\partial A}{\partial y},\quad \Gamma^2_{12} = \Gamma^2_{21} = \frac{1}{2A}\frac{\partial A}{\partial x},$$

$$\Gamma^1_{13} = \Gamma^1_{31} = \frac{1}{2A}\frac{\partial A}{\partial z},\quad \Gamma^3_{13} = \Gamma^3_{31} = \frac{1}{2A}\frac{\partial A}{\partial x}$$

$$\Gamma^0_{22} = \frac{1}{2cD}\frac{\partial A}{\partial t},\quad \Gamma^1_{22} = \frac{1}{2A}\frac{\partial A}{\partial x},\quad \Gamma^2_{22} = \frac{1}{2A}\frac{\partial A}{\partial y}$$

$$\Gamma^3_{22} = -\frac{1}{2A}\frac{\partial A}{\partial z},\quad \Gamma^0_{33} = \frac{1}{2cD}\frac{\partial A}{\partial t},\quad \Gamma^1_{33} = -\frac{1}{2A}\frac{\partial A}{\partial x}$$

$$\Gamma^2_{33} = -\frac{1}{2A}\frac{\partial A}{\partial y},\quad \Gamma^3_{33} = \frac{1}{2A}\frac{\partial A}{\partial z}$$

$$\Gamma^2_{23} = \Gamma^2_{32} = \frac{1}{2A}\frac{\partial A}{\partial z},\quad \Gamma^3_{23} = \Gamma^3_{32} = \frac{1}{2A}\frac{\partial A}{\partial y} \tag{4}$$

From the components of the affine connection given in Equation (4), we ob-

tain

$$R_{11}=\frac{1}{2c^2D}\frac{\partial^2 A}{\partial t^2}-\frac{1}{A}\frac{\partial^2 A}{\partial x^2}-\frac{1}{2A}\frac{\partial^2 A}{\partial y^2}-\frac{1}{2A}\frac{\partial^2 A}{\partial z^2}+\frac{3}{4c^2AD}\left(\frac{\partial A}{\partial t}\right)^2+\frac{1}{A^2}\left(\frac{\partial A}{\partial x}\right)^2+\frac{1}{4A^2}\left(\frac{\partial A}{\partial y}\right)^2+\frac{1}{4A^2}\left(\frac{\partial A}{\partial z}\right)^2$$

$$R_{22}=\frac{1}{2c^2D}\frac{\partial^2 A}{\partial t^2}-\frac{1}{2A}\frac{\partial^2 A}{\partial x^2}-\frac{1}{A}\frac{\partial^2 A}{\partial y^2}-\frac{1}{2A}\frac{\partial^2 A}{\partial z^2}+\frac{3}{4c^2AD}\left(\frac{\partial A}{\partial t}\right)^2+\frac{1}{4A^2}\left(\frac{\partial A}{\partial x}\right)^2+\frac{1}{A^2}\left(\frac{\partial A}{\partial y}\right)^2+\frac{1}{4A^2}\left(\frac{\partial A}{\partial z}\right)^2$$

$$R_{33}=\frac{1}{2c^2D}\frac{\partial^2 A}{\partial t^2}-\frac{1}{2A}\frac{\partial^2 A}{\partial x^2}-\frac{1}{2A}\frac{\partial^2 A}{\partial y^2}-\frac{1}{A}\frac{\partial^2 A}{\partial z^2}+\frac{3}{4c^2AD}\left(\frac{\partial A}{\partial t}\right)^2+\frac{1}{4A^2}\left(\frac{\partial A}{\partial x}\right)^2+\frac{1}{4A^2}\left(\frac{\partial A}{\partial y}\right)^2+\frac{1}{A^2}\left(\frac{\partial A}{\partial z}\right)^2$$

$$R_{00}=-\frac{3}{2c^2A}\frac{\partial^2 A}{\partial t^2}+\frac{3}{4c^2A^2}\left(\frac{\partial A}{\partial t}\right)^2 \tag{5}$$

Using the relation $R=g^{00}R_{00}+g^{11}R_{11}+g^{22}R_{22}+g^{33}R_{33}$ the Ricci scalar curvature can be found as

$$R=-\frac{3}{c^2DA}\frac{\partial^2 A}{\partial t^2}+\frac{2}{A^2}\nabla^2 A+\frac{3}{2A^3}(\nabla A)^2 \tag{6}$$

Using the relation

$$R(x,y,z,t)=\left(M\Big/\left(\sqrt{4\pi kt}\right)^3\right)\mathrm{e}^{-\left(x^2+y^2+z^2\right)/4kt} \tag{7}$$

Then we finally arrive at

$$-\frac{3}{c^2DA}\frac{\partial^2 A}{\partial t^2}+\frac{2}{A^2}\nabla^2 A+\frac{3}{2A^3}(\nabla A)^2=\frac{M}{\left(\sqrt{4\pi kt}\right)^3}\mathrm{e}^{-\frac{x^2+y^2+z^2}{4kt}} \tag{8}$$

Appendix 2

In this appendix, we will show that Schrödinger wavefunctions can be used for the construction of spacetime structures of the quantum states of a quantum system. Schrödinger's original works were on the time-independent quantum states of the hydrogen atom, commencing with the Hamilton-Jacobi equation, written in terms of the Cartesian coordinates (x,y,z) as

$$\left(\frac{\partial S}{\partial x}\right)^2+\left(\frac{\partial S}{\partial x}\right)^2+\left(\frac{\partial S}{\partial x}\right)^2-2m\left(E+\frac{kq^2}{r}\right)=0 \tag{1}$$

However, in order to obtain a partial differential equation that would give rise to the required results, Schrödinger introduced a new function ψ, which is real, single-valued and twice differentiable, through the relation $S=\hbar\ln\psi$, where the action S is defined by $S=\int L\mathrm{d}t$ and L is the Lagrangian defined by $L=T-\varphi$, with T is the kinetic energy and φ is the potential energy. In terms

of the new function ψ, Equation (1) takes the form

$$\left(\frac{\partial\psi}{\partial x}\right)^2+\left(\frac{\partial\psi}{\partial x}\right)^2+\left(\frac{\partial\psi}{\partial x}\right)^2-\frac{2m}{\hbar^2}\left(E+\frac{kq^2}{r}\right)\psi^2=0 \tag{2}$$

Then by applying the principle of least action $\delta\int L\mathrm{d}t=0$, Schrödinger arrived at the required equation

$$\nabla^2\psi+\frac{2m}{\hbar^2}\left(E+\frac{kq^2}{r}\right)\psi=0 \tag{3}$$

Now we show that Schrödinger wavefunction ψ can be used to construct the spacetime structures of the quantum states of the hydrogen atom. By using the relations $L=\mathrm{d}S/\mathrm{d}t$, $\mathrm{d}S/\mathrm{d}t=\partial_t S+\sum_{\mu=1}^{3}\partial_\mu S\left(\mathrm{d}x^\mu/\mathrm{d}t\right)$, $T=m\sum_{\mu=1}^{3}\left(\mathrm{d}x^\mu/\mathrm{d}t\right)^2$ and $\varphi=T-L$, we obtain

$$\varphi=m\sum_{\mu=1}^{3}\left(\mathrm{d}x^\mu/\mathrm{d}t\right)^2-\partial_t S+\sum_{\mu=1}^{3}\partial_\mu S\left(\mathrm{d}x^\mu/\mathrm{d}t\right) \tag{4}$$

In terms of the Schrödinger wavefunction ψ, Equation (4) can be rewritten as

$$\varphi=m\sum_{\mu=1}^{3}\left(\mathrm{d}x^\mu/\mathrm{d}t\right)^2-\hbar\frac{\partial_t\psi+\sum_{\mu=1}^{3}\partial_\mu\psi\left(\mathrm{d}x^\mu/\mathrm{d}t\right)}{\psi} \tag{5}$$

From Poisson equation we can assume the relation $\varphi=kmR$ then the following relation between the Schrödinger wavefunction ψ and the Ricci scalar R can be established [1]

$$R=\frac{1}{k}\left(\sum_{\mu=1}^{3}\left(\mathrm{d}x^\mu/\mathrm{d}t\right)^2-\frac{\hbar}{m}\frac{\partial_t\psi+\sum_{\mu=1}^{3}\partial_\mu\psi\left(\mathrm{d}x^\mu/\mathrm{d}t\right)}{\psi}\right) \tag{6}$$

Journal of Modern Physics, 2019, 10, 128-144
http://www.scirp.org/journal/jmp
ISSN Online: 2153-120X
ISSN Print: 2153-1196

Spin Supercurrent in Phenomena of Quantum Non-Locality (Quantum Correlations, Magnetic Vector Potential) and in Near-Field Antenna Effect

Liudmila B. Boldyreva

The State University of Management, Moscow, Russia
Email: boldyrev-m@yandex.ru

How to cite this paper: Boldyreva, L.B. (2019) Spin Supercurrent in Phenomena of Quantum Non-Locality (Quantum Correlations, Magnetic Vector Potential) and in Near-Field Antenna Effect. *Journal of Modern Physics*, **10**, 128-144.
https://doi.org/10.4236/jmp.2019.102010

Received: December 31, 2018
Accepted: February 23, 2019
Published: February 26, 2019

Abstract

It is shown that such phenomena as quantum correlations (interaction of space-separated quantum entities), the action of magnetic vector potential on quantum entities in the absence of magnetic field, and near-field antenna effect (the existence of superluminally propagating electromagnetic fields) may be explained by action of spin supercurrents. In case of quantum correlations between quantum entities, spin supercurrent emerges between virtual particles pairs (virtual photons) created by those quantum entities. The explanation of magnetic vector potential and near-field antenna effect is based on contemporary principle of quantum mechanics: the physical vacuum is not an empty space but the ground state of the field consisting of quantum harmonic oscillators (QHOs) characterized by zero-point energy. Using the properties of the oscillators and spin supercurrent, it is proved that magnetic vector potential is proportional to the moment causing the orientation of spin of QHO along the direction of magnetic field. The near-field antenna effect is supposed to take place as a result of action of spin supercurrent causing secondary electromagnetic oscillations. In this way, the electromagnetic field may spread at the speed of spin supercurrent. As spin supercurrent is *an inertia free process*, its speed may be greater than that of light, which does not contradict postulates of special relativity that sets limits to the speed of inertial systems only.

Keywords

Spin Supercurrent, Quantum Correlations, Magnetic Vector Potential, Near-Field Antenna Effect, Zero-Point Energy, Quantum Harmonic Oscillator, Virtual Particles Pair, Virtual Photon

1. Introduction

The following phenomena are discussed in this work: 1) quantum correlations—mutual dependence of characteristics of wave function of so-called entangled quantum entities while there is space separation; 2) a change in characteristics of wave function of quantum entities while they are passing in the region of non-zero magnetic vector potential (magnetic field may be absent); 3) the near-field antenna effect—the existence near antenna (an oscillating electric dipole) of superluminally propagating electromagnetic field. The common property of the phenomena is the following: they are not described by action of well-known physical fields: electric, magnetic, gravitational. For description of these phenomena, the mathematical apparatus of quantum mechanics is used: Heisenberg's uncertainty principle, Schrödinger equation for wave function of quantum entities [1] [2] [3].

Let us consider these phenomena in detail.

Quantum correlations belong to the category of phenomena that are collectively called "quantum non-locality" [4] [5]. The essence of the phenomena can be described using the following example. Let two quantum entities (**Figure 1**) ***a*** and ***b*** emitted by the same source and having the same wave function at the initial moment of time move in different directions.

Entity ***a*** is directed, depending on the position (1 or 2) of switch P, either towards detector A_1 or detector A_2 (these detectors have different characteristics); entity ***b*** is directed towards detector B. According to postulates of quantum mechanics, the wave properties of entity ***b*** being detected will depend on that which detector detects ***a***. In the early years of studies of quantum correlations, it was supposed that these correlations take place only between "entangled" quantum entities emitted by one source and described by a single wave function [5]. However, the discovery of quantum correlation between the photons having equal frequencies, emitted by different sources [4], suggests that for the existence of quantum correlations, it is only necessary for the interacting quantum entities to have equal wave function frequencies and at least for photons to have a definite mutual spin polarization. Quantum correlations have a non-electric and non-magnetic nature and take place independent of the distance between the interacting quantum entities [5] [6]. The speed of quantum correlations is greater than the speed of light; it follows from the possibility of correlations of photons separated in space and simultaneously emitted. The experiments exist [7] in which it is shown that the speed of quantum correlations is 10^4 times greater than the speed of light. If quantum correlations are accomplished by *an inertia-free process* (it is not accompanied by emergence of mass), this does not contradict the postulates of special relativity that set limits to the speed of motion of inertial systems only [8].

It should be noted that Einstein, Podolsky and Rosen with reference to the measurement problem of entangled quantum entities wrote [9]: "… the description of reality given by the wave function in quantum mechanics is not complete", which in fact admits a possibility of existence of a physical process re-

sponsible for quantum correlations.

Field-free magnetic vector potential. In classical electrodynamics, the magnetic field of induction **B** is determined [10] by equation $\mathbf{B} = curl\mathbf{A}$, where **A** is a magnetic vector potential. In shielding of magnetic field, $\mathbf{B} = 0$, the following may take place: $\mathbf{A} \neq 0$. This case is referred to as the field-free vector potential. Magnetic vector potential has a physical meaning of its own. In 1949, Erenberg and Siday predicted the ability of magnetic vector potential to influence directly the characteristics of quantum entities even though there is no electromagnetic field at the location of the entities [11]. In 1959, the possibility of such an effect was considered by Aharonov and Bohm [12]. Subsequently, a great number of experiments have been conducted which confirmed the theoretical predictions [13]. In general, these experiments were as follows (see Figure 2): the beam of electrically charged quantum entities emitted by a source is split into two beams: C_1 and C_2. Beam C_1 propagates through the region where $\mathbf{A} = 0$. Beam C_2 passes through an energized toroidal solenoid (region δ). The solenoid is shielded in such a way that outside the solenoid there is no magnetic field, $\mathbf{B} = 0$, but the vector potential is present: $\mathbf{A} \neq 0$. Both beams of quantum entities arrive at the entrances of an interferometer. The interference rings obtained suggest that there is a change in the wave function phase of quantum entities passing through the region where $\mathbf{B} = 0$ and $\mathbf{A} \neq 0$.

In quantum mechanics, the description of action of the field-free magnetic vector potential is based on Schrödinger's equation [2] without introducing any physical process. As the action of the field-free magnetic vector potential takes place in space where electromagnetic field is absent, this potential has both non-electric and non-magnetic nature.

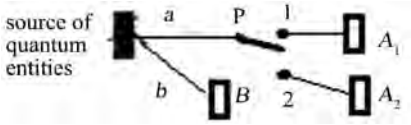

Figure 1. Schematic diagram of the experiment that illustrates quantum correlations between quantum entities. *a* and *b* are quantum entities; A_1, A_2, and *B* are detectors; *P* is a switch with positions 1 and 2.

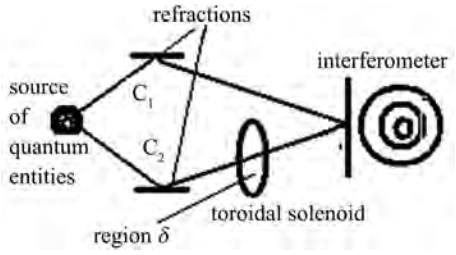

Figure 2. Schematic diagram of the experiment on the study of the effects of magnetic vector potential on quantum entities. The source of quantum entities emits two beams. Beam C_1 propagates through the region where $\mathbf{A} = 0$. Beam C_2 passes through the shielded energized toroidal solenoid in the region (region δ) of the field-free magnetic vector potential. Interference rings are produced by the interferometer.

Near-field antenna effect. There is experimental evidence of existence near antenna (an oscillating electric dipole) of superluminally propagating electromagnetic field [14] [15]. The well-known explanation of this phenomenon [14] is based on the assumption that a superluminal motion takes place at distances of about one wavelength from the source of oscillations. The wavelength of wave function of quantum entities (for photon it is equal to photon's wavelength) is the size on which the Heisenberg's uncertainty principle [1] holds true. That is the uncertainty Δp_x in the measured value of component p_x of momentum $\mathbf{p}$ of quantum entity is determined as: $\Delta p_x \geq \hbar/\Delta x$ (Δx is the uncertainty in the measured value of coordinate x of quantum entity). As momentum is a function of speed of quantum entity, the uncertainty in measured value of momentum means the uncertainty in the value of speed of quantum entity. Thus the suggested explanation of near-field antenna effect is in accordance with the second postulate of special relativity asserting the constancy of the velocity of light.

This work suggests essentially a new approach to description of the above-considered phenomena: namely it is shown that it is possible to describe these phenomena in terms of such physical process as spin supercurrent. The spin supercurrent emerges between objects having spin, and its action tends to make equal the respective characteristics of precession of spins of interacting objects. (Note that Yuri Bunkov, Vladimir Dmitriev and Igor Fomin were awarded the Fritz London Memorial Prize in 2008 for the studies of spin supercurrents in superfluid ^{3}He-B [16] [17] [18]). The specific feature of the approach to description of the above-considered phenomena is as well that it takes into account the properties of the physical vacuum.

In quantum field theory, the physical vacuum, free from magnetic and electric fields (without regard to gravitational energy), is defined not as an empty space but as the ground state of the field consisting of quantum harmonic oscillators (called QHOs from now on) characterized by zero-point energy [19]. The concept of zero-point energy was developed in Germany in 1913 by a group of physicists, including M. Planck, A. Einstein, and O. Stern [20]. A quantum entity (its characteristics are determined by the wave function) which is a singularity in electric or magnetic fields (electric charge or/and magnetic dipole) creates a virtual photon (virtual particles pair) having spin in the physical vacuum [21].

It is proved in this work that the properties of quantum correlations, the action of magnetic vector potential on quantum entities, and near-field antenna effect are determined by the properties of spin supercurrent arising between virtual photons created by quantum entities participating in these phenomena and of spin supercurrents emerging between virtual photons created by the quantum entities, on the one hand, and QHOs that constitute the physical vacuum, on the other hand.

The findings of this work can be used, for example, for optimization of channels intended for performing quantum correlations between quantum entities

owing to increasing the number of characteristics by which the correlation of the quantum entities is effected.

The paper below consists of the following sections. Section 2 (titled as "The Characteristics of Spin Supercurrent") contains equations describing the conditions of emergence of spin supercurrent and effects of the latter, energy properties of the current and features of its propagation (the speed, the impossibility of shielding by electromagnetic screens). Section 3 (titled as "The Properties of QHOs") contains the description of such characteristics of QHO as the electric dipole moment, mass, precessing spin and connection of QHO speed with magnetic phenomena. Section 4 (titled as "Results") provides explanations of phenomena of quantum correlations, the action of magnetic vector potential on quantum entities, and near-field antenna effect as based on both the properties of spin supercurrent and those of the physical vacuum consisting of QHOs.

Below are specified the main variables used in this paper.

The characteristics of spin supercurrent: α_1 and α_2 are angles of precession, θ_1 and θ_2 are angles of deflection, $\boldsymbol{\omega}_1$ and $\boldsymbol{\omega}_2$ are frequencies of precession of spins, J_z is spin supercurrent.

The characteristics of QHO: $\mathbf{S}_{QHO}$ is spin, m_{QHO} is mass, $\boldsymbol{\Omega}_{QHO}$ is precession frequency, $\mathbf{d}_{QHO}$ is electric dipole moment, $\mathbf{u}$ is velocity of QHO, $\mathbf{A}$ is magnetic vector potential, $\mathbf{E}_{QHO}$ is electric field inside the QHO, $\mathbf{M}_{QHO}$ is the moment causing precession of spin $\mathbf{S}_{QHO}$.

2. The Characteristics of Spin Supercurrent

1) The spin supercurrent arises between objects with precessing spins (spin structures) [16] [17] [18]. **Figure 3** contains the schema of such spin structures with the following characteristics: α_1 and α_2 are precession angles, θ_1 and θ_2 are deflection angles, $\boldsymbol{\omega}_1$ and $\boldsymbol{\omega}_2$ are the frequencies of precession of spins $\mathbf{S}$ of the structures, J_z is spin supercurrent between the spin structures.

2) The spin supercurrent tends to equalize the respective characteristics of spins of interacting spin structures: angles (phases) of precession and angles of deflection. For example, the value of spin supercurrent J_z in the direction of orientation (axis $\boldsymbol{z}$ in **Figure 3**) of precession frequencies of spins is determined as follows:

$$J_z = g_1\left(a_1 - \alpha_2\right) + g_2\left(\theta_1 - \theta_2\right), \tag{1}$$

where g_1 and g_2 are coefficients depending on deflection angles and the properties of the medium where spin supercurrent emerges. Let us assume that before the action of spin supercurrent the angles of precession α_1 and α_2 are determined as $\alpha_1 = \omega_1 t + \alpha_{01}$ and $\alpha_2 = \omega_2 t + \alpha_{02}$, where α_{01} and α_{02} are the values of angles of precession respectively α_1 and α_2 at t=0. If $\alpha_{01} = \alpha_{02} = 0$, then

$$\alpha_1 = \omega_1 t, \tag{2}$$

$$\alpha_2 = \omega_2 t. \tag{3}$$

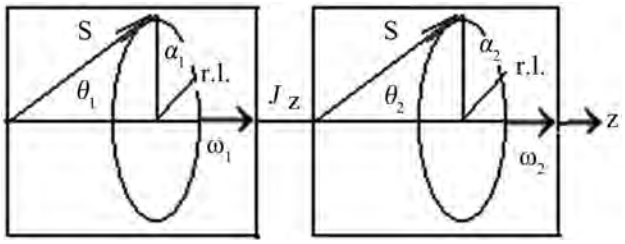

Figure 3. The schema of spin structures. J_z is spin supercurrent between spin structures with the following characteristics: α_1 and α_2 are precession angles, θ_1 and θ_2 are deflection angles, $\boldsymbol{\omega}_1$ and $\boldsymbol{\omega}_2$ are precession frequencies oriented along axis z, **S** is spin, r.l. is a reference line.

As a result of the action of spin supercurrent at arbitrary moment *t*, according to definition of this current, the following holds: $|\theta_1 - \theta_2| > |\theta_1' - \theta_2'|$ and:

$$|\alpha_1 - \alpha_2| > |\alpha_1' - \alpha_2'|, \tag{4}$$

where: θ_1' and θ_2' are respectively the values of deflection angles θ_1 and θ_2 of precessing spins of interacting spin structures after the action of spin supercurrent; α_1' and α_2' are respectively the values of precession angles α_1 and α_2 of precessing spins of interacting spin structures after the action of spin supercurrent. As a result of changes in precession angles, the change in frequencies ω_1 and ω_1 of interacting spin structures may also take place:

$$|\omega_1 - \omega_2| > |\omega_1' - \omega_2'|, \tag{5}$$

where ω_1' and ω_2' are the values of spin structures precession frequencies ω_1 and ω_1 after the action of spin supercurrent.

3) At a definite nonzero difference in the values of angles of precession

$$\Delta\alpha_c = \alpha_1 - \alpha_2 \neq 0, \tag{6}$$

a phase slippage, that is, the drop in the value and change in the sign of spin supercurrent may take place. In this case, Equation (1) does not hold. Consequently, as follows from Equations (2)-(3) and (6), for the effective equalization of respective characteristics of interacting spin structures the following is necessary: 1) a definite mutual orientation of precession frequencies of the interacting spin structures; 2) the absence of phase slippage, in particular, this takes place if the difference between their precession frequencies, $\omega_1 - \omega_2$, satisfy the following condition:

$$\Delta\omega \to 0. \tag{7}$$

4) The effectivity of action of spin supercurrent between spin structures does not depend on the distance between them. For example, the action of spin supercurrent in superfluid ^{3}He-B is limited only by the volume of superfluid.

5) Spin supercurrent is not an electric or magnetic process and consequently it is not shielded by electromagnetic screens.

6) The changes in the precession and deflection angles of precessing spins of interacting spin structures due to the action of spin supercurrent may be

considered as spin orientation transfer in the physical vacuum. Through the example of photon it may be shown that the spin orientation transfer in the physical vacuum is a dissipation-free process.

According to [22], the photon spin $\mathbf{S}_{ph}$ is perpendicular to its velocity $\mathbf{c}$, $\mathbf{S}_{ph} \perp \mathbf{c}$, and in the pure state (circular polarization) the photon spin performs precession motion with frequency $\boldsymbol{\omega}_{ph}$, $\boldsymbol{\omega}_{ph} \uparrow\uparrow \mathbf{c}$. According to [23], the energy W_{prec} of precession with frequency $\boldsymbol{\omega}_{ph}$ of angular momentum $S_{ph} = \hbar$ at $\mathbf{S}_{ph} \perp \boldsymbol{\omega}_{ph}$ is determined as:

$$W_{prec} = \hbar\omega_{ph}. \tag{8}$$

Energy U_{ph} of photon must be the sum of two components: energy W_{prec} of precession motion of spin and energy W_S of spin orientation transfer in space. From experiments [3] it follows that the total energy of photon is equal to $\hbar\omega_{ph}$. Taking into account Equation (8), this means that the total energy of photon U_{ph} equals only energy W_{prec} of precession motion of spin and the energy of spin orientation transfer equals zero:

$$W_S = 0. \tag{9}$$

Due to spreading of spin supercurrent without dissipation, the energies of interacting spin structures as a result of action of this current change by the same value. As, according to Equation (8), the energy of precessing spin is proportional to the frequency of precession, then from condition (5) it follows that $\omega_1 - \omega_1' = -(\omega_2 - \omega_2')$ or:

$$\Delta\omega_1 = -\Delta\omega_2, \tag{10}$$

where $\Delta\omega_1 = \omega_1 - \omega_1'$ and $\Delta\omega_2 = \omega_2 - \omega_2'$. Then according to Equations (2)-(4), $\alpha_1 - \alpha_1' = -(\alpha_2 - \alpha_2')$ or:

$$\Delta\alpha_1 = -\Delta\alpha_2, \tag{11}$$

where $\Delta\alpha_1 = \alpha_1 - \alpha_1'$ and $\Delta\alpha_2 = \alpha_2 - \alpha_2'$.

7) As energy is intrinsically associated with mass, then, according to Equation (9), spin supercurrent performing spin orientation transfer is not accompanied by emergence of any mass, that is, it is *an inertia free process* and consequently the speed y_{ss} of spin supercurrent may be greater than the speed of light:

$$y_{ss} > c. \tag{12}$$

This does not contradict the postulates of special relativity which set limits to the speed of inertial systems only [8].

3. The Properties of QHOs

According to contemporary principle of quantum mechanics, the physical vacuum is defined not as an empty space but as the ground state of the field consisting of QHOs characterized by zero-point energy. Let us consider the properties of QHO in detail (see also [19] [24] [25]).

1) The energy of QHO is equal to $\hbar\Omega_{QHO}/2$, the energy is referred to as zero-point energy. This expression for energy of QHO coincides with the expres-

sion for energy of object having angular momentum $\hbar$ and performing oscillations with frequency $\boldsymbol{\Omega}_{QHO}$ [26].

2) The QHO has mass m_{QHO} associated with the energy of QHO.

3) The existence of electric polarization of physical vacuum [3] suggests that QHO is an electric dipole (let us denote the electric dipole moment as $\mathbf{d}_{QHO}$).

4) There are some phenomena which testify that QHOs constituting the physical vacuum must have precessing spin for example: 1) the Cherenkov effect [27], the production of photons having spin by an electron moving at a superluminal speed while saving the value of its own spin; 2) the creation of virtual photons having precessing spin [21] by a quantum entity while saving the value of its own spin. If the principle of conservation of angular momentum holds true in the physical vacuum, then spin of virtual photon consists of spins of QHOs that constitute this vacuum.

That is, it may be supposed that QHO has spin $\mathbf{S}_{QHO}$ and the frequency of oscillations $\boldsymbol{\Omega}_{QHO}$ is the precession frequency of $\mathbf{S}_{QHO}$. That is, QHO as well as a virtual photon is a spin vortex.

5) Since QHO is a spin vortex, then for it as well as for analogous characteristics (spin, electric dipole moment, the precession frequency of spin, the deflection angle) of other spin vortices (photon, virtual photon)) the following takes place [24] [25] [28].

$$\mathbf{d}_{QHO} \uparrow\downarrow \mathbf{S}_{QHO}. \tag{13}$$

As electric field $\mathbf{E}_{QHO}$ inside the electric dipole is antiparallel to its electric dipole moment, *i.e.* $\mathbf{E}_{QHO} \uparrow\downarrow \mathbf{d}_{QHO}$ [10], from condition (13) we have:

$$\mathbf{E}_{QHO} \uparrow\uparrow \mathbf{S}_{QHO}. \tag{14}$$

$$\boldsymbol{\Omega}_{QHO} \parallel \mathbf{u}, \tag{15}$$

where u is the speed of QHO,

$$\sin\theta = u/c, \tag{16}$$

where θ is the angle between $\mathbf{S}_{QHO}$ and $\boldsymbol{\Omega}_{QHO}$ (angle of deflection), c is the speed of light.

6) That QHO has an electric dipole moment means that there is a repulsive force inside the QHO balancing the attractive Coulomb force between oppositely charged parts inside the QHO. The existence of such repulsive force may be treated as the existence of omniradial tensions inside the QHO.

7) It is shown in [26] that there is a complete analogy between the structures of formulas describing the magnetic interactions of current-carrying wires and the structures of formulas describing the interactions of vortices in an ideal incompressible liquid with positive density and negative pressure. The above considered properties of QHOs suggest that the physical vacuum consisting of QHOs is similar to such a liquid. The density ρ of this vacuum is formed by mass m_{QHO} of QHO; negative pressure p is a result of omniradial tensions inside the QHO. Hydrodynamically, the stationary motion of this vacuum as a

continuum may be described in the absence of shear viscosity as:

$$\rho u^2/2 - p = const\,. \tag{17}$$

Let us deduce the relationship between the speed of QHOs and magnetic induction by comparing the characteristics of the magnetic field and both force and kinematic characteristics of the medium described by Equation (17) [24] [25] [29]. These equations are written, first, for the vacuum whose permeability equals 1, and, secondly, they are written in the CGSE system of units, so that the equations include constant c which is a characteristic of the medium whose motion results in magnetic phenomena [10].

The magnetic induction $\mathbf{B}$ generated by a loop with current I [10] is determined by the Biot-Savart law and in the CGSE system of units defined as $\mathbf{B} = \frac{I}{c}\int_{L'} \frac{\mathrm{d}\mathbf{l}\times\mathbf{r}}{r^3}$, where L' is the length of the loop, $\mathrm{d}\mathbf{l}$ is the wire element, $\mathbf{r}$ is a radius vector from $\mathrm{d}\mathbf{l}$ to the point of observation. The field of velocities $\mathbf{u}$ generated by a closed vortex line having circulation $\mathbf{\Gamma}$ along an arbitrary loop enclosing the vortex line is defined [26] as $\mathbf{u} = \frac{\Gamma}{4\pi}\int_{L'} \frac{\mathrm{d}\mathbf{l}\times\mathbf{r}}{r^3}$, where $\mathrm{d}\mathbf{l}$ is an infinitesimal vector element of the vortex line, L' is the length of the line. Equating the expressions for $\mathbf{B}$ and $\mathbf{u}$, we obtain the relationship between $\mathbf{\Gamma}$ and $\mathbf{I}$:

$$\mathbf{\Gamma} = \mathbf{I}\sqrt{4\pi}\Big/\left(c\sqrt{\rho}\right). \tag{18}$$

Note. As shown in [24] [25], the electric current $\mathbf{I}$ creates the circulation $\mathbf{\Gamma}$ in the physical vacuum consisting of QHOs due to precession motion of spins of virtual photons (virtual particles pairs) that are created by moving charged quantum entities in the current-carrying wire.

The force F_Γ acting on a unit length of either of the two infinite mutually parallel vortex lines having the same values of circulation $\mathbf{\Gamma}$ equals: $F_\Gamma = \rho\Gamma^2/(2\pi r_w)$, where r_w is the distance between the vortex lines with circulation $\mathbf{\Gamma}$ [26]. The force F_I acting on a unit length of either of the two infinite mutually parallel current-carrying wires having the same values of current $\mathbf{I}$ equals: $F_I = 2I^2/(r_w c^2)$, where r_w is here the distance between the current-carrying wires [10]. Equating the expressions for F_Γ and F_I and taking into account Equation (18), we obtain.

$$\mathbf{B} = \mathbf{u}\sqrt{4\pi\rho}\,. \tag{19}$$

Thus the motion of physical vacuum consisting of QHOs characterized by zero-point energy is a cause of magnetic phenomena.

The QHO characteristics considered in this section are given in **Figure 4**: spin $\mathbf{S}_{QHO}$, frequency of the spin precession $\mathbf{\Omega}_{QHO}$, electric dipole moment $\mathbf{d}_{QHO}$, mass m_{QHO}, QHO velocity $\mathbf{u}$, electric field inside the QHO $\mathbf{E}_{QHO}$, angle of deflection θ, magnetic vector potential $\mathbf{A}$, $\mathbf{M}_{QHO}$ is the moment causing precession of spin. The latter two characteristics are considered in Section 4.

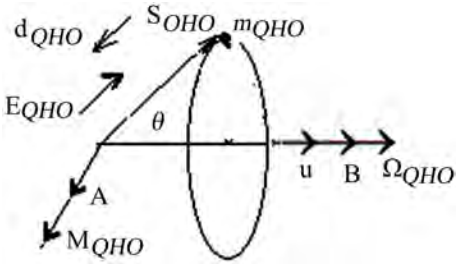

Figure 4. The characteristics of a quantum harmonic oscillator (QHO): $\mathbf{S}_{QHO}$ is spin, m_{QHO} is the mass, on the assumption that it is a point-like mass, $\boldsymbol{\Omega}_{QHO}$ is the precession frequency, $\mathbf{d}_{QHO}$ is the electric dipole moment, **u** is the velocity of QHO, **A** is the magnetic vector potential, θ is the angle of deflection, $\mathbf{E}_{QHO}$ is the electric field inside the QHO, $\mathbf{M}_{QHO}$ is the moment causing precession of spin $\mathbf{S}_{QHO}$, **B** is magnetic induction.

4. Results

4.1. Quantum Correlations

Let us prove that the properties of quantum correlations considered in Introduction are in accordance with the properties of spin supercurrent (see also the study by L. Boldyreva [30]).

1) The quantum correlation takes place between quantum entities having equal frequencies of their wave functions. As follows from [30], the precession frequency ω_v of spin of the virtual photon (pair of virtual particles) created by the quantum entity equals the frequency ω_q of wave function of the entity:

$$\omega_q = \omega_v . \tag{20}$$

Consequently, the first property of quantum correlation is in accordance with condition (7) of effective action of spin supercurrent: the equality of the precession frequencies of interacting spin structures.

2) The quantum correlation between photons takes place at definite mutual polarization ($\mathbf{E}_{ph}$) of photons. Due to transverse orientation of photon spin $\mathbf{S}_{ph}$ ($\mathbf{S}_{ph} \perp \mathbf{c}$) it holds that $\mathbf{S}_{ph} \uparrow\uparrow \mathbf{E}_{ph}$. Thus the quantum correlation between photons takes place at definite mutual orientation of spins of photons. If to take into account that photon's frequency $\boldsymbol{\omega}_{ph}$ is oriented along **c**, $\boldsymbol{\omega}_{ph} \uparrow\uparrow \mathbf{c}$, then $\mathbf{S}_{ph} \perp \boldsymbol{\omega}_{ph}$. Consequently, quantum correlation takes place at definite mutual orientation of photons' frequencies. This property is in accordance with the definition of spin supercurrent, see Equation (1), according to which the orientation of spin supercurrent relates to the orientation of the precession frequencies of spins of interacting spin structures.

3) The quantum correlations take place independent of the distance between the interacting quantum entities. This property agrees with property 4 of spin supercurrent.

4) The quantum correlations have non-electric and non-magnetic nature [4] [5]. This property is in accordance with property 5 of spin supercurrent.

5) The speed of quantum correlations is greater than the speed of light. As it

follows from experiments [7], the speed of quantum correlations is 10^4 times greater than the speed of light. This property is in accord with condition (12) (property 7 of spin supercurrent).

6) The relation between the changes in phases and frequencies of waves in the two-photon interference, associated with quantum correlations, is analogous to the changes in phases (angles of precession) and frequencies of spin precession in spin structures under action of spin supercurrent. **Figure 5** shows a diagram of experimental setup, which illustrates two-photon interference provided both beams of photons undergo phase delays [4].

Fields γ_1 and γ_2 of frequency ω_γ and also fields ξ_1 and ξ_2 of frequency ω_ξ are mixed by respective beam splitters. The detectors and coincidence circuit measure the correlation of intensities of output fields γ and ξ, the correlation being dependent on phase delays ϑ_1 and ϑ_2.

Depending on the statistics of incident beams of light, two types of interference may take place: one with phase $\vartheta_1 - \vartheta_2$, the other with phase $\vartheta_1 + \vartheta_2$. The first interference is referred to as the Hanbury Brown and Twiss intensity interference, the second one is called the two-photon interference. Under definite conditions, both types of interference are a result of conversion by beam splitters of fluctuations of phases of input fields into fluctuations of intensities of output fields [4]. Let us consider these conditions. Let fields γ_k and ξ_k ($k = 1, 2$) have constant unit amplitudes and phases $x_k(t)$ and $z_k(t)$ drifting in time t. That is the following takes place: $\gamma_k(t) = \exp\left[-ix_k(t)\right]$, $\xi_k(t) = \exp\left[-iz_k(t)\right]$. Then the first condition for the ordinary interference of intensities is determined by equalities:

$$x_1 = z_1, \quad x_2 = z_2. \tag{21}$$

The second condition is as follows:

$$x_1 + z_1 = x_2 + z_2, \tag{22}$$

that is, fluctuations of light beam phases occur in such a way that the sum of the phases remains constant.

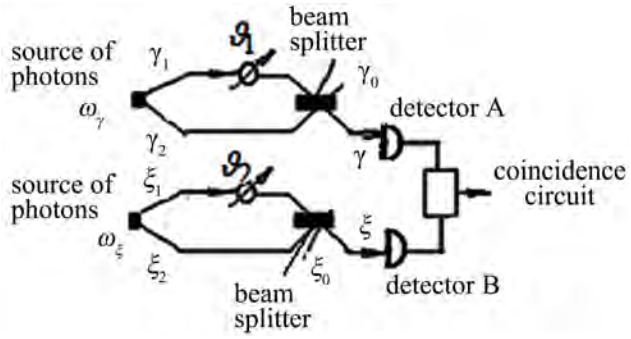

Figure 5. Diagram of a four-mode intensity interferometer. γ_1 and γ_2, ξ_1 and ξ_2 are input beams of light; ϑ_1 and ϑ_2 are phases of delay of light beams; ω_γ is the frequency of output beam γ; ω_ξ is the frequency of output beam ξ; γ_0 and ξ_0 may be classified as idle modes of respective beams. The detectors and coincidence circuit measure the correlation of intensities.

Equalities (21) can be called the conditions of "classical" correlation; it may be associated with thermal fluctuations; condition (22) is a condition of anticorrelation of phases which is a quantum phenomenon (related with quantum correlations [4]). From condition (22) it follows that for the changes in the phase of field γ, Δx, and field ξ, Δz, the following is valid:

$$\Delta x = -\Delta z . \tag{23}$$

Equality (23) is similar to Equation (11) describing the property of spin supercurrent (property 6 of spin supercurrent).

The frequencies of beams in the experiment on the two-photon interference as well as the phases drift in opposite directions, which is in accordance with condition (10) of property 6 of spin supercurrent.

Thus all properties of quantum correlations are in accordance with the properties of spin supercurrents.

4.2. Magnetic Vector Potential

According to condition (15) and Equation (19), in magnetic field **B** two types of motion of QHO that constitute physical vacuum take place: the translational motion with velocity $\mathbf{u} = \mathbf{B}/\sqrt{4\pi\rho}$ and precession of the QHO spin with frequency $\boldsymbol{\Omega}_{QHO}$. The value of $\boldsymbol{\Omega}_{QHO}$ is determined: first, by speed u of QHO and, secondly, by spin supercurrent emerging between the same QHO, on the one hand, and the virtual photons created by charged quantum entities constituting the current which, in turn, creates the magnetic field (or by "magnetic" electrons if the magnetic field is created by a permanent magnet), on the other hand. As spin supercurrent is not shielded by electromagnetic screens, the precession of QHO spin may exist in the physical vacuum under shielding of magnetic field, that is at **B** = 0 (**u** = 0).

For the description of magnetic vector potential let us introduce moment $\mathbf{M}_{QHO}$ causing the precession of spin of QHOs that constitute the physical vacuum (see **Figure 4**):

$$\mathbf{M}_{QHO} = \boldsymbol{\Omega}_{QHO} \times \mathbf{S}_{QHO} . \tag{24}$$

As $curl\mathbf{M}_{QHO} \uparrow\uparrow \boldsymbol{\Omega}_{QHO}$, then taking into account Equations (15) and (19) and introducing factor of proportionality b_s, we may write: $\mathbf{B} = curl\left(b_s \mathbf{M}_{QHO}\right)$. As according to definition of magnetic vector potential **A**, $\mathbf{B} = curl\mathbf{A}$, it may be assumed that:

$$\mathbf{A} = b_s \mathbf{M}_{QHO} . \tag{25}$$

Note. Using Equations (16), (19) and (24), magnetic induction B may be expressed as $B = M_{QHO}\sqrt{4\pi\rho}\cdot c/\left(\Omega_{QHO}\cdot S_{QHO}\right)$.

Let us return to **Figure 2** and explain the emergence of interferometer rings at the output of interferometer, that is, explain a change in wave characteristics of quantum entities of beam C_2 moving in region δ (in the region of action of field-free vector potential). To this end let us denote the precession frequency of spin of QHO in region δ as $\left(\Omega_{QHO}\right)_\delta$ and precession frequency of spin of

virtual photon created by a quantum entity of beam C_2 as $(\omega_v)_{vp}$ (according to equality (20) $(\omega_v)_{vp}$ is also the wave function frequency of quantum entities).

As a result of action of spin supercurrent between the virtual photon and QHO located in region δ and according to condition (5), the following takes place:

$$\left|\left(\Omega_{QHO}\right)_{\delta}-\left(\omega_v\right)_{vp}\right| \geq \left|\left(\Omega_{QHO}\right)'_{\delta}-\left(\omega_v\right)'_{vp}\right|, \tag{26}$$

where $\left(\Omega_{QHO}\right)'_{\delta}$ and $\left(\omega_v\right)'_{vp}$ are the values of respectively $\left(\Omega_{QHO}\right)_{\delta}$ and $(\omega_v)_{vp}$ after the action of spin supercurrent. As quantum entities of beams C_1 and C_2 at the output of the source of quantum entities have equal wave function frequencies, $(\omega_v)_{vp}$, the difference $\Delta(\omega_v)_{vp}$ in those frequencies at the input of interferometer according to inequality (26) is determined as: $\Delta(\omega_v)_{vp}=(\omega_v)'_{vp}-(\omega_v)_{vp}$. This difference results in appearance of interference rings.

It should be noted that the characteristics of quantum entities placed in the region of action of magnetic vector potential influence the value of the magnetic vector potential in the region. Let us prove it. According to Equation (26), in general the following holds:

$$\left(\Omega_{QHO}\right)_{\delta} \neq \left(\Omega_{QHO}\right)'_{\delta}. \tag{27}$$

Consequently, according to Equations (24) and (27), at placing of quantum entities in region δ of the physical vacuum the moment causing the precession of spin of QHO in region δ will be changed from $\left(\boldsymbol{\Omega}_{QHO}\right)_{\delta}\times\mathbf{S}_{QHO}$ to $\left(\boldsymbol{\Omega}_{QHO}\right)'_{\delta}\times\mathbf{S}_{QHO}$. Thus according to Equation (27) a problem of measurement of magnetic vector potential arises, because the measurement system may influence the value of the magnetic vector potential.

4.3. Near-Field Antenna Effect

The explanation of near-field antenna effect as well as of magnetic vector potential effect is based on the properties of the physical vacuum consisting of QHOs characterized by zero-point energy.

The antenna generating electromagnetic oscillations is an oscillating electric dipole [14] [15]. This electric dipole interacts with QHOs located near antenna, like with electric dipoles. As a result of this interaction, the oscillations of electric dipole moment $\left(\mathbf{d}_{QHO}\right)_a$ of QHOs located near antenna arise, that is we have

$$\frac{\partial\left(\mathbf{d}_{QHO}\right)_a}{\partial t} \neq 0. \tag{28}$$

As according to condition (13) $\left(\mathbf{d}_{QHO}\right)_a \uparrow\downarrow \left(\mathbf{S}_{QHO}\right)_a$, the following takes place in the physical vacuum consisting of QHOs:

$$\frac{\partial\left(\mathbf{S}_{QHO}\right)_a}{\partial t} \neq 0, \tag{29}$$

where $\left(\mathbf{S}_{QHO}\right)_a$ is spin of QHO located near antenna. The change in $\left(\mathbf{S}_{QHO}\right)_a$ means a change in precession and deflection angles of the precessing spins of QHOs located near antenna. According to Equation (1), spin supercurrent J emerges between QHOs located near antenna, on the one hand, and QHOs located in other regions of physical vacuum, on the other hand. As a result of action of spin supercurrent, the characteristics of spin $\left(\mathbf{S}_{QHO}\right)_{phys.vac.}$ of QHOs located in other regions of physical vacuum change, that is, the following takes place in other regions:

$$\frac{\partial\left(\mathbf{S}_{QHO}\right)_{phys.vac.}}{\partial t} \neq 0. \tag{30}$$

According to condition (14), the electric field $\left(\mathbf{E}_{QHO}\right)_{phys.vac.}$ relates to spin $\left(\mathbf{S}_{QHO}\right)_{phys.vac.}$ of QHO, and it follows from Equation (30):

$$\frac{\partial\left(\mathbf{E}_{QHO}\right)_{phys.vac.}}{\partial t} \neq 0. \tag{31}$$

Thus, according to Equations (1) and (28)-(31), electric oscillations with characteristics of electric oscillations generated by antenna emerge in the physical vacuum. That is, the following transformations take place in the physical vacuum:

$$\frac{\partial\left(\mathbf{d}_{QHO}\right)_a}{\partial t}\left(\frac{\partial\left(\mathbf{S}_{QHO}\right)_a}{\partial t}\right) \neq 0 \Rightarrow J \neq 0 \Rightarrow \frac{\partial\left(\mathbf{S}_{QHO}\right)_{phys.vac.}}{\partial t}\left(\frac{\partial\left(\mathbf{E}_{QHO}\right)_{phys.vac.}}{\partial t}\right) \neq 0 \tag{32}$$

These electric oscillations accompany spin supercurrent; consequently, the speed of their spreading in the physical vacuum consisting of QHOs equals the speed of spin supercurrent, which is greater than the speed of light, see Equation (12). It is a little similar to Cherenkov's radiation [27]: the electron moving at a speed greater than the speed of light radiates photons. If to observe only radiated photons, we discover that the speed of motion of photons is greater than the speed of light.

Note. The researchers of near-field antenna effect discover also the oscillation of gravitational field near antenna [31]. Let us discuss this phenomenon on the basis of properties of QHOs.

Due to the action of spin supercurrent in the near antenna region, which equalizes respectively the angles of precession and angles of deflection of precessing spins (Equation (1)), the orientation of QHOs' spins in the same direction in the antenna region may take place (let us denote the total spin of oriented QHOs' spins as $\left(\mathbf{S}_{QHO}\right)_{total}$). According to condition (13), the orientation of total electric dipole moment $\left(\mathbf{d}_{QHO}\right)_{total}$ of the QHOs in the region also takes place:

$$\left(\mathbf{d}_{QHO}\right)_{total} \uparrow\downarrow \left(\mathbf{S}_{QHO}\right)_{total}. \tag{33}$$

In an external nonhomogeneous electric field $\mathbf{E}_e$, the force $\mathbf{F}_{QHO}$ acts on these QHOs. The force $\mathbf{F}_{QHO}$ is determined [10] as

$$\mathbf{F}_{QHO} = \left(\left(\mathbf{d}_{QHO}\right)_{total} \nabla\right)\mathbf{E}_e , \tag{34}$$

where ∇ is the nabla operator. In particular, if $\left(\mathbf{S}_{QHO}\right)_{total}$ directs towards the Earth, then in the negative electric field of the Earth the force $\mathbf{F}_{QHO}$ acts oppositely to the gravitation force. As all quantum entities create virtual photons which are vortices in the physical vacuum consisting of QHOs, the force $\mathbf{F}_{QHO}$ emerging in this vacuum will act on the virtual photons and consequently on the quantum entities creating the virtual photons.

As an example of action of force $\mathbf{F}_{QHO}$, let us consider the results of experiments on gyroscope's rotations around the vertical axis relative to the Earth [32]. At the right-hand rotation, the decrease in weight of gyroscope took place. The magnitude of decrease in weight did not depend on shielding the gyroscope from external magnetic field (0.35 G). That is, the change in weight was not of magnetic nature. This phenomenon can be accounted for by the emergence of force $\mathbf{F}_{QHO}$ under the action of the electric field of the Earth. Due to the Barnett effect [33], at rotation of gyroscope the orientation of spins of the QHOs at the location of gyroscope takes place. At the right-hand rotation these spins are pointed downwards, that is towards the Earth. If to take into account that the surface of Earth has a negative charge, then, according to Equations (33) and (34), force $\mathbf{F}_{QHO}$ acting on QHOs that constitute this vacuum is directed from the Earth, that is, opposite to the vector of gravitation. In the experiments, it may look as a decrease in the weight of the objects in this region of vacuum.

5. Conclusions

Quantum correlations between quantum entities may be performed by spin supercurrent emerging between virtual photons (virtual particles pairs) created by those quantum entities.

Magnetic vector potential is proportional to the moment causing the precession of spin of quantum harmonic oscillators (QHOs), which constitute the physical vacuum and are characterized by zero-point energy; in the region of non-zero magnetic field, the frequency of this precession is oriented along the direction of magnetic field. The spin supercurrent emerging between these QHOs and virtual photons (virtual particles pairs) produced by the quantum entities creating magnetic field affects the frequency of this precession.

The near-field antenna effect takes place as a result of action of spin supercurrent between quantum harmonic oscillators (that constitute the physical vacuum) located near antenna, on the one hand, and quantum harmonic oscillators located in other regions, on the other hand. The spin supercurrent gives rise to oscillations of electric field of quantum harmonic oscillators, the latter being electric dipoles. Thus, electric oscillations may spread at the speed of spin supercurrent in the physical vacuum consisting of quantum harmonic oscillators characterized by zero-point energy. As spin supercurrent is *an inertia free process*, its speed may be greater than the speed of light, which does not contradict postulates of special relativity that set limits to the speed of inertial

systems only.

(It is a little similar to Cherenkov's radiation: the electron moving at a speed greater than the speed of light in the medium radiates photons. If to observe only radiated photons, we discover that the speed of motion of photons is greater than the speed of light.)

Acknowledgements

The author is grateful to Mr. Mikhail Boldyrev for his assistance in translating this paper into English.

Conflicts of Interest

The author declares no conflicts of interest regarding the publication of this paper.

References

[1] Heisenberg, W. (1927) *Zeitschrift für Physik*, **43**, 172-198. (In German) https://doi.org/10.1007/BF01397280

[2] Schrödinger, E. (1936) *Mathematical Proceedings of the Cambridge Philosophical Society*, **32**, 446-452.

[3] Wichmann, E.H. (1971) Quantum Physics. Berkeley Physics Course, McGraw-Hill Book Company, New York.

[4] Klyshko, D.N. (1994) *Physics Uspekhi*, **37**, 1097-1122. https://doi.org/10.1070/PU1994v037n11ABEH000054

[5] Belinskii, A.V. (2003) *Physics Uspekhi*, **46**, 877-881. https://doi.org/10.1070/PU2003v046n08ABEH001393

[6] Tittel, W., Brendel, J., Gisin, B., *et al.* (1998) *Physical Review A*, **57**, 3229. https://doi.org/10.1103/PhysRevA.57.3229

[7] Scarani, V., Tittel, W., Zbinden, H. and Gisin, N. (2000) *Physics Letters A*, **276**, 1-7. https://doi.org/10.1016/S0375-9601(00)00609-5

[8] Born, M. (1962) Einstein's Theory of Relativity. Dover Publications, New York.

[9] Einstein, A., Podolsky, B. and Rosen, N. (1935) *Physical Review*, **47**, 777. https://doi.org/10.1103/PhysRev.47.777

[10] Purcell, E.M. (1965) Electricity and Magnetism. Berkeley Physics Course, Vol. 2, McGraw-Hill Book Company, New York.

[11] Ehrenberg, W. and Siday, R.E. (1949) *Proceedings of the Physical Society* (*London*) *B*, **62**, 8-21.

[12] Aharonov, Y. and Bohm, D. (1959) *Physical Review*, **115**, 485-491. https://doi.org/10.1103/PhysRev.115.485

[13] Chambers, G. (1960) *Physical Review Letters*, **5**, 3. https://doi.org/10.1103/PhysRevLett.5.3

[14] Walker, W.D. (1999) Superluminal Near-Field Dipole Electromagnetic Fields. *International Workshop "Lorentz Group CPT and Neutrinos" Zacatecas*, Mexico, 23-26 June 1999, 16 p.

[15] Walker, W.D. (2000) Experimental Evidence of Near-Field Superluminally Propagating Electromagnetic Fields. In: Amoroso, R.L., *et al.*, Eds., *Gravitation and Cos-*

mology: *From the Hubble Radius to the Planck Scale*, Kluwer Academic Publishers, Printed in Netherlands, 189-196.

[16] Borovic-Romanov, A.S., Bunkov, Yu.M., Dmitriev, V.V., Mukharskii, Yu.M. and Sergatskov, D.A. (1989) *Physical Review Letters*, **62**, 1631. https://doi.org/10.1103/PhysRevLett.62.1631

[17] Bunkov, Yu.M. (2009) *Journal of Physics*: *Condensed Matter*, **21**, Article ID: 164201. https://doi.org/10.1088/0953-8984/21/16/164201

[18] Dmitriev, V.V. and Fomin, I.A. (2009) *Journal of Physics*: *Condensed Matter*, **21**, Article ID: 164202. https://doi.org/10.1088/0953-8984/21/16/164202

[19] Puthoff, H.E. (1989) *Physical Review A*, **40**, 4857-4862. https://doi.org/10.1103/PhysRevA.40.4857

[20] Einstein, A. and Stern, O. (1913) *Annelen der Physik*, **345**, 551-560. https://doi.org/10.1002/andp.19133450309

[21] Milonni, P.W. (1994) The Quantum Vacuum. Academic Press, Inc., Harcourt Brace & Company Publishers, Cambridge, MA.

[22] Weber, M.H. and Lynn, K.G. (2000) *Radiation Physics and Chemistry*, **58**, 749-753. https://doi.org/10.1016/S0969-806X(00)00252-8

[23] Doctorovitch, Z.I. (2005) *Engineering & Automation*, No. 4, 115-118. (In Russian)

[24] Boldyreva, L.B. (2018) *International Journal of Physics*, **6**, 128-138.

[25] Boldyreva, L.B. (2019) *Journal of Modern Physics*, **10**, 20-34.

[26] Sedov, L.I, (1971-1972) A Course in Continuum Mechanics. Wolters-Noordhoff, Groningen, 1-4.

[27] Čerenkov, P.A. (1937) *Physical Review*, **52**, 378. https://doi.org/10.1103/PhysRev.52.378

[28] Boldyreva, L.B. (2017) *International Journal of Physics*, **5**, 141-146. http://pubs.sciepub.com/ijp/5/4/6/

[29] Boldyreva, L.B. and Sotina, N.B. (1992) *Physics Essays*, **5**, 510-513.

[30] Boldyreva, L.B. (2014) *International Journal of Quantum Information*, **12**, Article ID: 1450007. https://doi.org/10.1142/S0219749914500075

[31] Walker, W.D. and Dual, J. (1998) Propagation Speed of Longitudinally Oscillating Gravitational and Electrical Fields. https://arxiv.org/abs/gr-qc/9706082v2

[32] Hayasaka, H. and Takeuchi, S. (1989) *Physical Review Letters*, **63**, 2701-2704. https://doi.org/10.1103/PhysRevLett.63.2701

[33] Barnett, S.J. (1915) *Physical Review*, **6**, 239-270.

Journal of Modern Physics, 2019, 10, 145-156
http://www.scirp.org/journal/jmp
ISSN Online: 2153-120X
ISSN Print: 2153-1196

Further Improvement of Reflection Efficiency of a Magnetic Mirror and Replenishment against Loss of Escaping Deuteron Ions

Mitsuaki Nagata, Keiichi Sawada

Soft Creator Company, Kyoto, Japan
Email: nagata@heian-kogyo.jp

How to cite this paper: Nagata, M. and Sawada, K. (2019) Further Improvement of Reflection Efficiency of a Magnetic Mirror and Replenishment against Loss of Escaping Deuteron Ions. *Journal of Modern Physics*, **10**, 145-156.
https://doi.org/10.4236/jmp.2019.102011

Received: December 6, 2018
Accepted: February 24, 2019
Published: February 27, 2019

Abstract

We reported previously the idea to improve reflection-ability of a magnetic mirror by installing a cyclotron resonance space in the front part of the mirror. However, since the previous analysis was insufficient from the examination after that, we complement the following two things in this work: 1) A simpler procedure of design to make a supplemental magnetic mirror with the simplest magnetic configuration, compared with the procedure reported previously. 2) A peculiar characteristic arising only in reflection of a nonrelativistic charged particle (a deuteron ion).

Keywords

Magnetic Mirror, Cyclotron Resonance Heating, Reflection and Replenishment of Deuteron Ions

1. Introduction

We found the term seen in the rear of (9) to accelerate only a relativistic charged particle rapidly at a cyclotron resonance point and reported previously [1] applying a work of the term to decreasing the half-vertical angle (called the loss angle) of the loss cone of a magnetic mirror by installing a cyclotron resonance space within. However, based on the examination after that, we would complement two things here. One is about the simplest supplemental magnetic mirror. The procedure of design is mentioned in §3.1 together with **Figure 1**. Another thing is that we missed in Ref. [1] a factor which must be taken into consideration with respect to reflection of a nonrelativistic particle (a deuteron ion). The factor is that an electric field being installed in the front part of a magnetic mir-

ror does both the work of taking out ions from inside of the loss cone into outside and the reverse work. When we inquired into this problem, we met with a peculiar characteristic with respect to reflection of a deuteron ion. This thing is mentioned in §3.2. Finally, we have proposed an idea about a means for replenishing a large quantity of deuteron ions from outside, in order to make the length of a supplemental magnetic mirror as short as possible.

2. Relativistic Cyclotron Resonance

We first describe theoretical expressions to be necessary for after analysis. The relativistic equation of motion

$$\begin{aligned}&\frac{\partial}{\partial t}\frac{m_e\boldsymbol{\upsilon}(t,t_0)}{\left[1-\upsilon(t,t_0)^2/c^2\right]^{1/2}}\\&=\frac{m_e\,\partial\boldsymbol{\upsilon}(t,t_0)/\partial t}{\left[1-\upsilon(t,t_0)^2/c^2\right]^{1/2}}+\frac{\left[m_e\,\boldsymbol{\upsilon}(t,t_0)/c^2\right]\upsilon(t,t_0)\partial\upsilon(t,t_0)/\partial t}{\left[1-\upsilon(t,t_0)^2/c^2\right]^{3/2}}\\&=-q\boldsymbol{E}(t)-q\boldsymbol{\upsilon}(t,t_0)\times\boldsymbol{B}\end{aligned}$$

is changed into (1) below by the help of the following two relationships:

1) The time derivative of energy with respect to a relativistic electron

$$\begin{aligned}&\frac{\partial}{\partial t}\frac{m_ec^2}{\left[1-\upsilon(t,t_0)^2/c^2\right]^{1/2}}=\frac{m_e\upsilon(t,t_0)\partial\upsilon(t,t_0)/\partial t}{\left[1-\upsilon(t,t_0)^2/c^2\right]^{3/2}}\\&=-q\boldsymbol{E}(t)\cdot\boldsymbol{\upsilon}(t,t_0)\end{aligned}$$

2) The integration of the above equation from t_0 to t

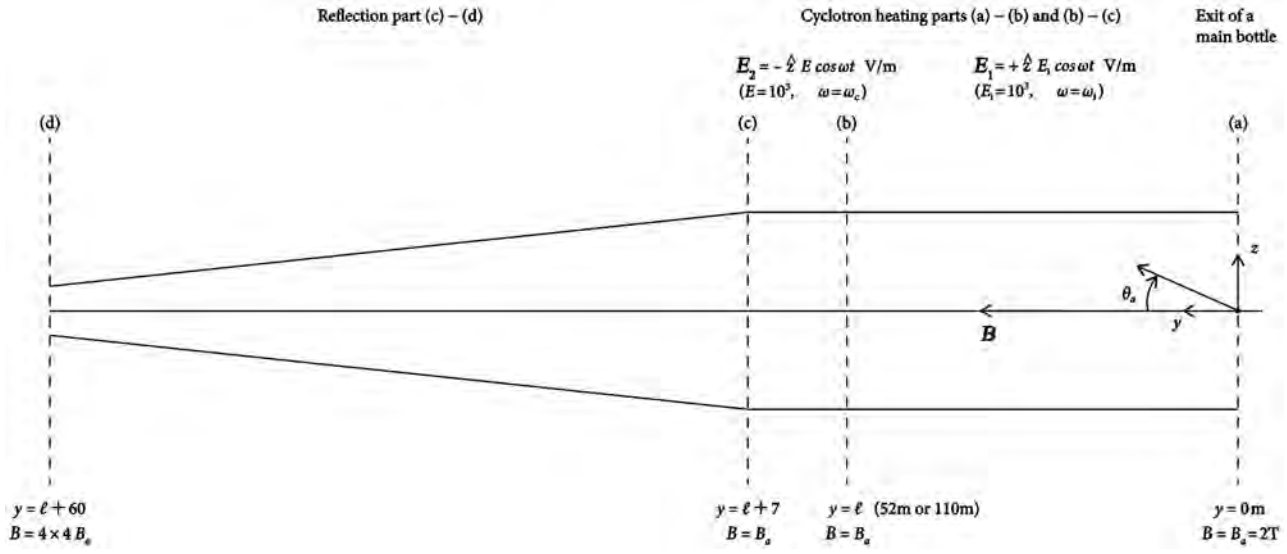

Figure 1. A supplemental magnetic mirror (a)-(d) for reclaiming charged particles to escape from the exit (plane (a)) of the main bottle. The half-vertical angle of the loss cone of mirror (c)-(d) is 14.5˚. It is tried to decrease the loss angle of mirror (a)-(d) from 14.5˚ to about 5˚ with the help of the electric fields $\boldsymbol{E}_1$ and $\boldsymbol{E}_2$. $\boldsymbol{E}_1$ is the electric field to accelerate deuteron ions, $\boldsymbol{E}_2$ is the electric field to accelerate electrons, ω_i is an ion cyclotron frequency and ω_c is an electron cyclotron frequency.

$$\frac{m_e c^2}{\left[1-\upsilon(t,t_0)^2/c^2\right]^{1/2}}-\frac{m_e c^2}{\left[1-\boldsymbol{\upsilon}_0^2/c^2\right]^{1/2}}=\int_{t_0}^{t}-q\boldsymbol{E}(t)\cdot\boldsymbol{\upsilon}(t,t_0)\,\mathrm{d}t$$

$$\left\{\frac{m_e}{\left[1-\boldsymbol{\upsilon}_0^2/c^2\right]^{1/2}}+\int_{t_0}^{t}\frac{-q\boldsymbol{E}(t)\cdot\boldsymbol{\upsilon}(t,t_0)}{c^2}\mathrm{d}t\right\}\frac{\partial\boldsymbol{\upsilon}(t,t_0)}{\partial t}+\boldsymbol{\upsilon}(t,t_0)\left(\frac{-q\boldsymbol{E}(t)\cdot\boldsymbol{\upsilon}(t,t_0)}{c^2}\right) \quad (1)$$
$$=-q\boldsymbol{E}(t)-q\boldsymbol{\upsilon}(t,t_0)\times\boldsymbol{B}$$

In the above four equations, m_e is the rest mass of an electron, $-q$ is the electron charge, c is the speed of light, $\boldsymbol{E}(t)$ is an electric field, $\boldsymbol{B}$ is a magnetic field, $\boldsymbol{\upsilon}(t,t_0)$ $(=\hat{x}\upsilon_x(t,t_0)+\hat{y}\upsilon_y(t,t_0)+\hat{z}\upsilon_z(t,t_0))$ is the velocity of an electron at time t after start with an initial velocity $\boldsymbol{\upsilon}_0$ $(=\hat{x}\upsilon_{0x}+\hat{y}\upsilon_{0y}+\hat{z}\upsilon_{0z})$ at time t_0, and $\upsilon(t,t_0)=\left|\boldsymbol{\upsilon}(t,t_0)\right|$.

Since a solution of (1), $\boldsymbol{\upsilon}(t,t_0)$, is to be given by a form of

$$\boldsymbol{\upsilon}(t,t_0)=\boldsymbol{\upsilon}_t+\boldsymbol{o} \qquad \begin{cases}\boldsymbol{\upsilon}_t=\boldsymbol{\upsilon}(t,t_0)_{(\boldsymbol{E}(t)=0)},\\ \boldsymbol{o}\text{ is a quantity which consists of components of }\boldsymbol{E}(t),\end{cases}$$

we neglect terms including products and squares with respect to components of $\boldsymbol{E}(t)$ in (1) and linearize (1) as

$$\frac{m_e}{\left(1-\dfrac{\boldsymbol{\upsilon}_0^2}{c^2}\right)^{\frac{1}{2}}}\frac{\partial\boldsymbol{\upsilon}(t,t_0)}{\partial t}+\left(\int_{t_0}^{t}\frac{-q\boldsymbol{E}(t)\cdot\boldsymbol{\upsilon}_t}{c^2}\mathrm{d}t\right)\frac{\partial\boldsymbol{\upsilon}_t}{\partial t}+\boldsymbol{\upsilon}_t\left(\frac{-q\boldsymbol{E}(t)\cdot\boldsymbol{\upsilon}_t}{c^2}\right) \quad (2)$$
$$=-q\boldsymbol{E}(t)-q\boldsymbol{\upsilon}(t,t_0)\times\boldsymbol{B}$$

First, we note the following problem which arises due to the linearization. It is that, in Figure 2 (shown after) for $\hat{z}\cdot\boldsymbol{\upsilon}(t,t_0)$ which is obtain from (2), maximum of $\hat{z}\cdot\boldsymbol{\upsilon}(t,t_0)$ goes over the speed c of light in long flight time. The magnitude of $\boldsymbol{\upsilon}(t,t_0)$ is estimated to be a function increasing together with time t under the resonance condition (an electric field frequency = a cyclotron frequency), and a mass increment per unit time is given by $-q\boldsymbol{E}(t)\cdot\boldsymbol{\upsilon}(t,t_0)/c^2$. Accordingly, we consider that the primary cause giving rise to this problem is underestimation in the linearization for the total mass $\left\{\dfrac{m_e}{\left[1-\boldsymbol{\upsilon}_0^2/c^2\right]^{1/2}}+\displaystyle\int_{t_0}^{t}\frac{-q\boldsymbol{E}(t)\cdot\boldsymbol{\upsilon}(t,t_0)}{c^2}\mathrm{d}t\right\}$ at time t. A more rapid increase of the total mass ought to reduce variation of $\left|\boldsymbol{\upsilon}(t,t_0)\right|$ to zero before $\left|\boldsymbol{\upsilon}(t,t_0)\right|$ arrives at the speed c of light.

We solve (2) for $\upsilon_z(t,t_0)$ and $\upsilon_y(t,t_0)$ under the following external force fields:

$$\begin{cases}\boldsymbol{E}(t)=-\hat{z}E\cos\omega t,\\ \boldsymbol{B}=\hat{y}B,\end{cases} \quad (3)$$

and under the following initial conditions at $t=t_0$ which are given by

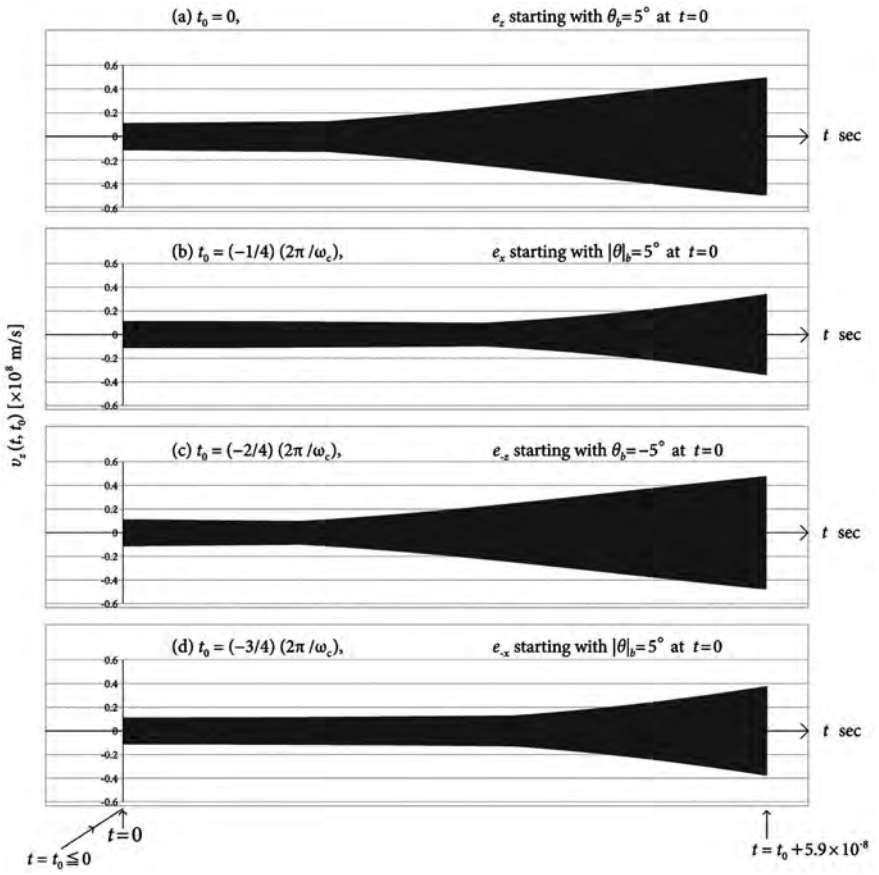

Figure 2. Dependence of $\upsilon_z(t,t_0)$ on t_0, based on Equation (6). The numerical conditions are: an initial velocity $\hat{z}\upsilon_{0z} = \hat{z}\upsilon\sin 5^\circ = \hat{z}0.105\times 10^8$ m/s in plane (b) at time t_0, $\boldsymbol{E}(t) = -\hat{z}10^3\cos\omega t$ V/m, $\boldsymbol{B} = 2$ T, $\omega_c/\omega = 1.0001$, the time variable $t = t_0 \sim t_0 + 7.0/(\upsilon\cos 5^\circ) = t_0 \sim t_0 + 5.9\times 10^{-8}$ sec. Note that the initial velocity at time t_0 is $+\hat{z}0.105\times 10^8$ m/s all in the four curves, but curves (a), (b), (c), (d) can be regarded to show velocity-variations for e_z, e_x, e_{-z}, e_{-x} starting with each different initial velocity from plane (b) at t = 0 ($\neq t_0$, expect for curve (a)).

$$\begin{cases} \boldsymbol{\upsilon}(t,t_0)_{(t=t_0)} = \hat{z}\upsilon_{0z} + \hat{y}\upsilon_{0y}, \\ \left(\dfrac{\partial \upsilon_z(t,t_0)}{\partial t}\right)_{(t=t_0)} = \dfrac{qE}{m}\cos\omega t_0 - \dfrac{qE}{mc^2}\upsilon_{0z}^2\cos\omega t_0, \\ \left(\text{where } m = m_e\left(1-\boldsymbol{\upsilon}_0^2/c^2\right)^{-1/2}\right). \end{cases} \tag{4}$$

The results are given in (5) and (6) below,

$$\upsilon_y(t,t_0) = \upsilon_{0y} + \upsilon_{0y}\upsilon_{0z}\frac{qE}{mc''}\left\{\frac{\sin\left[(\omega_c+\omega)(t-t_0)\right]}{2(\omega_c+\omega)} + \frac{\sin\left[(\omega_c-\omega)(t-t_0)\right]}{2(\omega_c-\omega)}\right\}. \tag{5}$$

Here, $c'' = c^2$ (The speed c of light appears always in the form of square in after analysis. Then, we have introduced the symbol c'' for c^2, because we would like to use c as the symbol for $\cos\omega t$), and $\omega_c = qB/m$. Since the second term

of (5) is extremely small compared with the first term υ_{0y} in after analysis under the conditions of $\omega \simeq \omega_c$ and $\omega_c(t-t_0) \gg 1$, $\upsilon_y(t,t_0)$ is regarded to be constant υ_{0y} in this work.

$$\upsilon_z(t,t_0) = a_1 s + (a_2 s)S^2 + (a_3 s)C^2 + (a_4 c)SC + a_5 tS + C_1 C + C_2 S, \tag{6}$$

(We have used $\boldsymbol{\upsilon}_t \left(= \hat{x}\upsilon_{0z}\sin\omega_c(t-t_0) + \hat{y}\upsilon_{0y} + \hat{z}\upsilon_{0z}\cos\omega_c(t-t_0)\right)$).

Here,

$$C = \cos\omega_c(t-t_0), S = \sin\omega_c(t-t_0), c = \cos\omega t, s = \sin\omega t,$$

$$a_1 = \frac{qE}{m}\frac{-\omega}{\omega_c^2-\omega^2},$$

$$a_2 = \frac{qE}{mc''}\frac{1}{\left(\omega_c^2-\omega^2\right)^2}\left[-2\omega_c^2\omega\upsilon_{0z}^2\right],$$

$$a_3 = \frac{qE}{mc''}\frac{1}{\left(\omega_c^2-\omega^2\right)^2}\left[\left(\omega_c^2\omega-\omega^3\right)\upsilon_{0z}^2\right],$$

$$a_4 = \frac{qE}{mc''}\frac{2\omega_c^3}{\left(\omega_c^2-\omega^2\right)^2}\left(-\upsilon_{0z}^2\right),$$

$$a_5 = \frac{qE}{mc''}\frac{\omega_c}{\omega_c^2-\omega^2}\left(\upsilon_{0z}^2\omega\sin\omega t_0\right),$$

$$C_1 = \upsilon_{0z} - a_1\sin\omega t_0 - a_3\sin\omega t_0,$$

$$C_2 = \frac{qE}{m\omega_c}\cos\omega t_0 - \frac{qE}{mc''}\frac{1}{\omega_c}\upsilon_{0z}^2\cos\omega t_0 - a_1\frac{\omega}{\omega_c}\cos\omega t_0 - a_3\frac{\omega}{\omega_c}\cos\omega t_0 - a_4\cos\omega t_0 - a_5 t_0.$$

Next let us obtain velocities perpendicular to the magnetic field at the resonance point $\omega \to \omega_c$, in the simple case where $t_0 = 0$:

$$\begin{aligned}\upsilon_{zr} &\equiv \lim_{\omega\to\omega_c}\upsilon_z(t,t_0)_{(t_0=0)} = \lim_{\omega\to\omega_c}(6)_{(t_0=0)} \\ &= \upsilon_{0z}C_0 + \frac{qE}{m}\left(1-\frac{\upsilon_{0z}^2}{c''}\right)\frac{1}{\omega_c}S_0 + \frac{qE}{m}\left(\frac{1}{-2\omega_c}\left(S_0-\omega_c tC_0\right)\right) \\ &\quad + \frac{qE}{m}\frac{\upsilon_{0z}^2}{c''}\left(\frac{1}{8\omega_c^2}\left(2\omega_c^3t^2S_0 - 4\omega_c^2tC_0 + 4\omega_cS_0 + 6\omega_cS_0^3\right)\right),\end{aligned} \tag{7}$$

$$\begin{aligned}\upsilon_{xr} &\equiv \lim_{\omega\to\omega_c}\upsilon_x(t,t_0)_{(t_0=0)} \\ &= \upsilon_{0z}S_0 + \frac{1}{2}\frac{qE}{m}tS_0 + \frac{qE}{m}\frac{\upsilon_{0z}^2}{c''}\left(\frac{1}{8\omega_c^2}\left(-4\omega_c^2tS_0 - 2\omega_c^3t^2C_0 - 6\omega_cS_0^2C_0\right)\right),\end{aligned} \tag{8}$$

$$\upsilon_r \equiv \left(\upsilon_{zr}^2+\upsilon_{xr}^2\right)^{\frac{1}{2}} \simeq \left\{\left[\upsilon_{0z} + \frac{qEt}{2m}\left(1-\frac{\upsilon_{0z}^2}{c''}\right)\right]^2 + \left[\frac{qEt}{m}\cdot\frac{\upsilon_{0z}^2}{c''}\cdot\frac{\omega_c t}{4}\right]^2\right\}^{1/2}, \quad (\omega_c t \gg 1). \tag{9}$$

Here, $C_0 = C_{(t_0=0)}$, $S_0 = S_{(t_0=0)}$, and $\upsilon_x(t,t_0)_{(t_0=0)}$ is given in Equation (15) of Ref. [1]. It should be noted that the second term within the root in (9) works

greatly only for a relativistic charged particle but the relativistic work of the second term will reduce more and more than the estimation in (9) as time t passes, because of the underestimation in (2) for the mass increment $-q\boldsymbol{E}(t)\cdot\boldsymbol{\upsilon}(t,t_0)/c''$ per unit time. Also, it must be noted that there is some difference between υ_r of (9) and an amplitude of a curve of $\hat{z}\cdot\boldsymbol{\upsilon}(t,t_0)$ seen in **Figure 2** (discussed in §3.1). However, we try designing a magnetic mirror for electrons based on a time-variation of an amplitude of $\hat{z}\cdot\boldsymbol{\upsilon}(t,t_0)$.

3. Design of a Supplemental Magnetic Mirror

In order to return back deuteron ions (called D^+ ions) and electrons escaping from a main bottle as many as possible, we consider installing (at the exit of the main bottle) a supplemental magnetic mirror which has a cyclotron resonance space within, as shown in **Figure 1**. We intend to reduce a loss angle of the supplemental mirror by increasing magnitudes of velocities perpendicular to a magnetic field $\boldsymbol{B}$ of the escaping particles within the cyclotron resonance space [2] [3] [4] [5]. The supplemental mirror is divided to three spaces by plane (j) (j = a, b, c, d). We define the *x, y, z* coordinate-system, as shown in plane (a). Also, we assume the *y*-coordinate and a strength B of a magnetic field $\boldsymbol{B}$ in each plane as shown in the figure. The magnetic field is regarded to be only in the $+y$-direction. Electric fields $\boldsymbol{E}_1$ and $\boldsymbol{E}_2$ are supplied within spaces (a) - (b) and (b) - (c), respectively. For an incident angle when a charged particle crosses plane (j), we denote an angle from $+y$-axis in the y-z plane by θ_j $\left(-90^\circ < \theta_j < 90^\circ\right)$ and a mere inclination from $+y$-axis by $|\theta|_j$ $\left(0 \le |\theta|_j < 90^\circ\right)$. A plasma temperature for fusion reaction to continue is assumed to be 4×10^8 K. Then, each mean thermal velocity for electrons and D^+ ions is about 1.2×10^8 m/s (= $\overline{\upsilon}$) and 2×10^6 m/s (= $\overline{\upsilon}_i$), respectively. To simplify after discussion, we assume that every electron and every D^+ ion are flying about within the main bottle, with each mean thermal velocity $\overline{\upsilon}$ and $\overline{\upsilon}_i$. Also, we disregard interactions between charged particles through Coulomb force within the supplemental mirror. Also in **Figure 1**, an electron or a D^+ ion is regarded to actually interact only with the electric field having ω_c or ω_i, respectively.

3.1. Reflection of Electrons

First we show in **Figure 2** the *z*-component of velocity, $\upsilon_z(t,t_0)$ given in (6), in the time range of ($t_0 \le t \le t_0 + 5.9\times10^{-8}$ sec) for an electron which starts from plane (b) with an initial velocity $\hat{z}\overline{\upsilon}\sin\theta_b + \hat{y}\overline{\upsilon}\cos\theta_b$ ($\overline{\upsilon} = 1.2\times10^8$ m/s, $\theta_b = +5^\circ$) at time t_0. The numerical conditions are shown in the figure. Curves (a), (b), (c), (d) are for four cases of t_0. Here, we note the following thing. In the short time range of $t_0 \sim 0$ (note that $t_0 \le 0$), both the velocity-magnitude and the gyration frequency of the electron hardly vary compared with each initial value at $t = t_0$. Therefore, since $\omega_c \simeq \omega$, curves (a), (b), (c), (d) can be regarded to show time-variations of the *z*-components of velocities perpendicular to $\boldsymbol{B}$ for four electrons (called e_z, e_x, e_{-z}, e_{-x}), starting from plane (b) with initial velocities shown below at time $t = 0$ ($\neq t_0$, except for curve

(a)):

1) $\hat{z}\bar{\upsilon}\sin\theta_b + \hat{y}\bar{\upsilon}\cos\theta_b$ ($\theta_b > 0$) for e_z,
2) $\hat{x}\bar{\upsilon}\sin|\theta|_b + \hat{y}\bar{\upsilon}\cos|\theta|_b$ ($|\theta|_b = |\theta_b|$) for e_x,
3) $\hat{z}\bar{\upsilon}\sin\theta_b + \hat{y}\bar{\upsilon}\cos\theta_b$ ($\theta_b < 0$) for e_{-z}, ($\theta_b = \pm 5^\circ$ in **Figure 2**)
4) $-\hat{x}\bar{\upsilon}\sin|\theta|_b + \hat{y}\bar{\upsilon}\cos|\theta|_b$ ($|\theta|_b = |\theta_b|$) for e_{-x},

(Note that the above four velocities are initial velocities at $t = 0$ all).

In the characteristics of curve (a) for e_z and curve (c) for e_{-z}, the difference is hardly seen, which is due to that the second term within the root in Equation (9) is much more predominant than the first term within the root in magnitude. We consider making these four electrons reflect by mirror (c) - (d) all. For this purpose, the four electrons must satisfy the following reflection condition:

$$\frac{\upsilon_{r(c)}}{\left(\upsilon_{r(c)}^2 + \bar{\upsilon}^2\cos^2\theta_c\right)^{1/2}} > \left(\frac{B_a}{4\times 4B_a}\right)^{1/2} \quad \text{or} \quad \upsilon_{r(c)} > 0.26\bar{\upsilon}\cos\theta_c \simeq 0.26\bar{\upsilon}\cos\theta_b \quad (10)$$

(The loss angle of mirror (c) - (d) is 14.5˚).

Here, $4\times 4B_a$ is the magnetic field in plane (d) and $\upsilon_{r(c)}$ is a minimum in velocity-magnitudes perpendicular to **B** of the four electrons when those cross plane (c). Accordingly, the electric field $\boldsymbol{E}_2\left(=-\hat{z}10^3\cos\omega t, \omega_c/\omega = 1.0001\right)$ in **Figure 1** must increase the value of $\upsilon_{r(c)}$ from $\bar{\upsilon}\left|\sin\theta_b\right|\left(=\bar{\upsilon}\left|\sin\pm 5^\circ\right| = 0.105\times 10^8 \text{ m/s}\right)$ at time $t = 0$ to $0.26\bar{\upsilon}\cos\theta_b$ (= 0.31 × 10^8 m/s). We regard the amplitudes of $\upsilon_z(t, t_0)$ in curves (a), (b), (c), (d) to show time-variations of velocity-magnitudes perpendicular to $\boldsymbol{B}$ of e_z, e_x, e_{-z}, e_{-x}, respectively. Then, the velocity-magnitudes in curves (a), (b), (c), (d) become larger than $0.26\cos\theta_b = 0.31\times 10^8$ m/s all when $t \simeq t_0 + 5.9\times 10^{-8}$ sec (A necessary length between planes (b) and (c) is about 7m). If the four electrons are reflected by mirror (c) - (d), we estimate that the most of electrons with $|\theta|_b = 5^\circ \sim 90^\circ$ will return to the main bottle.

Here, we would note the following thing. We tried obtaining from (9) values corresponding to the maxima of $\upsilon_z(t, t_0)$ near $t = t_0 + 5.9\times 10^{-8} \simeq 5.9\times 10^{-8}$ sec (because of $-\pi/\omega_c \simeq -10^{-11}$ sec) which are seen in curves (a) and (c) in **Figure 2** which is drawn based on (6).

$$\text{The maxima of } \upsilon_z(t, t_0) \simeq \begin{cases} 0.51\times 10^8 \text{ m/s in curve } (a), \\ 0.49\times 10^8 \text{ m/s in curve } (c). \end{cases}$$

Substituting into (9)

$$\begin{cases} c'' = \left(3\times 10^8 \text{ m/s}\right)^2, \ E = 10^3 \text{ V/m}, \ B = 2 \text{ T}, \\ \bar{\upsilon} = 1.2\times 10^8 \text{ m/s}, \\ \upsilon_{0z} = \bar{\upsilon}\sin\theta_b = \begin{cases} 0.105\times 10^8 \text{ m/s} & \theta_b = +5^\circ \text{ in curves } (a), \\ -0.105\times 10^8 \text{ m/s} & \theta_b = -5^\circ \text{ in curves } (c), \end{cases} \\ \upsilon_{0y} = \bar{\upsilon}\cos\theta_b = 1.192\times 10^8 \text{ m/s}, \\ q/m = 1.76\times 10^{11}\times\left(1 - \left(\upsilon_{0z}^2 + \upsilon_{0y}^2\right)/c''\right)^{1/2} = 1.61\times 10^{11} \text{ C/kg}, \\ \omega_c = qB/m = 3.22\times 10^{11} \text{ sec}^{-1}, \ t = 5.9\times 10^{-8} \text{ sec}, \end{cases}$$

we obtain

$$\upsilon_r = \begin{cases} 0.57\times10^8 \text{ m/s} & \text{for curve (a)}, \\ 0.55\times10^8 \text{ m/s} & \text{for curve (c)}. \end{cases}$$

There are some differences between the maxima in curves (a), (c) and the above values of υ_r. Then, considering that the differences have come from some approximation, we re-examined the calculation process from (15) of Ref. [1] and (6) to (7) and (8). However, there were no mathematical approximations. On the other hand, in the process from (7) and (8) to (9), there were two approximations below:

$$\left.\begin{aligned} &\frac{1}{2}\frac{qE}{m\omega_c}\left(1-\frac{\upsilon_{0z}^2}{c''}\right)S_0 \to 0, \\ &\frac{1}{4}\frac{qE}{m}\frac{\upsilon_{0z}^2}{c''}\left(\frac{3S_0^2}{\omega_c}\right)C_0 \to 0, \end{aligned}\right\} \quad (\omega_c t \to \infty).$$

However, the above approximations are right when $\omega_c t \simeq 2\times10^4$. So, we consider that the cause of "υ_r > the maximum of $\upsilon_z(t,t_0)$" is in that, of $\left(\upsilon_{zr}^2+\upsilon_{xr}^2\right)^{1/2}$ in (9), υ_{xr} is not zero when the magnitude of υ_{zr} becomes maximum.

3.2. Reflection of D^+ Ions

We aim a D^+ ion which starts from plane (a) in **Figure 1** with an initial velocity $\hat{z}\upsilon_{ioz}+\hat{y}\upsilon_{ioy} = \hat{z}\overline{\upsilon_i}\sin\theta_a + \hat{y}\overline{\upsilon_i}\cos\theta_a$ at time t_0 and goes to plane (b). An expression (called Equation (11)) for a D^+ ion corresponding to (6) is obtained by the following change for the symbols of an electron:

$$\begin{cases} -q \to q,\ -E \to E_i,\ \upsilon_{0z} \to \upsilon_{i0z}\left(=\overline{\upsilon_i}\sin\theta_a\right), \\ m_e \to m_i\left(=3680m_e\right),\ m \to m_{ii}\left(=m_i\Big/\left(1-\left(\upsilon_{i0z}^2+\upsilon_{i0y}^2\right)\Big/c''\right)^{1/2}\right), \\ \omega_c \to \omega_i\left(=qB/m_{ii}\right),\ \upsilon_z(t,t_0) \to \upsilon_{iz}(t,t_0). \end{cases} \quad (11)$$

We show in **Figure 3** dependences of $\upsilon_{iz}(t,t_0)$ on four cases of time t_0, for a D^+ ion which starts from plane (a) with an initial velocity $\hat{z}\overline{\upsilon_i}\sin\theta_a + \hat{y}\overline{\upsilon_i}\cos\theta_a\left(\theta_a=+3^\circ\right)$ at time t_0. The numerical conditions are shown in the figure. Based on the same consideration with in §3.1, the amplitudes in curves (a), (b), (c), (d) in **Figure 3** are regarded to show time-variations of velocity-magnitudes perpendicular to $\boldsymbol{B}$ of four D^+ ions (called $D_z^+, D_x^+, D_{-z}^+, D_{-x}^+$) starting from plane (a) with initial velocities shown below at time $t = 0$ ($\neq t_0$, except for curve (a)):

1) $\hat{z}\overline{\upsilon_i}\sin\theta_a + \hat{y}\overline{\upsilon_i}\cos\theta_a$ ($\theta_a > 0$) for D_z^+,
2) $\hat{x}\overline{\upsilon_i}\sin|\theta|_a + \hat{y}\overline{\upsilon_i}\cos|\theta|_a$ ($|\theta|_a = |\theta_a|$) for D_x^+, ($\theta_a = \pm3^\circ$ in **Figure 3**),
3) $\hat{z}\overline{\upsilon_i}\sin\theta_a + \hat{y}\overline{\upsilon_i}\cos\theta_a$ ($\theta_a < 0$) for D_{-z}^+,
4) $-\hat{x}\overline{\upsilon_i}\sin|\theta|_a + \hat{y}\overline{\upsilon_i}\cos|\theta|_a$ ($|\theta|_a = |\theta_a|$) for D_{-x}^+,

(Note that the above four velocities are initial velocities at $t = 0$ all).

The amplitude in curve (c) changes from decrease into increase halfway. This

variation can be explained based on an expression ($\upsilon_r \to \upsilon_{ir}$) for a D^+ ion corresponding to (9):

$$\upsilon_{ir} \simeq \left\{ \left[\upsilon_{i0z} + \frac{qE_i t}{2m_{ii}} \left(1 - \frac{\upsilon_{i0z}^2}{c''} \right) \right]^2 + \left[\frac{qE_i t}{m_{ii}} \frac{\upsilon_{i0z}^2}{c''} \frac{\omega_i t}{4} \right]^2 \right\}^{1/2}, \quad (\omega_i t \gg 1) \tag{12}$$

Since $\overline{\upsilon}_i^2 / c'' = 4.4 \times 10^{-5}$, (12) is approximated as

$$\upsilon_{ir} \simeq \left| \overline{\upsilon}_i \sin\theta_a + \frac{qE_i t}{2m_i} \right|, \quad (\omega_i t \gg 1) \tag{13}$$

Since $\theta_a = -3^\circ$ in curve (c) for D^+_{-z} in Figure 3, (13) becomes zero when $\left| \overline{\upsilon}_i \sin\left(-3^\circ\right) \right| = qE_i t / (2m_i)$.

Now, we consider again making four D^+ ions ($D^+_z, D^+_x, D^+_{-z}, D^+_{-x}$) reflect by mirror (c) - (d) all. Denoting by $\upsilon_{ir(b)}$ a minimum in velocity-magnitudes perpendicular to $\boldsymbol{B}$ of the four D^+ ions when those cross plane (b), $\upsilon_{ir(b)}$ must satisfy

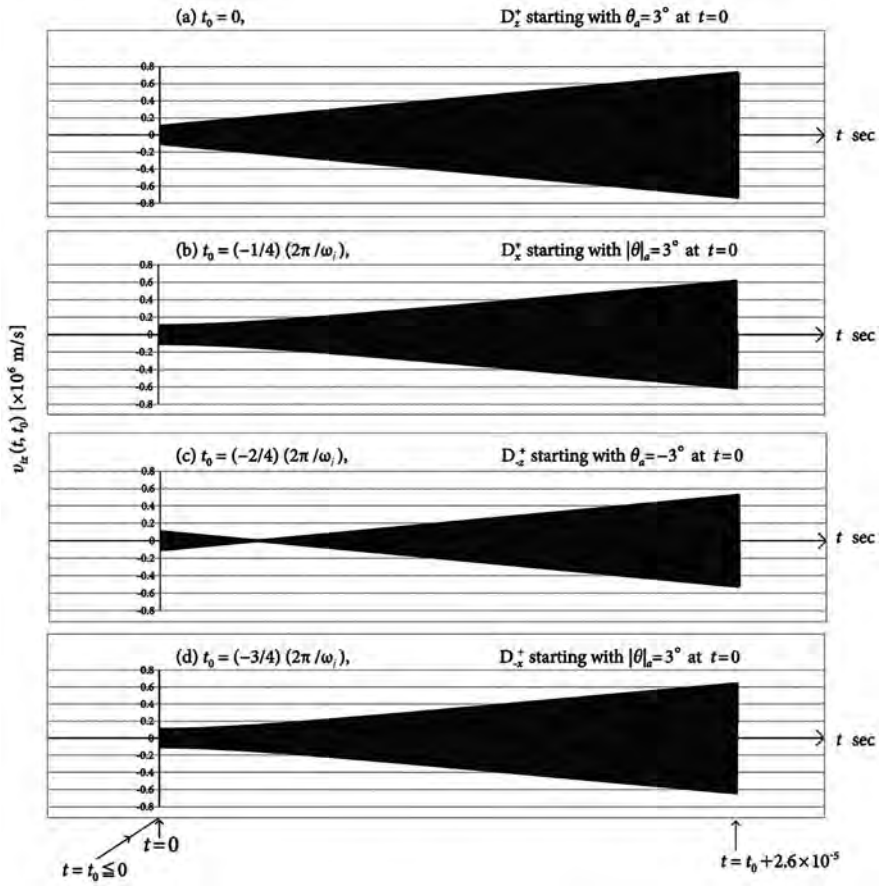

Figure 3. Dependence of $\upsilon_{iz}(t, t_0)$ on t_0, based on Equation (11). The numerical conditions are: An initial velocity $\hat{z}\upsilon_{i0z} = \hat{z}\overline{\upsilon}_i \sin 3^\circ = \hat{z}0.105 \times 10^6$ m/s in plane (a) at time t_0, $\boldsymbol{E}_1 = +\hat{z}10^3 \cos\omega t$ V/m, $\boldsymbol{B} = 2$ T, $\omega_i / \omega = 1.0001$, the time variable $t = t_0 \sim t_0 + \ell / \left(\overline{\upsilon}_i \cos 3^\circ \right) = t_0 \sim t_0 + 52 / \left(2 \times 10^6 \times \cos 3^\circ \right) = t_0 \sim t_0 + 2.6 \times 10^{-5}$ sec.

$$\upsilon_{ir(b)} > 0.26\bar{\upsilon}_i \cos\theta_b \simeq 0.26\bar{\upsilon}_i \cos\theta_a \equiv \upsilon_{reflect}. \quad (14)$$

Accordingly, the electric field $\boldsymbol{E}_1\left(=+\hat{z}10^3\cos\omega t, \omega_i/\omega = 1.0001\right)$ in **Figure 1** must increase the value of $\upsilon_{ir(b)}$ from $\bar{\upsilon}_i\left|\sin\theta_a\right|\left(=\bar{\upsilon}_i\left|\sin\left(\pm 3^\circ\right)\right| = 0.105\times 10^6 \text{ m/s}\right)$ at time $t = 0$ to $\upsilon_{reflect}$ of (14) $\left(=0.26\bar{\upsilon}_i\cos\left(\pm 3^\circ\right) = 0.52\times 10^6 \text{ m/s}\right)$. From the characteristics in **Figure 3**, the condition mentioned above is satisfied when an acceleration time is about 2.6×10^{-5} sec (A necessary length ℓ between planes (a) and (b) is about 52 m) and mirror (c) - (d) can reflect the four D^+ ions ($D_z^+, D_x^+, D_{-z}^+, D_{-x}^+$). However, when we had examined about reflection-characteristics of a D^+ ion (in the range of $-90^\circ < \theta_a \le 0^\circ$ in the y-z plane) starting from plane (a) at $t = 0$, we met with a peculiar dependence on θ_a. We missed this factor in Ref. [1]. To mention this thing with respect to a D^+ ion, we show in **Figure 4(a)**, **Figure 4(b)** dependences (on θ_a) of the following four quantities in plane (b):

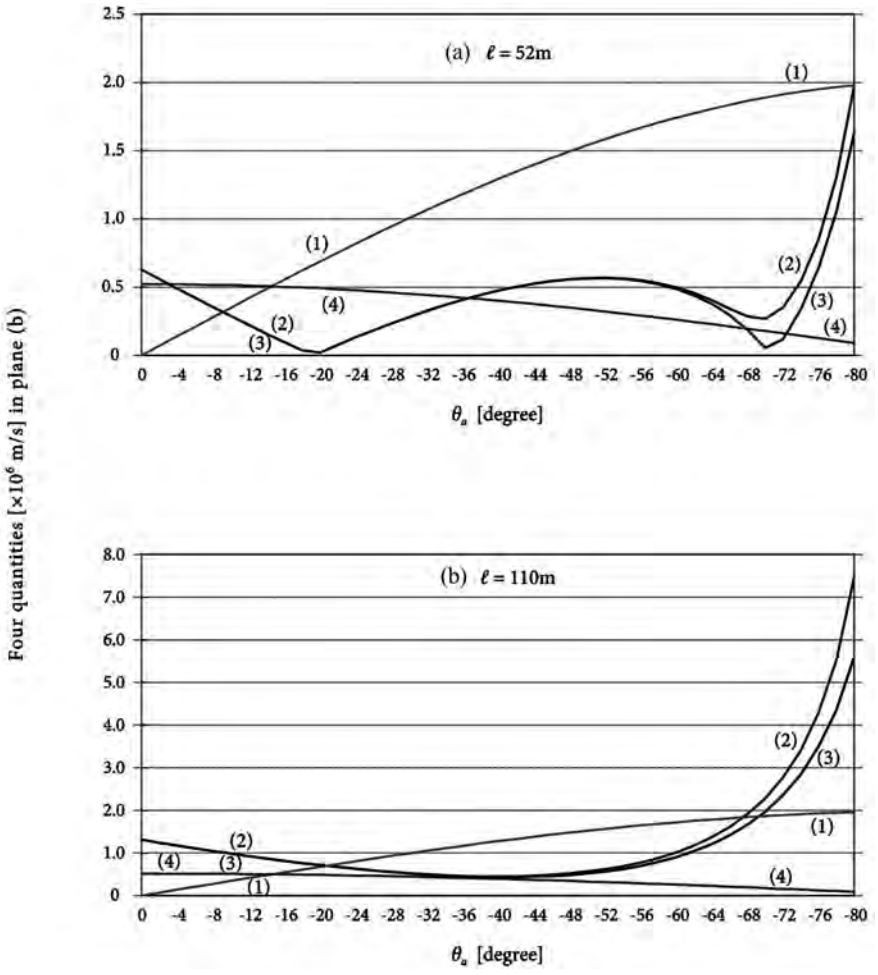

Figure 4. (a) (b) Dependence of four kinds of velocities perpendicular to the magnetic field with respect to reflection of a D^+ ion on $\theta_a\left[0^\circ \ge \theta_a \ge -80^\circ\right]$. (a) is for $\ell = 52$ m and (b) is for $\ell = 110$ m, where ℓ is the length between planes (a) and (b) as shown in **Figure 1**. (1) $\left|\bar{\upsilon}_i\sin\theta_a\right|$, (2) υ_{ir} of Equation (12), (3) υ_{ir} of Equation (13), (4) $\upsilon_{reflect}$ of Equation (14).

1) $|\overline{\upsilon_i}\sin\theta_a|$, which is the velocity-magnitude perpendicular to $\boldsymbol{B}$ of the initial velocity in plane (a) at $t=0$. This value is constant when $\boldsymbol{E}_1=0$.

2) υ_{ir} of Equation (12), which is the velocity-magnitude perpendicular to $\boldsymbol{B}$ in plane (b) when $\omega_i/\omega = 1.0001$.

3) υ_{ir} of Equation (13) (= Equation (12) with $c''\to\infty$).

4) $\upsilon_{reflect}$ of Equation (14). This is the minimum of υ_{ir} in plane (b) which is required for a D^+ ion to be reflected by mirror (c) - (d).

It was a peculiar variation that, in curves (2) and (3) of Figure 4(a), minima had appeared at two points of θ_a.

In Figure 4(a), Figure 4(b), when $\boldsymbol{E}_1=0$, from curves (1) and (4), a D^+ ion in the range of $0^\circ\geq\theta_a>-14.5^\circ$ are not reflected but those in the range of $-14.5^\circ\gtrsim\theta_a\geq-80^\circ$ are reflected. On the other hand, when $\boldsymbol{E}_1\neq0$, from curves (2) and (4) in Figure 4(a), a D^+ ion in the range of $0^\circ\geq\theta_a\gtrsim-3^\circ$ are reflected, but a D^+ ion in the range of $-3^\circ\gtrsim\theta_a\gtrsim-36^\circ$ is not reflected, that is, the acceleration by $\boldsymbol{E}_1$ has brought about such a disadvantage for reflection of a D^+ ion. We missed previously this factor. About relativistic electrons, such a problem does not arise, because the second term increasing together with υ_{oz}^2 within the root of (9) is much more predominant than the first term within the root in magnitude. In Figure 4(a), Figure 4(b), from comparison between curves (2) and (3), relativistic effects are seen from around $\theta_a\simeq-50^\circ$. In the case where ℓ =110 m (Figure 4(b)), it is seen that a D^+ ion starting from plane (a) in the range of $0^\circ\geq\theta_a\geq-80^\circ$ are reflected all. Under the assumption that every D^+ ion has the velocity-magnitude of $\overline{\upsilon_i}$, the loss angle of mirror (a) - (d) becomes nearly zero in the case of $\ell=110$ m. But in the case of $\ell=52$ m, it is presumed that the loss angle of mirror (a) - (d) will be larger than 3˚, due to the minus factor mentioned above with respect to a D^+ ion escaping from plane (a) with a velocity-component in the direction of $-z$ near the y-z plane.

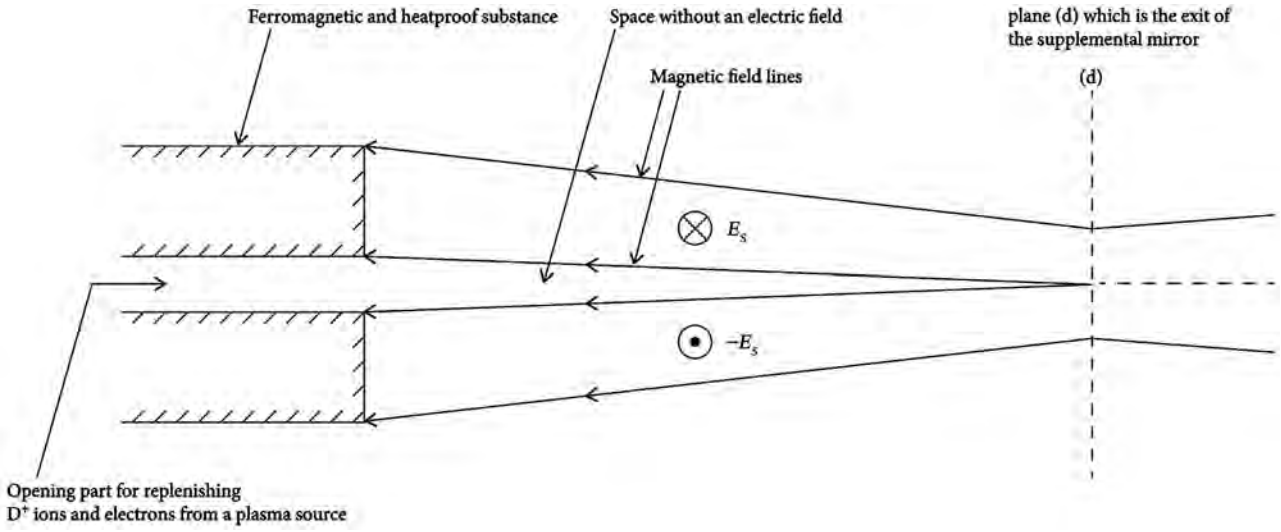

Figure 5. A schematic diagram of an apparatus for replenishing a large quantity of D^+ ions and electrons. Static electric fields $\pm\boldsymbol{E}_S$ are ones for decreasing the number of charged particles colliding with the metal plate by the forces of $\pm\boldsymbol{E}_S\times\boldsymbol{B}$. Escaping D^+ ions must be sent to a plasma source.

4. Conclusion

We have made it clear that, in order to reclaim escaping D^+ ions whose incident directions make small angles for a direction of $\boldsymbol{B}$ by a magnetic mirror of a linear type, a very long cyclotron resonance space is necessary. Though the loss angle, about 5˚, of the mirror (a) - (d) designed in Section 3 is presumed to be still too large from the viewpoint of plasma confinement, the mirror (a) - (d) shown in Figure 1 is a sufficiently too long apparatus. Therefore, we consider that, for shortening a length of acceleration space, a powerful means replenishing a large quantity of D^+ ions and electrons from the outside ought to be introduced. We show with Figure 5 an idea about a means for replenishment. This apparatus must be protected from heating and damage of the metal surface due to collisions of escaping D^+ ions.

Conflicts of Interest

The authors declare no conflicts of interest regarding the publication of this paper.

References

[1] Nagata, M. and Sawada, K. (2018) *EPJ Techniques and Instrumentation*, **5**, 1.

[2] Turlapov, A.V. and Semenov, V.E. (1998) *Physical Review E*, **57**, 5.

[3] Caspi, R. and Jerby, E. (1999) *Physical Review E*, **60**, 2.

[4] Savrukhin, P.V. and Shestakov, E.A. (2016) *Physics of Plasmas*, **23**, 112509-1.

[5] Soldatkina, E., Anikeev, M., Bagryansky, P., Korzhavina, M., Maximov, V., Savkin, V., Yakovlev, D., Yushmanov, P. and Dunaevsky, A. (2017) *Physics of Plasmas*, **24**, 022505-1.

Journal of Modern Physics, 2019, 10, 157-162
http://www.scirp.org/journal/jmp
ISSN Online: 2153-120X
ISSN Print: 2153-1196

Meaning of Gravitation

Walter Petry

Mathematical Institute of the University Duesseldorf, Duesseldorf, Germany
Email: wpetry@meduse.de

How to cite this paper: Petry, W. (2019) Meaning of Gravitation. *Journal of Modern Physics*, **10**, 157-162.
https://doi.org/10.4236/jmp.2019.102012

Received: February 2, 2019
Accepted: February 24, 2019
Published: February 27, 2019

Abstract

It is well-known that two bodies attract one another by gravitation. The theory of Newton gives a formula for this attraction depending on the masses of the bodies. General relativity of Einstein explains gravitation as geometry. There exists no satisfactory explanation for the meaning of gravitation. A theory of gravitation in flat space-time gives non-singular, cosmological models. In the beginning of the universe, there is no matter and all the energy is uniformly distributed gravitational energy. This energy is attractive and converts to dark matter generating our universe. Gravitational energy is the reason for attraction and not the mass of the bodies. It is well known that each body is surrounded by a gravitational field. This field gives the attraction of bodies.

Keywords

Gravitation in Flat Space-Time, Gravitational Energy, Universe, Dark Matter, No Singularity, No Big Bang

1. Introduction

General Relativity (GR) gives good agreements of theory and experimental results for weak gravitational fields. This result is considered as proof for GR. GR states for homogeneous, isotropic, cosmological models of the universe a point-singularity, called big bang, which is in general considered as beginning of the universe. Hence, the universe starts with infinite density of matter. It is worth to mention that infinities are physically not realistic. Furthermore, an inflationary expansion of space after the beginning (called cosmic inflation) is needed to get at present the big, flat universe. Nevertheless, the big bang is at present always considered as best description of the universe.

In the year 1979, I have studied a theory of gravitation in flat space-time (GFST) which gives for weak gravitational fields the same results as GR to measurable accuracy. The energy-momentum of gravitation of GFST is a tensor in

contrast to that of GR. Hence, gravitational energy by GFST is well defined contrary to that of GR. This energy is important for studying the universe and for the meaning of gravitation. The result for the universe by the theory of GFST is quite different from that of GR. The theory of GFST starts from uniformly distributed gravitational energy and no matter exists in the beginning of the universe. Gravitation is attractive yielding inhomogeneous distribution of gravitational energy which is converted to matter. Locally, only a part of the contracted gravitational energy is used to give a body with mass whereas the rest of the gravitational energy surrounds the body. This is important because otherwise the universe would consist of bodies without gravitational field. But gravitational energy is the reason for attraction of bodies and not the mass of them. A greater mass is surrounded by a bigger gravitational field. Hence, we get the meaning of gravitation, in particular for the attraction formula of two bodies already stated by Newton. There is no electrical charge or electromagnetic field. Therefore, the generated matter of the gravitational energy is the dark matter of the universe. Luminous matter is generated by electro-magnetic field. All physical quantities are finite, *i.e.* no big bang, and space is non-expanding. Shortly after the big bang, the results of the two theories agree to high accuracy for a flat universe of GR. It is worth to mention that astrophysical observations indicate that our universe is flat. The theory of GFST with applications is given in the book [1]. Further studies of GFST, especially with applications to cosmological models, are found in the articles [2] [3] [4] [5] and [6]. In these articles, the formulae for the universe are given. In the beginning of the universe, there was only uniformly distributed gravitational energy and matter didn't exist. The matter arises in the course of time and the universe is not expanding.

2. GFST and Cosmology

GFST is already studied in the article [7] in pseudo-Euclidean metric and in the article [8] in general covariant form. The theory with applications can e.g. be found in the book [1].

Let $\left(x^i\right)$ be a four-vector of space-time with flat space-time line-element

$$\left(\mathrm{d}s\right)^2 = -\eta_{ij}\mathrm{d}x^i\mathrm{d}x^j . \tag{2.1}$$

Put

$$\eta = det\left(\eta_{ij}\right).$$

Let g_{ij} be the gravitational field and define g^{ij} by

$$g_{ik}g^{kj} = \delta_i^j .$$

The proper-time is defined by

$$\left(c\mathrm{d}\tau\right)^2 = -g_{ij}\mathrm{d}x^i\mathrm{d}x^j . \tag{2.2}$$

Put

$$G = det\left(g_{ij}\right).$$

The Lagrangian of the gravitational field g_{ij} is given by

$$L(G) = -\left(\frac{-G}{-\eta}\right)^{1/2} g_{ij} g_{kl} g^{mn} \left(g^{ik}_{/m} g^{jl}_{/n} - \frac{1}{2} g^{ij}_{/m} g^{kl}_{/n} \right)$$

where the bar/denotes the covariant derivative relative to the metric (2.1).

Define the differential operator

$$D^i_j = \left(\left(\frac{-G}{-\eta}\right)^{1/2} g^{mn} g_{jk} g^{ki}_{/m} \right)_{/n} .$$

Then, the differential equation for the gravitational field is

$$D^i_j - \frac{1}{2}\delta^i_j D^k_k = 4\pi\kappa T^i_j \tag{2.3}$$

where T^i_j is the total energy-momentum tensor of matter and gravitational field, *i.e.*

$$T^i_j = T^i_j(M) + T^i_j(G).$$

The energy-momentum $T^i_j(G)$ of gravitation is also a tensor. The equations of motion are

$$T(M)^k_{i/k} = \frac{1}{2} g_{kl/i} T(M)^{kl}. \tag{2.4}$$

Cosmological models of GFST which are homogeneous and isotropic are already studied previously. Put

$$u^i = 0 \quad (i = 1,2,3)$$

and

$$p = p_r + p_m, \quad \rho = \rho_r + \rho_m$$

where r and m denote radiation and matter.

Subsequently, we use the pseudo-Euclidean metric. It holds

$$p_m = 0, \quad p_r = \frac{1}{3}\rho_r .$$

We have for homogeneous, isotropic, cosmological models

$$g_{ij} = \begin{cases} a^2(t) & (i = j = 1,2,3) \\ 1/h(t) & (i = j = 4) \\ 0 & (i \neq j) \end{cases}$$

The initial conditions at present time $t_0 = 0$ are

$$a(0) = h(0) = 1, \quad \dot{a}(0) = H_0, \quad \dot{h}(0) = \dot{h}_0, \quad \rho_m(0) = \rho_{m0}, \quad \rho_r(0) = \rho_{r0}$$

where H_0 is the Hubble constant and $(\dot{h}_0)$ is an additional constant.

It follows by the use of the field Equations (2.3) and the conservation of the total energy by longer calculations

$$\left(\frac{\dot{a}}{a}\right)^2 = \frac{H_0^2}{\left(2\kappa c^4 \lambda t^2 + \varphi_0 t + 1\right)^2} \left(-\Omega_m \kappa_0 + \Omega_r a^2 + \Omega_m a^3 + \Omega_\Lambda a^6 \right). \tag{2.5}$$

Here, λc^2 is the conserved total energy, Ω_r, Ω_m and Ω_Λ are the density parameters of radiation, matter and cosmological constant.

Define the abbreviations

$$\varphi_0 = 3H_0\left(1+\frac{1}{6}\frac{\dot{h}_0}{H_0}\right),\quad \Omega_m\kappa_0 = \frac{1}{12}\left(\frac{8\kappa c^4\lambda}{H_0^2}-\left(\frac{\varphi_0}{H_0}\right)^2\right) \tag{2.6}$$

Then it follows

$$a^3\sqrt{h} = 2\kappa c^4\lambda t^2+\varphi_0 t+1. \tag{2.7}$$

Relation (2.5) yields at present time $t_0 = 0$ and the initial conditions

$$\Omega_r+\Omega_m+\Omega_\Lambda = 1+\Omega_m\kappa_0. \tag{2.8}$$

Relation (2.5) gives non-singular solutions under the condition

$$0 < \Omega_m\kappa_0$$

which implies by the use of (2.7) and (2.6)

$$2\kappa c^4\lambda t^2+\varphi_0 t+1 > 0 \tag{2.9}$$

for all $t\in\mathcal{R}$. Furthermore, assume

$$\Omega_m\kappa_0 \ll 1$$

that is the full assumption

$$0 < \Omega_m\kappa_0 \ll 1. \tag{2.10}$$

Then, it follows from (2.5) the existence of a_1 with $0 < a_1 \ll 1$ and

$$\Omega_r a_1^2+\Omega_m a_1^3+\Omega_\Lambda a_1^6 = \Omega_m\kappa_0. \tag{2.11}$$

That is that there exists $t_1 < t_0 = 0$ such that

$$a_1 = a(t_1),\quad \dot{a}(t_1) = 0.$$

Relation (2.5) gives

$$\frac{\dot{a}}{a} = \pm\frac{H_0}{2\kappa c^4\lambda t^2+\varphi_0 t+1}\left(-\Omega_m\kappa_0+\Omega_r a^2+\Omega_m a^3+\Omega_\Lambda a^6\right)^{1/2}. \tag{2.12}$$

The upper sign holds for $t\ge t_1$ with increasing $a(t)$ and for $t\le t_1$ with decreasing $a(t)$. Let us introduce the proper time $\tilde{\tau}$ by

$$\mathrm{d}\tilde{\tau} = 1/\sqrt{h(t)}\,\mathrm{d}t. \tag{2.13}$$

Then, the differential Equation (2.12) can be rewritten by the use of (2.7) in the form

$$1/a\frac{\mathrm{d}a}{\mathrm{d}\tilde{\tau}} = \pm H_0\left(-\frac{\Omega_m\kappa_0}{a^6}+\frac{\Omega_r}{a^4}+\frac{\Omega_m}{a^3}+\Omega_\Lambda\right)^{1/2}. \tag{2.14}$$

The Equation (2.14) is with the upper sign and by virtue of (2.10) for sufficiently large *a*, *i.e.* not to near to the big bang nearly identical to the cosmological model of GR with flat space.

Non-singular cosmological models of GFST are already given in article [9]. More detailed studies of chapter 2 are found in the articles [2] [3] [4] [5] [6] and

[10] where the theory of GFST and the results are compared to those of GR, too.

3. Meaning of Gravitation

The study of GFST with applications show that GFST and GR are logically quite different from one another, e.g. GFST has flat space-time as metric and the energy-momentum is a tensor where the total energy-momentum is the source of the gravitational field. Nevertheless, the results of the two theories agree with one another for weak gravitational fields to measurable accuracy. But cosmological models are in the beginning of the universe quite different whereas at later times the results approximately agree if the universe of GR is flat. The universe of GFST has no singularity and is non-expanding. The interpretation of expanding space is also possible by virtue of the general covariance of the theory. In contrast to GR where the space must expand GFST gives non-expanding universes which are already studied in article [11]. An expanding space makes little sense and it was introduced by the curious solution of a point-singularity of the universe by GR. The universe of GFST starts from uniformly distributed gravitational energy in space. Gravitational energy is attractive implying non homogeneities which are converted to dark matter. This gives the dark matter of our universe because no electrical charges are active. The luminous matter arises by electro-magnetic fields. Not the whole clumpy inhomogeneity of the gravitational field is converted to matter and the non-converted gravitational energy surrounds the body. This is important because gravitational energy yields attraction and bodies without gravitation field could not attract one another. Hence, the reason for the attraction of two bodies is the surrounding gravitational fields of the bodies and not the masses. This gives an explanation of Newton's law of the attraction of two bodies. Therefore, a body with bigger mass must have a stronger gravitational field. Hence, we have received the meaning of gravitation, that is, the gravitational field is attractive and not the mass of the body. GFST cannot give an explanation of the generation of the uniformly distributed gravitational energy in space in the beginning of the universe. This may be an indication for the existence of GOD.

Hence, we have also got an explanation for the attraction of two bodies, a long not answered problem.

4. Conclusion

GFST gives non-singular cosmological models (no Big Bang), the generation of dark matter in the universe by virtue of the attractive gravitational field and an explanation of the "Meaning of Gravitation". Gravitational field is attractive and bodies are surrounded by gravitational fields. The mass of a body doesn't attract.

Conflicts of Interest

The authors declare no conflicts of interest regarding the publication of this paper.

References

[1] Petry, W. (2014) A Theory of Gravitation in Flat Space-Time. Science Publishing Group.

[2] Petry, W. (2013) *Journal Modern Physics*, **4**, 20-25. https://doi.org/10.4236/jmp.2013.47A1003

[3] Petry, W. (2015) *Journal Modern Physics*, **6**, 1085-1094. https://doi.org/10.4236/jmp.2015.68113

[4] Petry, W. (2016) *Journal Modern Physics*, **7**, 1432-1439. https://doi.org/10.4236/jmp.2016.712135

[5] Petry, W. (2017) *Journal Applied Mathematics and Physics*, **5**, 882-872.

[6] Petry, W. (2018) *Journal Modern Physics*, **9**, 1441-1447. https://doi.org/10.4236/jmp.2018.97088

[7] Petry, W. (1979) *General Relativity and Gravitation*, **10**, 599-608. https://doi.org/10.1007/BF00757210

[8] Petry, W. (1981) *General Relativity and Gravitation*, **13**, 865-872. https://doi.org/10.1007/BF00764272

[9] Petry, W. (1981) *General Relativity and Gravitation*, **13**, 1057-1071. https://doi.org/10.1007/BF00756365

[10] Petry, W. (1990) *General Relativity and Gravitation*, **22**, 1045-1065. https://doi.org/10.1007/BF00757815

[11] Petry, W. (2007) arXiv: 0705.4359.

Journal of Modern Physics, 2019, 10, 163-175
http://www.scirp.org/journal/jmp
ISSN Online: 2153-120X
ISSN Print: 2153-1196

Scenario for the Origin of Matter (According to the Theory of Relation)

Russell Bagdoo

Independent Searcher, Saint-Bruno, Quebec, Canada
Email: rbagdoo@gmail.com, rbagdoo@yahoo.ca

How to cite this paper: Bagdoo, R. (2019) Scenario for the Origin of Matter (According to the Theory of Relation). *Journal of Modern Physics*, **10**, 163-175.
https://doi.org/10.4236/jmp.2019.102013

Received: February 20, 2019
Accepted: February 24, 2019
Published: February 27, 2019

Abstract

Where did matter in the universe come from? *Where does the mass of matter come from*? Particle physicists have used the knowledge acquired in matter and space to imagine a standard scenario to provide satisfactory answers to these major questions. The dominant thought to explain the absence of antimatter in nature is that we had an initially symmetrical universe made of matter and antimatter and that a dissymmetry would have sufficed for more matter having constituted our world than antimatter. This dissymmetry would arise from an anomaly in the number of neutrinos resulting from nuclear reactions which suggest the existence of a new type of titanic neutrino who would exceed the possibilities of the standard model and would justify the absence of antimatter in the macrocosm. We believe that another scenario could better explain why we observe only matter. It involves the validation of the negative energy solution of the Dirac equation, itself derived from the Einstein energy equation. The theory of Relation describes a negative energy ocean with the creation of real particle/antiparticle pairs. The origin of the masses of the particles would come from this ocean. A physical mechanism would allow their separation in the opposite direction and, therefore, the matter would be enriched at the expense of the ocean. The matter would be favored without resorting to negation or annihilation of negative energy, without the need for a CP (the behavioral difference between particle and antiparticle) violation that would be responsible for matter/antimatter asymmetry in the universe. And without the savior contribution of an undetectable obese neutrino: his search appears to us more a desperate act towards an "ultra-massive catastrophe" than a real effort to try to discover what really happened.

Keywords

Matter and Antimatter, Sterile Neutrino, Ocean of Negative Energy, Theory of Relation, Pair of Real Particles, Principle of Compensation

1. Introduction

The standard model of the big bang makes it possible to reconstruct the history of the cosmos in large part, in good agreement with the astronomical observations, until the first fractions of a second that followed the zero-time. In spite of this, we have not succeeded in combining the three fields, electromagnetic, electro-weak and strong into a single one at very high interaction energies, and we are unable to reconcile the requirements of quantum mechanics with those of general relativity to quantify the gravitational field. This has not prevented the theoreticians of particle physics, astrophysics, and cosmology from engaging in the craziest speculations to answer some of the great questions that aspire to explain our universe.

One of the questions that seem to have found a satisfactory answer concerns particle physicists: *How did matter appear*? The consensus is reached on the idea that in the moments following the initial moment of the big bang, when the universe is in a neutral matter state of photons for the most part and neutrinos, this neutral matter will transform and separate into matter and antimatter which will re-annihilate, etc., up to the present stage. The question of whether at the beginning the universe was completely neutral, which would imply that there is now as much antimatter as matter, seems to be discarded since one does not find constituted antimatter. The current dominant idea is that of the Soviet physicist Andrei Sakharov: the universe was slightly biased on the matter side, which would explain its predominance at the present time [1] [2].

To corroborate the idea of Sakharov, physicists rely on certain physics experiments, some disintegrations which generate a dissymmetry coupled with the particle/antiparticle symmetry. It is believed that a small dissymmetry, similar to that of kaons which decompose differently from their antiparticle, would suffice to leave a tiny excess of baryons with respect to the antibaryons. But we now prefer experiments with leptons. Thus, the first results of the T2K experiment carried out since 2011 in Tokai, Japan, indicate that a very slight imbalance may have appeared during the disintegration of certain particles: heavy neutrinos. This reaction gives birth to leptons (electron, muon, tau) or antileptons, but not in equal proportions: for 100,000 antileptons, 100,001 leptons would be formed. It suggests that during the big bang, slightly more matter was created than antimatter.

In our view, the thesis of a small violation of particle/antiparticle symmetry at the first moments of the universe is not a theoretical necessity. The argument that this difference will prove to be crucial to demonstrate that after the appearance of matter and antimatter at about 10^{-30} seconds, obese, ultra-massive neutrinos would have broken the equilibrium of the cosmos, seems to us unfounded and desperate.

The intention of this article is to propose an alternative to the direction taken to answer the question *How did matter appear*? In Section 2, we show that Sakharov's idea of an original dissymmetry that would have privileged matter is biased and causes particle physics towards dead-end directions. Any solution of

negative energy is treated as non-physical, despite the fact that they are mathematically valid predictions of the Dirac equation. Several experiments have highlighted the concept of oscillation which surmises that neutrinos can change their flavor throughout their journey because they have a mass. It has been found that the number of antineutrinos produced by a reactor is lower than theoretically expected, which evokes an original dissymmetry. Physicists speculate the existence of heavy neutrinos at the exit of the reactors which would accredit the process of oscillation, could constitute the dark matter and would explain the absence of the antimatter of our universe. We think they are putting their finger in the eye too quickly. In Section 3, we show that Dirac's negative energy solution, banned from physics, is a reality. But it is a question of a virtual reality in which the sea of negative energy materializes above the surface of the pairs of particle/antiparticle which annihilate immediately. We present an alternative in Section 4, namely the solution of the negative energy of the theory of Relation. Throughout the expansion, the highly intense electromagnetic field of the ocean spontaneously converts energy into particles/antiparticles, both for matter and space. A separation mechanism allows the creation of real particles of positive energy. A new variable (M_{vp}^2), from the equation of the theory of Relation, gives mass to these particles.

2. Origin of the Matter According to the Idea of Sakharov

2.1. Sakharov's Idea of a Dissymmetry at the Origin of Matter in the Universe

Today, the consensus is that although there would have been an initially symmetrical universe made of matter and antimatter, there would still have been some dissymmetry in the particle laws, and this dissymmetry would have sufficed so that more particles remain than antiparticles, and this would explain why there would have been a small excess of particles which would have served to fabricate the cosmos we know [3].

This consensus starts from the idea of Sakharov of an original dissymmetry that would have advantaged matter. He posed the problem in the form of three conditions. The first—that the universe is in a state of violent thermal imbalance—is fulfilled by the standard cosmological model of the big bang. The second—that matter can be transformed into antimatter—is, also, already authorized by the standard model of particles. The third condition dives at the heart of the problem. To build a world filled with matter, the processes that transform matter into antimatter must violate the combination of two symmetries: the symmetry C (charge), which stipulates that a process remains unchanged if the charges of the particles involved are changed; and the symmetry P (parity), according to which if a transformation occurs in nature, then the transformation which would be the image in a mirror is just as possible. In the early 1960s, it was observed that some unstable particles, kaons, decompose slightly differently from their antiparticle. It was thought that this small violation of parti-

cle/antiparticle destroyed the initial perfection of nature. It has been anticipated that a small similar dissymmetry between baryons with respect to the anti-baryons which would leave a tiny excess of baryons would prove that the universe is only made by baryons. So far no proton disintegration has ever been observed. The physicists then turned to the leptons, concentrating on the neutrinos. The T2K experiment (Tokkai to Kamioka) has been working to observe the transformation of a neutrino type, the muon neutrino, into an electron neutrino. They then compared with the transformation of muonic antineutrinos into electronic antineutrinos. After two years of measurements, they found too many neutrinos detected and not enough antineutrinos, proof of a violation of the CP symmetry [2].

This second anomaly is, for theorists, an indicator of a violation of symmetry between matter and antimatter. Such a violation goes against the current standard particle model and, moreover, has the theoretical consequence of sowing a disorder that invalidates its current formulation [4]. But it must be recognized, until today, neutrinos of the standard model do not agree with the data of the observation and do not allow, in particular, to explain the deficit of antineutrinos compared to the excess neutrinos. According to experts, these anomalies should be the manifestation of a particle still unknown. A particle which, on the one hand, is the result of the mutation of a standard neutrino, from which their disappearance, and which, on the other hand, is capable of transforming into a standard neutrino, what would explain the excesses observed. This particle would be a neutrino of a fourth type not yet detected. They called it "sterile neutrino" because it is not sensitive to any of the three basic interactions of the standard model. Not even to the weak nuclear force. It interacts only through gravitation (almost zero intensity at the particle scale and undetectable in the context of a microscopic physics experiment). They suspect it endowed with a state of right-handed helicity. Such a particle could not only explain how matter prevailed over antimatter but it could also be the original particle from which the mass of matter comes.

2.2. The Original Particle from Which Comes the Mass of Matter

Only a few years ago, the particle that confers its mass on all the others was the Higgs boson which represented the Brout-Englert-Higgs (BEH) field. It is an unstable particle that survives barely 10^{-22} seconds after its production. The boson is not observed since it disintegrates immediately by splitting into other particles which can be observed. In fact, it is only an excitation of the BEH field which can be compared to an ocean surface. To excite the ocean and produce waves, it is enough to supply energy, whether through wind, tidal power or an earthquake. We excite the ocean of BEH by supplying it with energy with particle accelerators. This excitation or wave is none other than the scalar boson of Higgs and it is manufactured exactly as is manufactured the antiparticle in the accelerators.

Theorists had suggested that the universe was filled with an ocean of BEH. Other physicists have proved that this ocean (or field) exists by creating excitations of this field in the form of Higgs bosons, thus completing the standard particle model. In the end, most physicists are disappointed because there are no waves without water and no Higgs boson without BEH ocean. For them, conceptually, the incoherence of an ocean of negative energy (that it bears the name of Dirac, Higgs, or other) is monumental: it deals with an ocean that physically has no consistency, even if it holds some exotic properties; An ocean that connects two kinds of energy that ignore each other is very inconsistent. Detection of the boson of Higgs completes the standard model but to go beyond, towards an ocean of negative energy, is forbidden by the official Physics and excluded from the model [5].

In fact, the problem is circumvented from the moment we perpetuate the hypothesis that everything is only of positive energy. By deciding that the physical properties of particles and antiparticles are only positive energy, physicists impose ipso facto a radical dissymmetry that violates CP symmetry and annihilates the antimatter. For the hypothesis to continue to work, it is imperative to put in the closet the particle of God, that has become cumbersome and without future. Dethroned, it will quickly be replaced by the sterile neutrino, the fourth type. The new physics of neutrinos, with this invisible savior, should explode the standard model and entail vast cosmological consequences, such as making dark matter, justify the absence of antimatter in the universe.

2.3. The Sterile Neutrino, the Perfect Phantom Particle that Succeeds the Higgs Boson

According to specialists, the tiny relic of the disintegration of super heavy neutrinos and antineutrinos would have tipped the cosmic balance towards the matter. The imbalance of the cosmos towards 10^{-30} seconds would have been transmitted to the quarks, then to the protons and neutrons until the great annihilation towards 10^{-4} seconds, destroying all the antiparticles to leave alone the grains of matter which will be structured in atoms, stars, planets. This undetectable particle would explain the failure counts in the neutrino flux measured for more than fifteen years near nuclear reactors. Detectors at the output of nuclear reactors have detected more neutrinos than antineutrinos. The number of antineutrinos measured is 7% lower than that theoretically expected. As if they had mysteriously disappeared. This flagrant anomaly would not only break the restrictive framework of the standard model of particle physics but would also have unbalanced the cosmos 10^{-27} seconds after the big bang, having thus given birth to all the matter of the universe and having been able to constitute dark matter, *i.e.*, 85% of the mass of the natural world.

This scenario uses data from the T2K experiment that argue in favor of the CP symmetry violation, about 1000 times stronger than in processes involving quarks. Even with this asymmetry, these neutrinos do not make the weight to explain the predominance of matter in the universe. According to the models,

the smallness of the masses of the three classic neutrinos can only be explained by means of a fourth type of neutrino, heavy as tens of billions of protons. A primordial version of the current neutrinos, that must have existed at the beginning of the creation. Theoreticians are obliged to introduce a titanic sterile neutrino, with a mass-energy of the order of 10^9 teraelectronvolts (TeV). However, such energy far exceeds the possibilities of describing the standard model, whose equations become crazy when they attempt to describe elementary phenomena involving energy greater than a few TeV.

The tracking down to these obese neutrinos susceptible to solve the problem of the mass of their congeners is already launched. Current experiments use the oscillation phenomenon, valid for any type of neutrino, to flush them out. An alternation of appearances and disappearances of standard neutrinos, near nuclear power stations for several months, should suffice to conclude that the undetectable sterile neutrino is unmasked [2] [6].

2.4. Neutrino with Neither Faith Nor Law

In view of the experimental success of the discovery of the Higgs boson, it is expected that the sterile neutrino will not be a theorist's simple whim, but will be demonstrated in the next few years through experiments [7]. And yet could it be that the thought of the neutrino specialists was misled? Is the neutrino oscillations phenomenon, crowned by a Nobel Prize, merely a praise of error? Would not the building of twenty years of experience and data build upon a gigantic mistake?

Then if the sterile neutrino exists for nuclear reactors and acts on the electronic neutrinos, why would it not exist for the Sun, the ideal nuclear reactor which produces only electronic neutrinos? If the sterile neutrinos act on the electronic neutrinos of the Sun, before or at the photosphere exit, and we do not see why it would be otherwise, it would mean that the theory of the oscillation would be false.

It is known that two-thirds of the electron-type neutrinos produced by nuclear reactions in the core of the Sun are observed to change to muon- or tau-type neutrinos before reaching the Earth. The experience of the Sudbury Neutrino Observatory (SNO) would have demonstrated that a good part of the electronic neutrinos emitted by the Sun is transformed into muon and tau neutrinos along the way. The SNO detector, using heavy water, a substance allowing to detect the three flavors of neutrinos, could have verified that the sum of the three neutrino types corresponded to a number of electronic neutrinos produced by the Sun. The specific SNO measures would thus have demonstrated the ability of neutrinos to change from one type to another in transit to the Earth from the Sun, to "oscillate", proving by the very fact that they have finite masses. But would this demonstration be as well obvious with this new invisible parameter, the sterile neutrino?

With this fourth player, would the sum of the three neutrinos flavors corre-

spond to an amount of electronic neutrinos produced by the Sun? It is known that the missing standard neutrinos are transformed on the way into another type and that such a transformation requires at least a great distance. If the sterile neutrino changes the identity of the neutrinos without any distance, it is that there are not many oscillations over great distances. So the theory of neutrino oscillation would be wobbly. Especially since the neutrinos from the supernovae 1987A [8] were traveling at substantially the same speed as the photon, which would not have been the case if they had had a mass [9].

One would have the new parameter of the heavy neutrino for the very short distances which explains an unforeseen deficit and the oscillation of the mass states of the light neutrinos for the great distances which explains the total deficit. These two deficits are contradictory and one can apprehend an "ultra-massive catastrophe". Which reminds the "ultraviolet catastrophe" at the end of the 19th century concerning the radiation emitted by the bodies being heated; we had the Wien law which reported experimental observations for short wavelengths without being capable for long wavelengths, and Rayleigh's law for long wavelengths but which did not diverge for small wavelengths [10]. The neutrino oscillation hypothesis and the sterile neutrino hypothesis contradict each other. Which is false? What if both were false? What if the negative energy ocean existed? What if the antineutrinos were attracted by the ocean?

3. Dirac's Negative Energy Solution

3.1. The Original Swindle

At the outset, the thesis of an alleged symmetrical creation made of matter and antimatter, with an asymmetry in the laws concerning the particles that would have sufficed so that it remains a small excess of particles used to produce the universe, is not based on sound scientific evidence. It has been totally fabricated from an idea issued in 1967 by Sakharov. This idea goes beyond the hypothesis for practically all specialists. It takes on the dimension of a true scientific theory that explains the origin of matter. But it is also a form of scam. For the simple reason that we are talking here about a strictly positive energy solution framework and that physics has officially eliminated the negative energy solution. Which gives a speculative and unfounded character to the idea of an originally symmetrical universe, but in which a particular mechanism would have quickly preferred matter [11].

For those who might doubt it, it should be stressed that it is foolish to want to apply only the equations of Einstein's special relativity concerning positive energy at the moment when the age of the universe is equal to Planck's time. All physicists know that the energy-momentum-mass relationship of the Dirac equation $E^2 = c^2p^2 + m^2c^4$, which is always associated with Einstein's special relativity, has two roots. Those of positive energy and negative energy: $\pm E = (c^2p^2 + m^2c^4)^{1/2}$. The negative energy solution is that of Dirac sea. Under the pretext that it could not be observed directly, Heisenberg, Pauli, Jordan, and others, have ex-

cluded all negative energy solutions from classical physics; it is, therefore, illegitimate to use negative energy solutions in a quantum period where there are only particles and antiparticles. How do we want the concept of matter, a notion which is the basis of our universe, has a meaning at the particle and atom level, whereas the deep concept of antimatter is eliminated as a theoretical chimera from the equations and laws of quantum mechanics [2] [12]?

It was the original swindle which ended in the total annihilation of the antimatter. The so practical causal dissymmetry is equivalent to the exclusion of the negative energy solution from the equations. And it is, in our opinion, because of this negation of a Dirac sea, that particle physicists no longer know what to do with the Higgs boson, and that the BEH field (which is the Dirac sea under a new name) is now becoming a skeleton in the closet of particle physics.

3.2. Solution of Dirac Equation's Negative Energy

To solve this thorny problem, we postulate that contrary to what is assumed by classical physics, negative energy actually exists as much as positive energy. In a universe of only positive energy, the mechanism that was chosen to transform matter into antimatter is that of Sakharov: the universe would have been originally symmetrical, but soon after the materialization of particles and antiparticles, a mechanism of disintegration before annihilation would have quickly chosen matter. The other processes originally asymmetric universe, an originally symmetric universe where particles and antiparticles separate to form galaxies and anti-galaxies, an originally symmetric universe favoring the antimatter were ruled out. Several physicists have already proclaimed the existence of the Dirac sea of negative energy.

3.3. Creation of a Virtual Particle/Antiparticle Pair and Annihilation

The equation of Dirac gives to a particle of mass m the possibility of having negative as well as positive energies. Dirac interpreted the result assuming that all states of negative energy are occupied by unobservable electrons, forming an invisible "sea", the electrons of positive energy floating on this sea being the only observed ones. The hypothesis may seem *ad hoc*. However, Dirac added with the next argument: If a photon of energy hv greater than 2 mc^2 interacts with an electron of the sea of negative energy $-\varepsilon_o(\varepsilon_o > 0)$, he can communicate his energy and make it pass in a state of energy $hv - \varepsilon_o$; this electron is then observable. The two symmetrical solutions of this equation, one of positive energy and the other of negative energy, allowed him to postulate the existence of particles analogous to the electron but of opposite electrical charge. With Anderson who discovers the positron in 1932, appears the reality of the antimatter, as Dirac equation predicted, without physicists having discerned it. It will then be discovered that almost all the particles are matched to antiparticles [13] [14] [15].

Would we have created matter and electric charge from energy with the negative energy solution of Dirac equation? It is not believed because it has been as-

sumed that there is now a "bubble" or "hole" in the sea.

3.4. Dirac's Negative Energy Solution Unacceptable to Explain the Asymmetry between Matter and Antimatter

The Dirac sea despite the constant annihilations and creations of "pairs", total transformations of mass in energy, of energy in mass in no way diminishes its level of water in favor of the ground (matter). The emersion of the ground, which leaves a hole in the water, is immediately harpooned by the sea which hates the decreasing water levels, no matter how high the waves. In other words, the electromagnetic energy ($E = mc^2$) is turned into mass-energy of the particle and the antiparticle (which leaves only a hole in the sea because the antiparticle is only a mirror image) but the two are condemned to annihilate in a flash of energy to ensure the stability of the ocean. Despite their undeniable spectacular metamorphoses, these negative energy solutions remain virtual and are physically unacceptable to explain the asymmetry between matter and antimatter.

4. Origin of Matter According to the Theory of Relation

4.1. Negative Energy Solution Would Involve the Creation of a Pair of Real Particles

However, the ocean of the theory of Relation [16] [17] can explain why today the universe consists essentially of matter whereas matter and antimatter must have been produced in equal quantities after the big bang. It is worth remembering that according to the theory our universe has two structures: a structure of expansion with an expanding negative electromagnetic energy (identified or equivalent to dark energy, to BEH ocean or to the Dirac sea) and a structure of condensation that uses known matter and general relativity. There is cooperation, not competition, between these two antagonistic structures, and it is this cooperation that determines the nature of expansion. The structure of the expansion comes from a universe that has decomposed and has transferred its energy to the condensation structure of our universe that he gave birth to. The process would have started with a big bang (we assume a pre-existing quantum plenum) in the Planck era and would continue again. The compensation principle ensures that the negative energy of the structure of the expansion is transformed into positive energy of the structure of the condensation. The total energy density remains constant, although the two energy contributions respond to the expansion in a radically different way. The first, the energy density of the quantum "vacuum" of the structure of expansion, is progressively diluted, like that of any ordinary fluid housed in a volume that extends. It plays the role of a negative cosmological constant. It tends to decelerate the expansion and solves the problem of the *vacuum catastrophe*: The value of the energy of the vacuum today corresponds to the cosmological value observed, which is 10^{120} times smaller than that calculated by the quantum theory for the Planck era. The second, the density of the energy of the structure of the condensation, which comes

from the lost energy of the quantum vacuum, increases and condenses progressively, like that of any ordinary fluid lodged in a volume that shrinks. This is how stars, galaxies, clusters of galaxies are formed.

In addition to this duality, note that the Dirac sea applied to the atom while the ocean of the theory of Relation concerns the atom and the vacuum of space, hence the term "ocean" instead of "sea". Before elaborating further, let's say that the asymmetry between matter and antimatter is mainly explained by the creation of a pair of real particles (leaving two holes in the ocean); the antiparticle annihilates itself by regaining its oceanic hole while the particle is added to the matter leaving an oceanic hole. All in all, the hypothesis of the sea of Dirac is beautiful, but defective to explain the asymmetry between matter and antimatter. The particles of this sea are virtual whereas they are a reality in the ocean of the theory of Relation, which makes all the difference. The Dirac sea hypothesis is beautiful, but defective in explaining the asymmetry between matter and antimatter, while that of the ocean of the theory of Relation is effective.

4.2. Ocean of Negative Energy Seen by the Theory of Relation

Since all forms of energy is equivalent to mass, it is logical to expect that *electromagnetic energy* can also be converted spontaneously into particles. This is precisely the deep meaning of our mathematical model of the universe. The quantum vacuum is polarized by the very intense electromagnetic field that prevails in the ocean of negative energy. Above this ocean, pairs are constantly created and destroyed. The very intense electromagnetic field of the ocean spontaneously converts energy into particles. For a brief moment, a particle and its antiparticle separate. There are then four possibilities: Process 1: the two partners meet and annihilate.

Process 2: the negative energy antiparticle is captured by the negative energy ocean and the negative energy particle materializes in the outer world. The latter becomes an antiparticle of positive energy.

Process 3: The negative energy particle is captured by the ocean and its partner (negative energy antiparticle) escapes to become a positive energy particle.

Process 4: Both partners plunge into the negative energy ocean.

Since matter predominates, we incline towards process 3. The energy balance of the negative energy ocean of the theory of Relation shall be the following: by preferentially capturing particles of negative energy (the latter will encounter antiparticles of negative energy: they will annihilate each other in the ocean or they will materialize above) and by losing antiparticles of negative energy, the ocean spontaneously loses energy, hence mass. For an outside observer, lands of matter emerge on the horizon while the ocean evaporates by emitting radiation and particles. It is what explains the asymmetry between matter and antimatter.

4.3. Creation of a Real Particle/Antiparticle Pair and Separation

The ocean of the theory of Relation is filled with particles and antiparticles of all

kinds. If a photon of energy hv greater than 4 mc^2 interacts with an electron and a positron of the ocean of negative energy $-\varepsilon_o(\varepsilon_o > 0)$, it can communicate to them its energy and make them go in a state of energy $hv - \varepsilon_o$; This electron and this positron are then observable. There are now two "bubbles" or two "holes" in the ocean.

The holed ocean is equivalent to a full ocean and to two objects, one of positive energy $+\varepsilon_o$ and of charge +e opposite to those of the electron, the other of positive energy $+\varepsilon_o$ and of charge −e opposite to those of the positron. The initial photon disappeared and created a real electron and a real positron, that is, an electron with a positron hole and a positron with an electron hole. Four entities: two pairs of particle and antiparticle, a pair of positive energy over the ocean that can be observed and a pair of holes in the negative energy ocean.

The particularity of the mechanism would be this: a photon which has in itself its particle and its antiparticle makes cross a pair electron-positron of negative energy the barrier that separates the negative energy from the positive energy. The negative energy electron becomes a positron of positive energy while the positron of negative energy becomes the positive energy electron. There is then materialization of the electron-positron pair. Afterward, the electron and the positron separate each going in an opposite direction. The positron of positive energy will regain the negative energy ocean and will become again the negative energy electron. There will at that time annihilation equivalent to 2 mc^2. As for the positive energy electron, it will add 2 mc^2 to the matter and leave a hole in the ocean that will have the image of an electron of negative energy.

The conservation of energy is preserved but it can be said that there is a creation of matter and electric charge from energy since there is manifestly a preponderance of matter on antimatter. There is currently no evidence that antimatter exists in the world in the form of atoms, like matter, in appreciable quantities. Antimatter is only observed in the form of isolated antiparticles, which are produced either by cosmic radiation or by large accelerators. Negative energy appears to be liquid cement destined to produce matter.

4.4. How the Mass Comes to Particles

This cement also gives masses to the particles. It is akin to the Higgs mechanism. In the article "The Equation of the Universe" [18], we have seen that the flat spatiotemporal ocean of special relativity merges with the ocean of Higgs, itself assimilated with the Dirac sea, amalgamated with the ether ocean (minimum vacuum energy). Under the Principle of Compensation of the theory of Relation, there is a continuous transformation of so-called "negative" energy into "positive" energy. The principle of Compensation says that the decrement of negative electromagnetic energy-mass during the expansion induces a proportional and opposite increment of the positive gravitational energy-mass [16].

According to the equation $ke^2 = M_{vp}^2 t_o c$ of the theory of Relation [here M_{op} is the proton rest mass; $M_{op}(1/(1 - v^2/c^2)^{1/2})$ gives the relativized proton M_{vp}, *i.e.*, the rest mass + the kinetic energy; v = the estimated recessional velocity of the

galaxies], or more precisely $\pm ke^2 = \pm[M_{op}/(1 - v^2/c^2)^{1/2}]^2\ t_o c$, since the particles come in pairs, each with a counterpart antiparticle, the term M_{vp}^2, or $[M_{op}/(1 - v^2/c^2)^{1/2}]^2$, is a new fundamental variable in physics. Its value changes throughout the expansion. We suspect it to be the non-zero average value in the vacuum of the Higgs field. It would be the scalar field of the ocean of Higgs at the origin of the inertia of matter which measures the force that must be applied to an object to print it a given acceleration. It would follow a transformation of a space-time more and more flat into a space-time more and more locally curved.

Before being a boson that contains a particle and an antiparticle, M_{vp}^2 is a field that gives masses to the particles of the four forces. It blends in with the Higgs mechanism. Like him, he is as a mud in a field that sticks to the boots which thus become heavier. Similarly, particles-boots begin weighing.

5. Conclusions

Particle physicists assume the existence of an undetectable ultra-massive sterile neutrino which, not only would explain the anomalies in the neutrinos flux measured near nuclear reactors but which would have unbalanced the cosmos after the big bang, thereby giving birth to all matter in the universe, including dark matter [2] [6]. Excited, they hope that an alternation of appearances and disappearances of standard neutrinos near nuclear reactors for several months should suffice to conclude that the sterile neutrino is discovered. We think that the hypothesis of a fourth neutrino, very heavy, following the discovery of a deficit of antineutrinos, contributes more to invalidating the phenomenon of the oscillation of neutrinos than to fortify it. The contradiction is too blatant between the oscillation of standard neutrinos over long distances and the oscillation of the sterile neutrino with standard neutrinos over virtually non-existent distances.

Unlike neutrino physicists, we consider that such an alternation of neutrinos appearances and disappearances near nuclear power stations would mean a completely different phenomenon coming from a negative energy field. According to the theory of Relation, the origin of the masses of the particles would come from the ocean of negative energy. There would be a physical mechanism, likely beyond the standard model, at the origin of elementary particle masses. We have described it above: the creation of a pair of real particle/antiparticle and their separation in opposite direction, from which it follows that ground (matter) levels are rising while the ocean' levels are going down [7]. Energy power near the reactors would be better able to create neutrino-antineutrino pairs in favor of neutrinos. The natural tendency of antineutrinos would be to join the ocean of negative energy. One would not need a CP violation that would be responsible for the matter/antimatter asymmetry in the universe. It is ironic to think that Dirac's negative energy solution was perceived as non-existent. On the contrary, its relations with cosmology play in its favor and, more generally, it would be its origin.

Conflicts of Interest

The author declares no conflicts of interest regarding the publication of this paper.

References

[1] Lévy-Leblond, J.-M. (1981) La matière aujourd'hui. Seuil-Point, 119, 136.

[2] Grousson, M. (2016) *Science & Vie*, **1191**, 48, 56-59.

[3] Schaeffer, R. (1986) Chaos et Cosmos, L'anti-matière. Éditions Le Mail, 111.

[4] Schatzman, E. (1989) L'expansion de l'Univers. Hachette, 60, 61.

[5] Gagnon, P. (2016) Who Cares about Particle Physics? Oxford University Press, Oxford, 67-68. https://doi.org/10.1093/acprof:oso/9780198783244.001.0001

[6] Grousson, M. (2012) *Science & Vie*, **1137**, 52-53, 56-57, 66.

[7] Cohen-Tannoudji, G. and Spiro, M. (2013) Le boson et le chapeau mexicain. Gallimard, Folio Essais, 268-275, 318, 423.

[8] Bagdoo, R. (2011) Cosmological Inconstant, Supernovæ 1a and Decelerating Expansion. http://vixra.org/abs/1304.0169
https://www.academia.edu/5539777

[9] Bagdoo, R. (2016) Neutrino's Temporal Oscillations. 7, 11, 15.
http://vixra.org/abs/1605.0005
https://www.academia.edu/25111027

[10] Klein, É. (2007) Le facteur ne sonne jamais deux fois. Éditions Flammarion, Paris, 239.

[11] Magnan, C. (2011) Le théorème du jardin. amds édition, 203.

[12] Hotson, D.L. (2002) Dirac's Equation and the Sea of Negative Energy. Part 1, Infinite Energy, Issue 43.

[13] Zitoun, R. (1998) La physique des particules. Nathan Université, 32-34.

[14] Michaud, A. (2017) Electromagnetic Mechanics of Elementary Particles. Scholars' Press, 2nd Edition, 297-326, 329, 537.

[15] Pharabod, J.-P. and Pire, B. (1993) Le rêve des physiciens. Edition Odile Jacob.

[16] Bagdoo, R. (2008) The Pioneer Effect: A New Theory with a New Principle.
http://vixra.org/abs/0812.0005
https://www.academia.edu/5535864/

[17] Bagdoo, R. (2013) The Energy in Virtue of the Principle of Compensation.
http://vixra.org/abs/1301.0180
https://www.academia.edu/5539802/

[18] Bagdoo, R. (2017) The Equation of The Universe.
http://vixra.org/abs/1709.0033
https://www.academia.edu/34546347/

Journal of Modern Physics, 2019, 10, 176-194
http://www.scirp.org/journal/jmp
ISSN Online: 2153-120X
ISSN Print: 2153-1196

The de Broglie Waves and Joule-Lenz Law Applied in Examining the Electron Transitions in Small Quantum Systems

Stanislaw Olszewski

Institute of Physical Chemistry, Polish Academy of Sciences, Warsaw, Poland
Email: olsz@ichf.edu.pl

How to cite this paper: Olszewski, S. (2019) The de Broglie Waves and Joule-Lenz Law Applied in Examining the Electron Transitions in Small Quantum Systems. *Journal of Modern Physics*, **10**, 176-194.
https://doi.org/10.4236/jmp.2019.102014

Received: January 12, 2019
Accepted: February 24, 2019
Published: February 27, 2019

Abstract

A transformation of the electron states—say those enclosed in a potential box—into the de Broglie waves done in the paper, enabled us to calculate the energy change between two quantum levels as a function of the specific heat and difference of the temperature between the states. In consequence, the energy difference and that of entropy between the levels could be examined in terms of the appropriate classical parameters. In the next step, the time interval necessary for the electron transition between the levels could be associated with the classical electrodynamical parameters like the electric resistance and capacitance connected with the temporary formation of the electric cell in course of the transition. The parameters characterizing the mechanical inertia of the electron were next used as a check of the electrodynamical formulae referring to transition.

Keywords

The de Broglie Waves, Specific Heat, and Energy as Well as Entropy Transfer in Small Quantum Systems, Time Interval of the Electron Transition Associated with Parameters of the Classical Electrodynamics

1. Introduction

The spectacular results obtained by Planck (see e.g. [1]) at the very beginning of the quantum theory allowed him to couple the energy changes of the quantum oscillators with the temperature and entropy. The Planck's results concerning the probabilistic aspects of the changes of quantum oscillators were next generalized by Einstein [2]. Further development of the quantum theory led mainly to an accurate calculation of the stationary quantum states leaving the problem of

the electron transitions, and their properties, approximately on the level presented by Einstein. A step forwards was here the wave functions of the stationary states applied in calculating the transition probabilities between different quantum levels.

Another feature of the probabilistic Einstein theory was the assumption that a large, though rather undefined, number of the quantum objects should enter a given transition. This difficulty seems to be not involved in the Planck's approach where the number of the states which participate in transition can be definited and not necessarily large. This property allows us to consider also transitions in which the number of participating objects is relatively small. Moreover, when the Joule-Lenz classical approach [3] is applied on the quantum footing [4], the intensity of the energy emission can be estimated for a transition of a single particle without any reference to the probabilistic theory.

In effect, the aim of the present paper became to examine a single electron transition in small quantum systems on both probabilistic and non-probabilistic footing. An analysis of the classical physical parameters of mechanics, thermodynamics and electrodynamics which can be connected with the transition seems to be then of use.

2. Notion of Temperature Applied for a Small Number of Quantum Systems

Historically the quantum theory began as a statistics of photons emitted in course of the black-body radiation. Here the notion of temperature does accompany systematically the presentation of the energy distribution among the quantum levels. Somewhat later a concurrent quantum theory by Schrödinger banned essentially the notion of temperature and that of particle oscillations from the basic idea of the quantum states: the spectrum of levels has been replaced by a set of discrete entities being in general essentially different in their individual properties. The temperature is then assumed to be close to zero.

Nevertheless, for less or more numerous ensembles of particles, a reference between the temperature and energy remained of importance. The point became especially sound for the case of very low temperatures. Here we have, on one side, the well-known Nernst law representing a reference between the vanishing temperature and similar behaviour of the specific heat, but on the other side, the Planck's doubt does exist concerning the validity of the thermodynamical laws in general in case when the system absolute temperature T approaches zero [1].

The first step of the present paper is focused on a special problem of the electron specific heat. In general this heat is considered for large electron ensembles occupying a large number of the electron states. In consequence the problem is mainly reduced to the change of the Fermi level as an effect of the change of the temperature [5] [6] [7]. Such an approach seems to neglect details concerning the influence of the temperature on the individual levels. But the levels behaviour can be important also for small quantum systems, especially those having

low dimensionality. In such systems the number of considered quantum levels can be limited to only few states. Their examination as a function of the change of T becomes especially convenient when the dimensionality of the system is reduced together with the system size. An example can be a linear one-dimensional potential box represented by a very thin straight-linear tube. For, in this case, the system can be replaced by a set of the de Broglie waves. An advantage of such an approach is a transformation of the system into a frequency-and-temperature dependent ensemble similar to the photon system considered earlier by Planck.

3. The One-Dimensional Free-Electron System and Its Wave-Like Properties

The Schrödinger-like approach to such system is well known [8]. If we have the free-electron particles enclosed in a one-dimensional potential box of length L, their wave-mechanical properties are represented by the eigenenergies (see e.g. [8])

$$E_n = \frac{n^2 h^2}{8mL^2} \tag{1}$$

with the integer numbers

$$n = 1, 2, 3, 4, \cdots \tag{2}$$

indicating the quantum energy levels in (1), and the electron wave functions are

$$\psi_n = \left(\frac{2}{L}\right)^{1/2} \sin\left(\frac{n\pi}{L}x\right); \tag{3}$$

x is a position coordinate extended along the box. Here any ψ_n satisfies at the box boundaries the vanishing properties

$$\psi_n(x=0) = \psi_n(x=L) = 0. \tag{4}$$

The wave-like character can be attributed to the free-electron particles by taking into account, first, their kinetic energy in any state n, viz.

$$\frac{mv_n^2}{2} = E_n \tag{5}$$

where v_n is the velocity of the particle in the box. This gives

$$v_n = \left(\frac{2E_n}{m}\right)^{1/2} = \frac{nh}{2mL}. \tag{6}$$

The particle is moving in one or another of the box directions with the speed of (6).

The de Broglie wave representing the particle in state n has the frequency

$$\nu_n = \frac{1}{\tau_n} = \frac{v_n}{2L} = \frac{nh}{4mL^2} \tag{7}$$

so

$$v_n = \frac{2L}{\tau_n}. \tag{8}$$

In (7) the time period τ_n of the wave oscillation is characterized by assuming that the particle is passing twice the way of the length L.

The next requirement is that the energy possessed by the electron in state n is conserved by remaining equal to (1) also in the case of the de Broglie wave:

$$E_n = \frac{n^2h^2}{8mL^2} = \alpha nhv_n = \alpha nh\frac{nh}{4mL^2} = \alpha\frac{n^2h^2}{4mL^2}. \tag{9}$$

We find from (9) put equal to (1) that

$$\alpha = \frac{1}{2}. \tag{10}$$

Therefore the quantum

$$nhv_n = 2E_n \tag{11}$$

represents a full (non-interacting) energy of the electron pair occupying—according to the Pauli principle—a single level n.

4. Planck's Oscillator System as a Substitution of the Electron System

In effect of Sec. 3 we obtain the energy of the system of electron particles replaced by the energy of a system of the oscillators: each pair of particles situated on the level n is replaced by the oscillator having the energy nhv_n. The energy of the total system is therefore

$$2\sum_n E_n = \sum_n nhv_n, \tag{12}$$

where summation runs over the occupied states n.

A similar system of oscillators and its dependence on the temperature T has been considered by Planck [1]. The probability that a single oscillator has at any time the energy

$$\varepsilon_n = \varepsilon_0 + nhv_n \tag{13}$$

in the temperature bath of T is:

$$w_n = \mathrm{e}^{\frac{-nhv_n}{kT}}\left(1-\mathrm{e}^{-hv_n/kT}\right) \cong \mathrm{e}^{\frac{-nhv_n}{kT}}. \tag{14}$$

The last step in (14) is due to the assumption of a very low T.

In effect - by neglecting ε_0 which is the energy constant characteristic for all oscillator levels n - we have the energy

$$E_n(T) = w_n nhv_n = \mathrm{e}^{\frac{-nhv_n}{kT}} nhv_n. \tag{15}$$

The dependence of $E_n(T)$ on T can be examined by taking different n. In general we can look for the contribution of the state n to the specific heat. This is

$$c_V = \frac{\mathrm{d}}{\mathrm{d}T}E_n(T). \tag{16}$$

here the assumption of a constant volume V implies a constant box length L. We obtain

$$c_V = \mathrm{e}^{\frac{-nh\nu_n}{kT}} nh\nu_n \frac{\mathrm{d}}{\mathrm{d}T}\left(-\frac{nh\nu_n}{kT}\right) = \mathrm{e}^{\frac{-nh\nu_n}{kT}} \left(nh\nu_n\right)^2 \frac{1}{kT^2} = k\mathrm{e}^{-u}u^2 \tag{17}$$

where

$$u = \frac{nh\nu_n}{kT}; \tag{18}$$

k is the Boltzmann constant.

5. Examination of c_V

The function (17) gives

$$\frac{c_V}{k} = f(u) = \mathrm{e}^{-u}u^2. \tag{19}$$

The first derivative of $f(u)$ is

$$f'(u) = \mathrm{e}^{-u}\left(2u - u^2\right) \tag{20}$$

which gives

$$f'(u) = 0 \tag{21}$$

for

$$u = u_1 = 0 \tag{21a}$$

and

$$u = u_2 = 2. \tag{21b}$$

The second derivative of (19) is

$$f''(u) = \mathrm{e}^{-u}\left(u^2 - 4n + 2\right) \tag{22}$$

which for u_1 in (21a) becomes

$$f''(u_1) = 2 > 0 \tag{22a}$$

indicating a minimum of $f(u)$ equal to

$$f(u_1) = f(0) = 0. \tag{23}$$

For u_2 in (21b) we have

$$f''(u_2) = -2\mathrm{e}^{-2} < 0 \tag{22b}$$

which indicates a maximum of $f(u)$ equal to

$$f(u_2) = f(2) = 4\mathrm{e}^{-2}. \tag{24}$$

A characteristic point is that results (19)-(24) hold for any quantum number n. The result

$$u_2 = 2 = \frac{nh\nu_n}{kT_n} \tag{25}$$

implies that $T = T_n$ at the maxima of c_V satisfy the equation

$$T_n = \frac{nh\nu_n}{2k} = \frac{n^2h^2}{8mL^2k} \tag{26}$$

with the size of each maximum

$$c_V^{\max} = kf(u_2) = kf(2) = k\frac{4}{e^2} \tag{27}$$

independent of *n*. A similar property of the independence on *n* holds for the minima of c_V which are

$$c_V^{\min} = kf(u_1) = kf(0) = 0 \tag{28}$$

for all states *n*.

The formula (26) provides us with an important relation:

$$kT_n = \frac{n^2h^2}{8mL^2} = E_n. \tag{26a}$$

6. Heat Transfer Due to the Temperature Interval ΔT between Two Extrema of the Specific Heat

The heat transfer of the amount $\Delta E^{(h)}$ due to the temperature interval ΔT will be considered with the aid of a simplified formula

$$\Delta E^{(h)} = c_V \Delta T \tag{29}$$

where c_V is, first, an average specific heat

$$c_V = c_V^{av} \tag{30}$$

in the interval ΔT between two extrema (maxima) of the specific heat. In the second case c_V is put equal to a maximum of the specific heat, *i.e.*

$$c_V = c_V^{\max}, \tag{31}$$

where $c_V^{\max}$ is equal to the value obtained in formula (27). The both $\Delta E^{(h)}$, obtained respectively according to (29), (30) and (29), (31), will be next compared with the energy ΔE calculated from the energy difference between two quantum levels.

The temperature difference between two maxima of c_V can be derived from the formula (26):

$$\Delta T = T_{n+1} - T_n = \frac{(n+1)^2 - n^2}{8mL^2k}h^2. \tag{32}$$

The average c_V between these maxima is approximately equal to

$$\frac{2k}{2\times 2}\int_0^2 \mathrm{e}^{-u}u^2\mathrm{d}u = \frac{1}{2}k\int_0^2 \mathrm{e}^{-u}u^2\mathrm{d}u \tag{33}$$

where we assumed that the distance separating the maxima is roughly equal to a double distance between position of a minimum $(u=0)$ and that of the nearest maximum $(u=2)$ of c_V. In effect we obtain

$$c_V^{av} = \frac{1}{2}k\int_0^2 \mathrm{e}^{-u}u^2\mathrm{d}u = \frac{k}{2}(-1)\mathrm{e}^{-u}\left(u^2+2u+1\right)\Big|_{u=0}^{u=2} = \frac{1}{2}k0.65 \approx k0.33 \tag{34}$$

from which

$$\Delta E^{(h)} = \frac{1}{2}k0.65\Delta T \approx 0.33\frac{(n+1)^2 - n^2}{8mL^2}h^2 = 0.33\Delta E_n. \tag{35}$$

In the last step of (35) the energy difference between the electron states $n+1$ and n, viz.

$$\Delta E_n = \frac{(n+1)^2 - n^2}{8mL^2}h^2 \tag{36}$$

obtained from (1), is taken into account.

The case of $c_V = c_V^{\max}$ leads to result

$$\Delta E^{(h)} = kc_V^{\max}\Delta T = k\frac{2^2}{\mathrm{e}^2}\frac{(n+1)^2 - n^2}{8mL^2k}h^2 = \left(\frac{2}{\mathrm{e}}\right)^2 \Delta E_n \approx 0.54\Delta E_n. \tag{37}$$

which is not very much different from that obtained in (35).

7. Change of Entropy Referred to the Energy Change of a Quantum System

A well-known fact is that many ideas of classical physics did penetrate gradually into the quantum theory after being "only" submitted to modifications of a specific kind. The main idea of the modern theory was just to point out that physical parameters are quantum parameters. In general this means that a suitable size of parameter should be important for the physics of many phenomena in which the quantum situation can be involved.

The size limitations of the quantum theory did apply certainly to the energy and its changes. The aim of the present section and Secs. 8 and 10 is to examine from the quantum point of view the entropy parameter S systematically accompanying the changes of energy in thermodynamics according to the formula [1]

$$\mathrm{d}U + p\mathrm{d}V = T\mathrm{d}S; \tag{38}$$

here U is the internal energy of a system having the volume V, the external pressure p is exerted on V, and T is temperature.

Because of the presence of T and p the system is regularly considered as a many-particle ensemble submitted to the laws of a statistical theory. However, a difficulty connected with a many-particle approach can be circumvented by limiting the problem to that similar to a one-particle system. This is easy to demonstrate on the example of a single particle enclosed in a potential box by considering the particle, say an electron, as a de Broglie wave of matter spread into a one-dimensional box volume of the length L.

In order to meet a quantum situation we should assume that the de Broglie wave, corresponding to any quantum state n of the electron, has its special frequency ν_n. When the number of free electrons in the box is reduced to a pair occupying the same quantum state n, it can be demonstrated that the kinetic energy of such pair, *i.e.* obtained by neglecting the electrostatic interaction energy, is equal to (see [8]):

$$nh\nu_n = 2E_n = \frac{n^2h^2}{4mL^2}. \tag{38a}$$

A characteristic point is that a superposition of n de Broglie waves of the same frequency ν_n gives a conservation of the kinetic energy of the pair when this pair is transformed into the waves;
here

$$h\nu_n \tag{39}$$

is the energy carried by a single wave of the frequency

$$\nu_n = \frac{nh}{4mL^2}. \tag{40}$$

The reciprocal value of ν_n, viz.

$$\tau_n = \frac{1}{\nu_n} = \frac{4mL^2}{nh} \tag{41}$$

is the time period of the electron wave equal to the oscillation time necessary for the electron to travel twice—in two opposite directions—along the box length L.

8. Entropy Change and the Specific Heat

The formula (38) can be simplified by assuming that the volume increment $\mathrm{d}V$ is equal to zero, *i.e.* we can put

$$\Delta V = \Delta L = 0. \tag{42}$$

In this case the entropy increment $\mathrm{d}S$ in (38) is reduced to

$$\mathrm{d}U = T\mathrm{d}S. \tag{43}$$

Our aim becomes first to calculate a suitable specific heat c_V.

In Sec. 4 (see (14)) the problem—for the sake of simplicity—was reduced to a situation of a very low T by limiting the Planck's probability expression for the temperature bath of T

$$w_n = \mathrm{e}^{-\frac{nh\nu_n}{kT}}\left(1-\mathrm{e}^{-\frac{h\nu_n}{kT}}\right) \tag{44}$$

to the first component entering (14). In this case the formula (17) accompanied by (18) is obtained.

In the present case we apply a full probability expression (44), therefore

$$c_V^{\mathrm{tot}} = c_V + c_V^{\mathrm{suppl}}, \tag{45}$$

so c_V calculated in (17) is supplemented by the expression

$$c_V^{\mathrm{suppl}} = -\mathrm{e}^{(n+1)h\nu_n/kT}nh\nu_n(n+1)h\nu_n\frac{1}{kT^2} = -\mathrm{e}^{-\frac{u}{n}(n+1)}\frac{u}{n}(n+1)uk. \tag{46}$$

In result

$$c_V^{\mathrm{tot}} = k\mathrm{e}^{-u}u^2\left[1-\mathrm{e}^{-u/n}\left(1+\frac{1}{n}\right)\right]. \tag{47}$$

In the next step we examine the extremum position of c_V^{tot} divided by k. To

this purpose we calculate

$$\begin{aligned}\frac{\mathrm{d}}{\mathrm{d}u}\left(c_V^{\mathrm{tot}}/k\right) &= \frac{\mathrm{d}}{\mathrm{d}u}\mathrm{e}^{-u}u^2\left[1-\mathrm{e}^{-u/n}\left(1+\frac{1}{n}\right)\right] \\ &= \left(-\mathrm{e}^{-u}u^2+2\mathrm{e}^{-u}u\right)\left[1-\mathrm{e}^{-u/n}\left(1+\frac{1}{n}\right)\right]+\mathrm{e}^{-u}u^2\left[-\frac{1}{n}\mathrm{e}^{-u/n}\left(1+\frac{1}{n}\right)\right] \\ &\cong \mathrm{e}^{-u}\left(2u-u^2\right)\left(1-\mathrm{e}^{-u/n}\right)+\mathrm{e}^{-u}u^2\left(-\frac{1}{n}\mathrm{e}^{-u/n}\right) \\ &\cong \mathrm{e}^{-u}\left(2u-u^2\right)\left(1-1+\frac{u}{n}\right)+\mathrm{e}^{-u}u^2\left(-\frac{1}{n}+\frac{u}{n^2}\right) \\ &\cong \mathrm{e}^{-u}\left(2u-u^2\right)\frac{u}{n}-\mathrm{e}^{-u}u^2\frac{1}{n}\cong \mathrm{e}^{-u}u^2\frac{1}{n}\left(2-u-1\right)=0.\end{aligned} \tag{48}$$

In the end steps of calculations we assumed that n is large.

The extremal positions are obtained from (48) either for

$$u=u_1=0 \tag{49}$$

or

$$u=u_2=1 \tag{50}$$

The next derivative with respect to u performed with the expression in (48) gives

$$\frac{\mathrm{d}}{\mathrm{d}u}\mathrm{e}^{-u}u^2\left(1-u\right)=-\mathrm{e}^{-u}u^2\left(1-u\right)+\mathrm{e}^{-u}\left(2u-3u^2\right). \tag{51}$$

Evidently for $u=u_1=0$ the formula (51) gives again zero, but a similar substitution of u_2 into (51) indicates a negative result:

$$\left.\frac{\mathrm{d}}{\mathrm{d}u}\mathrm{e}^{-u}u^2\left(1-u\right)\right|_{u=1}=\mathrm{e}^{-1}\left(2-3\right)=-\frac{1}{\mathrm{e}}<0; \tag{52}$$

in effect the property of a maximum position can be attributed to u_2.

By assuming the approximation

$$1+1/n\cong 1 \tag{53}$$

we obtain for $u=u_2=1$ the maximum value of the specific heat equal to

$$\left.c_V^{\mathrm{tot}}=k\mathrm{e}^{-u}u^2\left(1-\mathrm{e}^{-\frac{u}{n}}\right)\right|_{u=1}=k\frac{1}{\mathrm{e}}\left(1-\frac{1}{\mathrm{e}^{1/n}}\right) \tag{54}$$

9. De Broglie Waves for the Electron Particle in a Potential Box Referred to a Harmonic Oscillator

Before the results for c_V^{tot} are applied to calculations of the entropy let us demonstrate a harmonic-like behaviour of the de Broglie oscillating waves. This is based on an analysis of the oscillation constant together with the frequency and energy carried by the oscillator [9].

For a particle enclosed in a potential box of the length L the amplitude a of the de Broglie wave can be assumed to be close to L, *i.e.*

$$a\approx L, \tag{55}$$

so a approaches the length of path allowed for the particle motion in one direction. This holds for any state n. The energy W_n of the oscillator in state n is coupled with a and the oscillation constant k_n by the formula [9]

$$W_n = \frac{k_n a^2}{2}. \tag{56}$$

In the next step k_n is coupled with the frequency ν_n of the oscillator by the relation

$$\omega_n = 2\pi\nu_n = \sqrt{\frac{k_n}{m}}. \tag{57}$$

Together with (55) and (56) this implies that the formula

$$a = L = \left(\frac{2W_n}{k_n}\right)^{1/2} \tag{58}$$

should be satisfied. Having

$$nh\nu_n = W_n, \tag{56a}$$

and the oscillator energy and particle energy formulae [see (7)] giving

$$2\pi\nu_n = 2\pi\frac{nh}{4mL^2} = \frac{\pi}{2}\frac{nh}{mL^2}, \tag{59}$$

we obtain [see (56a), (57) and (59)]:

$$\frac{k_n}{m} = \frac{2W_n}{a^2 m} = \frac{2nh\nu_n}{L^2 m} = \frac{2n^2h^2}{4mL^2}\frac{1}{L^2 m} = \frac{n^2h^2}{2m^2L^4}. \tag{60}$$

On the other side from (57)

$$\frac{k_n}{m} = 4\pi^2\nu_n^2 \tag{61}$$

which gives [see (59)]

$$\frac{k_n}{m} = 4\pi^2\frac{n^2h^2}{16m^2L^4} = \frac{\pi^2}{4}\frac{n^2h^2}{m^2L^4} \tag{62}$$

valid for any n. Evidently the last formula in (62) differs only slightly from the result obtained in (60).

10. Entropy Change Calculated with the Aid of the Specific Heat

We calculate the entropy change by applying to it a maximal value of the specific heat. In this case [see (54)]:

$$c_V^{\text{tot}} = k\mathrm{e}^{-u}u^2\left(1-\mathrm{e}^{-u/n}\right)\Big|_{u=1} \cong k\frac{1}{\mathrm{e}}\left(1-1+\frac{1}{n}\right) = \frac{k}{n\mathrm{e}} \tag{63}$$

since $u = u_2 = 1$ corresponds with a maximum value of c_V^{tot}.

Moreover in this case [see (18)]

$$u = 1 = \frac{nh\nu_n}{kT_n}, \tag{64}$$

so we obtain [see (40)]

$$T_n = \frac{nh\nu_n}{k} = \frac{1}{k}\frac{n^2h^2}{4mL^2} \tag{65}$$

or

$$nh\nu_n = kT_n. \tag{64a}$$

According to the formula (43) (see also [1]) we have

$$\Delta S = \frac{\Delta U}{T} = c_V^{\text{tot}}\frac{\Delta T}{T}. \tag{66}$$

Let us take the ΔT corresponding to the temperature difference between two neighbouring quantum states:

$$\Delta T = T_{n+1} - T_n = \left[(n+1)h\nu_{n+1} - nh\nu_n\right]\frac{1}{k}. \tag{67}$$

Therefore a maximal change of entropy corresponding to the change of the quantum number n by one is

$$\Delta S = c_V^{\text{tot}}\left[(n+1)^2\frac{h^2}{4mL^2} - n^2\frac{h^2}{4mL^2}\right]\frac{1}{k}\frac{4mL^2k}{n^2h^2} \cong \frac{k}{ne}\frac{2n}{n^2} = \frac{2k}{en^2} \tag{68}$$

which implies

$$\Delta S \sim \frac{1}{n^2}. \tag{69}$$

Let us note that ΔT between the neighbouring states obtained in virtue of (65) is twice as large as ΔT calculated in (32) with the aid of (26).

11. Classical Physical Parameters Associated with Electron Transitions in Small Quantum Systems

In many cases the treatment of quantum systems is considered as fundamentally separated from the classical physics and its results. Sometimes this view is dictated by the properties which are actually in our interest and are expected to belong mainly to a quantum domain. For example the statistics of the electron gas is usually a priori considered to be of a special character dictated by the Fermion-like classification of the electron particles and consequently, such kind of behaviour is from the beginning taken into account in course of the calculations performed on a given system. Another example concerns small quantum objects in which a special kind of the observable, say the energy connected with an electron transition, is mainly of interest. In this case the energy change due to transition is usually examined independently of other parameters which can be associated with the location of the electron particle and its change. In effect we obtain an exact or almost exact quantum result concerning the energy, but simultaneously an insight into numerous parameters describing the physical background of the transition process can be lost.

The aim of Sections 12 and 13 is to obtain some view on the classical secondary effects connected with the transition of an electron coupled mainly with the energy emission done in small quantum systems.

12. Transition Time between Quantum States and Its Reference to Parameters of the Classical Electrodynamics

In quantum mechanics the transition time Δt of an electron between two quantum energy levels is regularly difficult to assess. In fact the calculation of Δt is replaced by a probabilistic treatment of the electron transitions started by Einstein [2] already in reference to the old quantum theory. A step due to the modern quantum theory was to associate the probabilities of the electron transitions with the matrix elements of the electron transition operator calculated with the aid of the wave functions describing both the initial and final state of the examined transition; see e.g. [10] [11]. An evident advantage was the selection rules for transitions provided by the calculation of the mentioned matrix elements, as well as the dependence of these rules on the character of the applied operator. A drawback seemed to be the absence of a direct insight into the size of the interval Δt.

This difficulty could be at least partly removed by applying the classical Joule-Lenz law for the transition of energy between the quantum levels [4] [12]. If we have the energy difference ΔE defined by the formula

$$\Delta E = E_{n+1} - E_n, \tag{70}$$

so ΔE concerns a difference between two neighbouring quantum levels, the Joule-Lenz law states the relation [3] [4] [12]

$$\frac{\Delta E}{\Delta t} = Ri^2. \tag{71}$$

here R can be considered as a resistance due to the voltage V connected with ΔE and intensity i of the electron current between the states $n+1$ and n.

In other words we assume i to be associated with a condenser having the voltage

$$V = \frac{\Delta E}{e} \tag{72}$$

and the current in the condenser is

$$i = \frac{e}{t}, \tag{73}$$

where t is the time of the current effectiveness. Together with the well-known formula

$$R = \frac{V}{i} \tag{74}$$

we have for (71) on the basis of (72)-(74) the result

$$\frac{\Delta E}{\Delta t} = \frac{\Delta E}{e} \cdot \frac{t}{e} \left(\frac{e}{t}\right)^2 = \frac{\Delta E}{t} \tag{75}$$

which means that

$$\Delta t = t. \tag{76}$$

The ΔE in (72) and (75) is a parameter usually easy to obtain, whereas (76) can be associated classically with the resistance R in (74) and the capacitance C of the condenser by the formula

$$t \approx RC; \tag{77}$$

see e.g. [13]. We expect (77) to be a constant term. In fact C in (77) is given by the formula

$$C = \frac{e}{V} = \frac{e^2}{\Delta E}, \tag{78}$$

whereas R in virtue of (72) and (74) becomes

$$R = \frac{\Delta E}{e} \cdot \frac{t}{e} = \frac{\Delta E t}{e^2}. \tag{79}$$

In effect we obtain

$$RC = t \tag{80}$$

which is a confirmation of the expression given in (77).

This means that R and C should be known parameters in order to give the transition time (80). Beginning with R we have

$$R = \frac{V}{i} = \frac{\Delta E}{e} \cdot \frac{t}{e} = \frac{\Delta E \Delta t}{e^2} \tag{81}$$

where in the last step the result of (76) is applied. We postulate that

$$\Delta E \Delta t = h \tag{82}$$

which implies that t present in (77) should be a very special interval of time. This makes on the basis of (81)

$$R = \frac{h}{e^2}, \tag{83}$$

which is a result much independent of the examined quantum system; see [4]. The validity of the postulate in (82) is checked in Sec. 13 given below.

A consequence of the formula (83) is that R becomes equal to a well-known resistance value characteristic for the integer quantum Hall effect; see e.g. [14]. With the formula (83) for R and (78) for C we obtain

$$RC = \frac{h}{\Delta E} \tag{84}$$

or

$$RC\Delta E = h. \tag{85}$$

13. The Time Interval Equal to *RC* Characteristic for the Electron Transition in Different Quantum Systems

We demonstrate an invariance of RC in (84) for different quantum systems beginning with a free electron particle in a one-dimensional potential box. In this case (see e.g. [8])

$$\Delta E = E_{n+1} - E_n = \frac{(n+1)^2 - n^2}{8mL^2} h^2 \approx \frac{1}{4}\frac{nh^2}{mL^2}, \tag{86}$$

so from (84)

$$RC = \frac{h}{\Delta E} \cong \frac{4mL^2}{nh}. \tag{87}$$

It should be noted that RC in (87) is an interval equal to the time period characteristic for the free-electron oscillation in state n:

$$\tau_n = \frac{2L}{v_n} = \frac{2L}{nh} 2mL = \frac{4mL^2}{nh}. \tag{88}$$

This holds because for a free electron in state n the one-dimensional kinetic energy becomes

$$E_n = \frac{mv_n^2}{2} = \frac{n^2h^2}{8mL^2} \tag{89}$$

from which we obtain the electron velocity in n equal to:

$$v_n = \left(\frac{n^2h^2}{4mL^2}\right)^{1/2} = \frac{nh}{2mL}; \tag{90}$$

see also (6). The result obtained in (90) is applied in (88).

A corresponding RC can be calculated also for the electron transition in the hydrogen atom. By the virial theorem, we have the kinetic electron energy equal to the absolute value of the total electron energy:

$$\frac{mv_n^2}{2} = |E_n| = \frac{m}{2}\left(\frac{e^2}{n\hbar}\right)^2 = \frac{me^4}{2n^2\hbar^2}. \tag{91}$$

here

$$v_n = \frac{e^2}{n\hbar} \tag{92}$$

is the electron velocity on the nth orbit; see [15]. The energy difference in the hydrogen atom is

$$\begin{aligned} \Delta E = E_{n+1} - E_n &= \frac{m}{2}\frac{e^4}{\hbar^2}\left[\frac{1}{n^2} - \frac{1}{(n+1)^2}\right] \\ &= \frac{me^4}{2\hbar^2}\frac{(n+1)^2 - n^2}{n^2(n+1)^2} \cong \frac{me^4}{2\hbar^2}\frac{2n}{n^4} = \frac{me^4}{\hbar^2}\frac{1}{n^3}, \end{aligned} \tag{93}$$

where in the last step ΔE is simplified to the case of large n. The time period of the electron circulation along the orbit n becomes [15]

$$\tau_n = \frac{2\pi r_n}{v_n} = \frac{2\pi n^2\hbar^2}{me^2}\frac{n\hbar}{e^2} = \frac{2\pi n^3\hbar^3}{me^4}, \tag{94}$$

if we note that the radius r_n of the nth circular orbit in the hydrogen atom is equal to [15]

$$r_n = \frac{n^2\hbar^2}{me^2}. \tag{95}$$

On the other hand from the formula (84) for RC and (93) for ΔE we obtain

$$RC = \frac{h}{\Delta E} = \frac{h}{me^4}\hbar^2 n^3 = \frac{2\pi\hbar^3 n^3}{me^4}. \tag{96}$$

This means that RC becomes equal to the time period τ_n of the electron circulation given in (94).

The last small quantum system considered in the paper is the harmonic oscillator. For the oscillator having the frequency ν we have the time period of the oscillation equal to

$$\frac{1}{\nu} = T \tag{97}$$

and the energy difference between two neighbouring quantum levels is

$$\Delta E = h\nu = \frac{h}{T}. \tag{98}$$

This gives

$$RC = \frac{h}{\Delta E} = \frac{1}{\nu} = T. \tag{99}$$

In effect the formula (84) is satisfied for all examined cases, *i.e.* the electron particle in a one-dimensional potential box, the electron in a hydrogen atom and the harmonic oscillator. In the last case the electron mass m and charge e do not enter into an explicit calculation of RC.

14. Parameters of the Electron Mechanical Inertia Examined as a Check of the Formulae Applied for the Electron Transition

Interesting results gives the examination of parameters connected with the electron inertia exhibited in course of the electron transitions, say those represented by the change

$$n+1 \to n. \tag{100}$$

A similar reasoning was applied in considering the Tolman-Stewart effect characteristic for the slowing down of the motion of the electrons in metals; see e.g. [12] [13].

The energy difference

$$\Delta E = eV \tag{101}$$

can be represented by the product

$$mal = eV \tag{102}$$

where m is the electron mass, a —electron acceleration attained in course of the transition between the quantum levels, and l —the way length connected with the time characteristic for the transition. By the conservation of momentum this l should be not much different than a distance travelled by an electron with the

speed v_n characteristic for the electron level at the end of transition multiplied by the transition time which is

$$RC = \tau;$$

see respectively (88), (96) and (99) in different physical objects.

In effect we obtain

$$l_n = 2L \tag{103}$$

for a free particle in a one-dimensional potential box,

$$l_n = 2\pi r_n \tag{104}$$

in the hydrogen atom, and for the harmonic oscillator l_n should approximate four times the amplitude of the classical oscillator equal to the product of the maximal velocity in state n and time τ :

$$l_n = v_n^{\max}\tau. \tag{105}$$

In all these cases the acceleration a in (102) can be represented by the ratio

$$a = \frac{\Delta v}{\tau} \tag{106}$$

where Δv is the velocity change of the electron particle given by the difference

$$\Delta v = v_{n+1} - v_n. \tag{107}$$

In effect we obtain in place of (102) the equation

$$ml_n\Delta v = \tau eV = RCeV = \frac{V}{i}\frac{e}{V}eV = e^2\frac{V}{i} = e^2R = h, \tag{108}$$

because of the result (83) obtained for R.

We check below that in fact equation (108) is well satisfied.

For a free-electron particle in the box:

$$l_n = 2L \tag{109}$$

is independent of n and

$$\Delta v = v_{n+1} - v_n = \left(n+1-n\right)\frac{h}{2mL} = \frac{h}{2mL}; \tag{110}$$

see (90). The above two formulae give

$$ml_n\Delta v = m2L\frac{h}{2mL} = h. \tag{111}$$

For the hydrogen atomic orbit we have

$$l_n = 2\pi r_n = 2\pi\frac{n^2\hbar^2}{me^2} \tag{112}$$

and the absolute value of Δv is

$$\left|\Delta v\right| = v_n - v_{n+1} = \frac{e^2}{n\hbar} - \frac{e^2}{\left(n+1\right)\hbar} \cong \frac{e^2}{n^2\hbar}. \tag{113}$$

In this case the product entering the numerator of (102) becomes:

$$ml_n\left|\Delta v\right| = m2\pi\frac{n^2\hbar^2}{me^2}\frac{e^2}{n^2\hbar} = 2\pi\hbar = h. \tag{114}$$

The above reasonings confirm the value (83) obtained for the resistance R.

The case of the harmonic oscillator is slightly more complicated [9]. The maximal electron velocity in state n is given by the formula

$$(1/2)mv_{\max}^2 = nh\nu \tag{115}$$

from which the distance l obtained by the electron inertia in course of the time period of the electron oscillation T is

$$l = v_{\max}T = v_{\max}\frac{1}{\nu} = \frac{(2nh)^{1/2}}{m^{1/2}\nu^{1/2}}. \tag{116}$$

On the other hand the work performed by the electron on the distance l is

$$mla = ml\frac{\Delta v_{\max}}{\tau} = eV \tag{117}$$

where

$$\tau = T \tag{118}$$

is the time period connected with the electron current:

$$i = \frac{e}{\tau}. \tag{119}$$

The $\Delta v^{\max}$ in (117) is a difference of the maximal velocities associated respectively with the quantum state $n+1$ and n:

$$\Delta v^{\max} = \left(\frac{2h\nu}{m}\right)^{1/2}\left[(n+1)^{1/2} - n^{1/2}\right] = \left(\frac{2h\nu}{m}\right)^{1/2}\frac{n+1-n}{(n+1)^{1/2}+n^{1/2}} \cong \left(\frac{2h\nu}{m}\right)^{1/2}\frac{1}{2n^{1/2}}. \tag{120}$$

In effect we obtain for (117):

$$ml\Delta v^{\max} = m\frac{(2nh)^{1/2}}{m^{1/2}\nu^{1/2}}\left(\frac{2h\nu}{m}\right)^{1/2}\frac{1}{2n^{1/2}} = h \tag{121}$$

which is the expected result.

15. Summary

In the first step, by assuming the conservation of energy, the electron states enclosed in a one-dimensional potential box are transformed into the de Broglie waves having definite frequencies in time. The dependence of these waves on temperature can be studied according to the well-known Planck's formalism applied to the black-body radiation. When the specific heats due to the electron waves are examined, they show an extremal (maximal) behaviour at some temperature different from the absolute zero. In a further treatment, the difference of temperature characteristic for two extremal positions of the specific heat obtained for two quantum levels can be multiplied by a maximal specific heat due to these levels. This product estimates the amount of the heat transfer of energy associated with the electron transition. The amount occurs to be close to the change of the electron energy due to the quantum-mechanical transition.

The next step of the paper concerns the calculation of the changes of the entropy of a free-electron particle enclosed in a potential box. Usually the temper-

ature and entropy refer to a large ensemble of particles whose statistics and energy are known. However, at the early stage of the quantum theory, the particle ensembles were considered as sets of the oscillators having definite frequencies and remaining in equilibrium with respect to some external temperature. According to the de Broglie idea, it is easy to transform the behaviour of particles enclosed in a potential box into that of a system of the oscillating waves. In effect, the thermodynamical properties of the oscillators, like the specific heat, can be examined with the aid of the probabilistic formalism given by Planck. Because of the relation existent between the specific heat and entropy, the changes of entropy which accompany the energy transfer become easy to calculate with the aid of the temperature intervals defining the separations between the quantum levels.

In the last step, the aim of the paper was to point out that the time of the emission of energy between two neighbouring quantum states is associated—on a classical level—with production of the electric current due to a transport of a single electron particle. The current corresponds to a temporary formation of the electric cell in a quantum system and exhibits the properties of intensity and resistance known from the classical electrodynamics.

Having a known energy emission ΔE, the current parameters provide us—on the basis of the Joule-Lenz law—with the time Δt necessary for the dissipation of energy ΔE. But the same interval Δt can be obtained as a product of the current resistance R and capacitance C of the condenser represented by a temporary presence of the potential difference $\frac{\Delta E}{e}$ between two quantum levels.

The calculations are limited to three quantum objects considered as examples: the electron in a one-dimensional potential box, electron in a hydrogen atom and the electron representing a harmonic oscillator.

Classical parameters obtained for the examined objects in effect of the emission process are checked by considering the properties of the electron mechanical inertia exhibited in the same objects in course of the emission of the energy ΔE.

Conflicts of Interest

The author declares no conflicts of interest regarding the publication of this paper.

References

[1] Planck, M. (1932) Einführung in die Theorie der Wärme. S. Hirzel, Leipzig.

[2] Einstein, A. (1917) *Physikalische Zeitschrift*, **18**, 121.

[3] Lass, H. (1950) Vector and Tensor Analysis. McGraw-Hill, New York.

[4] Olszewski, S. (2015) *Journal of Modern Physics*, **6**, 1277.
ibid. (2016) **7**, 162; (2017) *Acta Physica Polonica*, **131**, 226.

[5] Sommerfeld, A. and Bethe, H. (1933) The Electron Theory of Metals. In H. Geiger

& K. Scheel (Eds.), *Handbuch der Physik* (Vol. 24, Part 2), Berlin: Springer. (In German)

[6] Mott, N.F. and Jones, H. (1936) The Theory of the Properties of Metals and Alloys. Oxford University Press, Oxford, New York.

[7] Ziman, J.M. (1972) Principles of the Theory of Solids. Cambridge University Press, UK. https://doi.org/10.1017/CBO9781139644075

[8] Eyring, H., Walter, J. and Kimball, G.E. (1957) Quantum Chemistry. Wiley, New York.

[9] Sommerfeld, A. (1949) Mechanik. 4th Ed., Akademische Verlagsgesellschaft, Leipzig.

[10] Schiff, L.I. (1968) Quantum Mechanics. 3rd Ed., McGraw-Hill, New York.

[11] Slater, J.C. (1960) Quantum Theory of the Atomic Structure. Vol. 2, McGraw-Hill, New York.

[12] Matveev, A.N. (1964) Electrodynamics and the Theory of Relativity. Izd, Wyzszaja Szkola, Moscow. (In Russian)

[13] Jauncey, G.E.M. (1948) Modern Physics. 3rd Ed., Van Nostrand, New York.

[14] MacDonald, A.H. (1989) Quantum Hall Effect. A Perspective, Kluwer, Milano. https://doi.org/10.1007/978-94-010-9709-3

[15] Sommerfeld, A. (1931) Atombau und Spektrallinien. 5th Ed., Vieweg, Braunschweig.

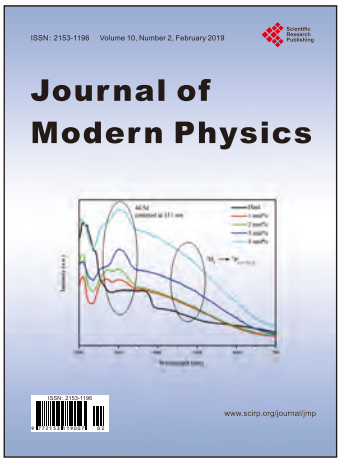

Call for Papers

Journal of Modern Physics

ISSN: 2153-1196 (Print) ISSN: 2153-120X (Online)
http://www.scirp.org/journal/jmp

Journal of Modern Physics **(JMP)** is an international journal dedicated to the latest advancement of modern physics. The goal of this journal is to provide a platform for scientists and academicians all over the world to promote, share, and discuss various new issues and developments in different areas of modern physics.

Editor-in-Chief

Prof. Yang-Hui He City University, UK

Subject Coverage

Journal of Modern Physics publishes original papers including but not limited to the following fields:

Biophysics and Medical Physics
Complex Systems Physics
Computational Physics
Condensed Matter Physics
Cosmology and Early Universe
Earth and Planetary Sciences
General Relativity
High Energy Astrophysics
High Energy/Accelerator Physics
Instrumentation and Measurement
Interdisciplinary Physics
Materials Sciences and Technology
Mathematical Physics
Mechanical Response of Solids and Structures
New Materials: Micro and Nano-Mechanics and Homogeneization
Non-Equilibrium Thermodynamics and Statistical Mechanics
Nuclear Science and Engineering
Optics
Physics of Nanostructures
Plasma Physics
Quantum Mechanical Developments
Quantum Theory
Relativistic Astrophysics
String Theory
Superconducting Physics
Theoretical High Energy Physics
Thermology

We are also interested in: 1) Short Reports—2-5 page papers where an author can either present an idea with theoretical background but has not yet completed the research needed for a complete paper or preliminary data; 2) Book Reviews—Comments and critiques.

Notes for Intending Authors

Submitted papers should not have been previously published nor be currently under consideration for publication elsewhere. Paper submission will be handled electronically through the website. All papers are refereed through a peer review process. For more details about the submissions, please access the website.

Website and E-Mail

http://www.scirp.org/journal/jmp **E-mail: jmp@scirp.org**

What is SCIRP?

Scientific Research Publishing (SCIRP) is one of the largest Open Access journal publishers. It is currently publishing more than 200 open access, online, peer-reviewed journals covering a wide range of academic disciplines. SCIRP serves the worldwide academic communities and contributes to the progress and application of science with its publication.

What is Open Access?

All original research papers published by SCIRP are made freely and permanently accessible online immediately upon publication. To be able to provide open access journals, SCIRP defrays operation costs from authors and subscription charges only for its printed version. Open access publishing allows an immediate, worldwide, barrier-free, open access to the full text of research papers, which is in the best interests of the scientific community.

- High visibility for maximum global exposure with open access publishing model
- Rigorous peer review of research papers
- Prompt faster publication with less cost
- Guaranteed targeted, multidisciplinary audience

Scientific Research Publishing

Website: http://www.scirp.org

Subscription: sub@scirp.org

Advertisement: service@scirp.org